Copy No. 24

RM No. L8G22

RESEARCH MEMORANDUM

DOWNWASH, SIDEWASH, AND WAKE SURVEYS BEHIND A 42° SWEPTBACK WING AT A REYNOLDS NUMBER OF 6.8 × 10^6 WITH AND WITHOUT A SIMULATED GROUND

By

G. Chester Furlong and Thomas V. Bollech

Langley Aeronautical Laboratory
Langley Field, Va.

NATIONAL ADVISORY COMMITTEE
FOR AERONAUTICS

WASHINGTON

December 13, 1948

NACA RM No. L8G22

NATIONAL ADVISORY COMMITTEE FOR AERONAUTICS

RESEARCH MEMORANDUM

DOWNWASH, SIDEWASH, AND WAKE SURVEYS BEHIND A 42° SWEPTBACK WING AT A REYNOLDS NUMBER OF 6.8×10^6 WITH AND WITHOUT A SIMULATED GROUND

By G. Chester Furlong and Thomas V. Bollech

SUMMARY

An investigation, with and without a simulated ground, has been conducted to provide flow inclination and wake data behind a 42° sweptback wing. Tests were made for two model configurations; namely, the plain wing and the wing with inboard trailing-edge split flaps and outboard leading-edge flaps deflected. Contour charts of downwash, sidewash, and dynamic-pressure ratio at two longitudinal stations behind the wing (2.0 and 2.8 mean aerodynamic chords) are presented. Integrations have been made to obtain variations of average downwash and dynamic-pressure ratio with angle of attack. The possibility of extending the lifting-line method used for calculating the downwash behind unswept wings to the case of a sweptback wing has been briefly investigated.

The qualitative results of the air-stream survey for the ground-out condition are, in general, consistent with the results which would be expected from a consideration of the span-load curve associated with sweptback wings. It was found also that without the ground present the tip vortices for the plain wing were shed and located at a position that would be expected for a straight tapered wing.

The variations of average downwash and average dynamic-pressure ratio with angle of attack indicate that for either model configuration the most preferable tail location would be below the chord plane extended and at the most rearward survey position. In the presence of the ground, negative variations of average downwash with angle of attack were obtained, and though such variations would increase the degree of stability, they may be undesirable from the standpoint of trim.

Calculations of downwash by the lifting-line method (as applied) underestimated the experimental downwash at the plane of symmetry but resulted in reasonable estimates of the experimental downwash outboard of the plane of symmetry.

INTRODUCTION

In order to obtain a satisfactory empennage design for a conventional airplane, a knowledge of the flow inclination and wake characteristics behind the wing is required.

Extensive theoretical and experimental studies have been made of the flow behind straight wings with the result that reasonable estimates of the flow inclination and wake characteristics can be made for a straight wing either with or without the ground present (references 1, 2, and 3). Theoretical and experimental studies of the flow behind sweptback wings are, at present, limited in scope and, hence, no adequate means for proper empennage design exist. The experimental data that are available for sweptback wings were obtained without the ground present and at relatively low values of Reynolds number (for example, reference 4). Recently some large-scale data have been published in reference 5.

An experimental investigation (Reynolds number 6.8×10^6) has been conducted in the Langley 19-foot pressure tunnel to provide not only additional flow inclination and wake data behind a sweptback wing not in the presence of the ground but also flow data obtained with the wing in the presence of the ground.

The model used for the present investigation had 42° sweepback of the leading edge, an aspect ratio of 4.01, a taper ratio of 0.625, and NACA 64_1-112 airfoil sections normal to the 0.273-chord line. Tests were made with and without a simulated ground for two model configurations; namely, the plain wing and the wing with inboard trailing-edge split flaps and outboard leading-edge flaps deflected. Force and moment data obtained through the angle-of-attack range for several values of Reynolds number have been presented in reference 6.

The present paper contains contour charts of downwash, sidewash, and dynamic-pressure ratios at two longitudinal stations behind the wing (2.0 and 2.8 mean aerodynamic chords). The locations of the tip vortices have been shown on the contour charts of dynamic-pressure ratios for the plain wing without the ground present. Integrations have been made to obtain variations of average downwash and dynamic pressure with angle of attack. Values of downwash have been calculated by extending the method presented in references 1 and 2 to account for the sweep of the 0.25-chord line.

The ground was simulated in the tunnel by means of a ground board. Although this method of ground representation is not ideal, the results of the present tests are believed to be indicative of the ground-interference effects on a sweptback wing.

SYMBOLS

C_L	lift coefficient $\left(\frac{\text{Lift}}{qS}\right)$
α	angle of attack of wing root chord, degrees
q	free-stream dynamic pressure, pounds per square foot $\left(\frac{\rho V^2}{2}\right)$
S	wing area, square feet
b	wing span, feet
c	local chord, feet
$\bar{c}$	mean aerodynamic chord, feet $\left(\frac{2}{S}\int_0^{b/2} c^2\,dy\right)$
ρ	mass density of air, slugs per cubic foot
V	stream velocity, feet per second
q_t	local stream dynamic pressure, pounds per square foot
ϵ	local downwash angle, degrees
Λ	sweep angle of 0.25-chord line, degrees
σ	sidewash angle, inflow positive, degrees
q_t/q	ratio of local-stream dynamic pressure to free-stream dynamic pressure
z	vertical distance, feet
x	longitudinal distance from 0.25-chord point of root chord
s	vortex semispan (always positive)
y	lateral distance from plane of symmetry
g	downwash factor
w	total induced downward velocity

c_l section lift coefficient

τ vortex strength

ϵ' calculated downwash angle, degrees

h downward displacement, measured normal to the relative wind, of the center line of the wake and the trailing vortex sheet from its origin at the trailing edge, feet

Integrated air-stream surveys:

$\left(q_t/q\right)_{av}$ average q_t/q, obtained by

$$\left[\left(\frac{q_t}{q}\right)_{av} = \frac{2}{S_t}\int_0^{b_t/2}\left(\frac{q_t}{q}\right)c_t\,dy_t\right]$$

ϵ_{av} average ϵ, obtained by

$$\left[\epsilon_{av} = \frac{2}{\left(\frac{q_t}{q}\right)_{av} S_t}\int_0^{b_t/2}\epsilon\left(\frac{q_t}{q}\right)c_t\,dy_t\right]$$

where

c_t chord of fictitious tail

b_t span of fictitious tail

S_t area of fictitious tail

y_t spanwise distance

$\frac{d\epsilon_{av}}{d\alpha}$ rate of change of ϵ_{av} with angle of attack

MODEL AND APPARATUS

Model

The model mounted on the normal wing-support system of the Langley 19-foot pressure tunnel is shown in figure 1. The wing had

42° sweepback of the leading edge, a taper ratio of 0.625, an aspect ratio of 4.01, and NACA 64_1-112 airfoil sections normal to the 0.273-chord line. The 0.20c trailing-edge split flaps were deflected 60° from the lower surface and extended from the root to $0.50\frac{b}{2}$. The leading-edge flaps extended from $0.400\frac{b}{2}$ to $0.975\frac{b}{2}$. The principal dimensions of the model and flaps are given in figure 2.

Prior to the present investigation, the wing had been equipped with a leading-edge slat which extended from $0.400\frac{b}{2}$ to $0.975\frac{b}{2}$. It was found that in the retracted position the slat slightly altered the NACA 64_1-112 airfoil sections and caused a slight discontinuity along the 0.20-chord line. The results obtained in the present tests, therefore, do not necessarily represent exactly those which would be obtained on a wing with true NACA 64_1-112 airfoil sections. The model was maintained in a smooth condition during the tests.

Apparatus

The aerodynamic forces were measured by a simultaneous-recording, six-component balance system.

Survey apparatus.- The Langley 19-foot-pressure-tunnel survey apparatus and multiple survey head (fig. 3) were used to obtain downwash and dynamic pressure behind the wing. The multiple survey head consists of six pitot-static tubes with pitch and yaw orifices in the hemispherical tips. The survey apparatus maintained the rake vertical as it was moved laterally along the span. The multiple survey head had been previously calibrated through known pitch and yaw angles. All pressure leads were conducted to a multiple-tube manometer and during the tests the data were photographically recorded.

A probe containing three tufts spaced 1.5 inches was used to locate the tip vortex. The probe was attached to the survey strut.

Ground board.- The ground board consisted of a steel framework covered with plywood on both the upper and lower surfaces, which resulted in an over-all thickness of 4 inches. (See fig. 4.) A slot extending the full width of the ground board and located 1 foot in front of the $0.25\bar{c}$ of the wing was provided as a means of boundary-layer control. The ground board was supported in the tunnel test section by means of wall brackets and center posts. (See figs. 1 and 4.) The support system allowed a ground-board travel from 16.0 to 31.9 inches below the center line of the tunnel (center of rotation of the model). A more detailed description of the ground board is contained in reference 6.

TESTS AND CORRECTIONS

Tests

The air in the tunnel was compressed to approximately 33 pounds per square inch absolute for all tests. The tests were made at a Reynolds number of 6.8×10^6 (based on the M.A.C. of the wing), which corresponded to a dynamic pressure of approximately 80 pounds per square foot and a Mach number of 0.14.

A preliminary investigation was conducted to determine the flow characteristics on the ground board and in the tunnel test section both with and without the model present. The results of these tests are summarized in reference 6.

Downwash, sidewash, and dynamic-pressure surveys were made for each model and ground-board configuration at two longitudinal stations. The positions for the survey apparatus were selected so that they approximated, through the angle-of-attack range of the tests, stations $2.0\bar{c}$ and $2.8\bar{c}$ behind the $0.25\bar{c}$ of the wing measured along the chord plane extended. The maximum variation of the stations $2.0\bar{c}$ and $2.8\bar{c}$ from the locations of the survey apparatus was only 0.5 inch through the angle-of-attack range of the test. Due to the fact that the trailing edge of the wing was swept back, the distance between the survey rake and the trailing edge of the wing decreased as the rake was moved from the plane of symmetry. Data were obtained at three angles of attack for the tests of the plain wing and at four angles of attack for the flapped wing. The angles of attack for the tests in the presence of the ground were selected so that the values of lift coefficient obtained were of approximately the same magnitude as those obtained with the ground board out.

In conjunction with the air-stream surveys, the tip vortex core was located by observing the rotational movement of a wool tuft on a probe.

Corrections

The lift data have been corrected for support-tare and strut interference as determined by tare tests. The values of angle of attack have been corrected for jet-boundary effects and air-stream misalinement.

The air-stream-survey data have been corrected for jet-boundary effects which consist of an angle change to the downwash and a downward displacement of the flow field.

Longitudinal survey position	$2.0\bar{c}$	$2.8\bar{c}$
$\Delta\epsilon$	$\frac{1.36C_L}{\sqrt{q_t/q}}$	$\frac{1.53C_L}{\sqrt{q_t/q}}$

With the ground board in the tunnel test section, it was not possible to obtain corrections for support-tare and strut interference. The ground-board-out corrections for support-tare and strut interference, however, have been applied to the ground-board-in lift data in the belief that they would be of the same nature, although not necessarily of the same magnitude, as would be obtained with the ground board in.

Calculations made for other ground investigations (such as reference 7) have shown that at small ground heights, jet-boundary corrections are negligible; hence, they have been neglected in the present tests.

RESULTS AND DISCUSSION

Ground Distance

The vertical distance from the $0.25\bar{c}$ of the wing to the ground board (regardless of boundary-layer thickness on the ground board) is referred to as the ground distance. Inasmuch as no standard point of reference exists, the $0.25\bar{c}$ has been used because it is the most convenient point of reference from considerations of test procedure. The model is supported in the tunnel at the $0.25\bar{c}$, and to maintain a constant ground distance for any other point of reference would have necessitated moving the ground board as the angle of attack of the wing was changed.

Based on the preceding definition of ground distance, the ground distances of the present tests were $0.68\bar{c}$ and $0.92\bar{c}$.

Air-Stream Surveys

The variations of lift coefficient with angle of attack obtained for both model configurations are presented in figure 5 to establish the locations of the test conditions for the air-stream surveys.

The air-stream-survey data have been cross-plotted to obtain contour charts of dynamic-pressure ratios, downwash, and sidewash in vertical planes $2.0\bar{c}$ and $2.8\bar{c}$ behind the $0.25\bar{c}$. The charts are presented in figures 6 to 17 and, for reference, the data presented are summarized in table I.

The effect of the model support struts on the flow at the survey planes was small even though tuft studies indicated that flow separation on the struts occurred at moderate angles of attack with the ground board present. The regions affected are easily discernable on the contours of dynamic-pressure ratio for the plain wing as areas of reduced dynamic-pressure ratio in the vicinity of $0.50\ b/2$. When the flaps were deflected the wing and strut wakes intermixed and hence the strut wake lost its identity.

The contours of dynamic-pressure ratio, downwash, and sidewash have been shown with reference to the chord plane extended. The intersection of the chord plane extended with the plane of survey has been arbitrarily selected as the reference line and any horizontal tail will remain a constant distance from this line as the angle of attack of the wing is changed. In order to indicate the position of the flow field of the wing with respect to the wing, the 0.25-chord line of the wing has been projected onto the plane of survey in the contours of dynamic-pressure ratio.

The qualitative results of the air-stream survey for the ground-out condition are, in general, consistent with the results which would be expected from a consideration of the span-lift curve associated with sweptback wings. The span lift for the unflapped wing, computed by the empirical method presented in reference 8, indicates that negative vorticity is shed over the inboard sections of the wing and, hence, it should be expected that the maximum downwash would occur outboard of the plane of symmetry. For an unswept wing of the same taper ratio, the lift would increase to the plane of symmetry and it would be here that the maximum downwash is reached. In the present tests, the reduced downwash at the plane of symmetry (figs. 6 and 7) is also due in part to the fact that the distance from the wing to the plane of survey is greatest at the plane of symmetry. The vortex sheet is displaced downward and the magnitude appears to be of the same order as for unswept wings. The wake center line traveled from just above the chord plane extended to a maximum height of $0.17\frac{b}{2}$ at the highest angle of attack ($\alpha = 16.0^\circ$) and most rearward survey position ($2.8\bar{c}$).

The air-stream surveys behind the flapped wing (figs. 8 and 9) show to some extent the strong effect of the flap tip vortex and secondary effect of the increase in strength of the bound vortex produced inboard by the flap on the flow field. The downwash is increased and the wake is lowered behind the flapped portion of the wing.

The tip vortices, as indicated by the present surveys for the plain wing, are shed and located in approximately the same position as would be expected for a straight tapered wing. In the range of the tests there is very little rolling in of the vortex, a fact not unreasonable when it is realized that the distance aft of the geometric tip is much less than the $2.8\bar{c}$ measured from $0.25\bar{c}$.

The presence of the ground caused for both model configurations (figs. 10 to 17) the usual reduction in downwash and upward displacement of the wake. Inasmuch as the reflected tip vortex is opposite in direction to the real tip vortex, it would increase the negative values of sidewash (outflow) and decrease the positive values of sidewash (inflow).

Average Values of Downwash and Dynamic Pressure

Variations of average downwash and dynamic-pressure ratio with angle of attack have been presented in figures 18 and 19 to show the effects of tail span and tail location (vertical and longitudinal) on the stability of a wing-tail combination. Integrations were made across the contour charts at various vertical positions and spans of a fictitious tail of constant chord and zero sweep. At each longitudinal survey plane (2.0 and 2.8$\bar{c}$), integrations were made across tail spans of 0.25 and $0.50\frac{b}{2}$ and at ground distances of $0.38\frac{b}{2}$ above, $0.25\frac{b}{2}$ above, on, and $0.25\frac{b}{2}$ below the chord plane extended. Where physical limitations prohibited obtaining data $0.25\frac{b}{2}$ below the chord plane extended, several variations have been presented for tail heights of $0.05\frac{b}{2}$ and $0.125\frac{b}{2}$ below the chord plane extended.

Inasmuch as the data presented are for a wing alone, the results are not necessarily indicative of those that would be obtained with a fuselage present. The results of an investigation of this wing tested in conjunction with a fuselage are presented in reference 9.

The data presented in figures 18(a) and 19(a) show that the size of tail span $\left(\text{up to } 0.50\frac{b}{2}\right)$ has very little effect on $d\epsilon/d\alpha$ either with or without the ground for the plain wing, whereas $d\epsilon/d\alpha$ increases with increased span for the flapped wing. The increased values of $d\epsilon/d\alpha$ for the flapped wing can be attributed to the influence of the flap-tip vortex.

Near maximum lift, the greater tail length resulted in a slight decrease in $d\epsilon/d\alpha$ for the plain wing and an even greater decrease for the flapped wing.

The most important parameter, as regards tail location for either the plain or flapped wing, appears to be the vertical position. Almost without exception, the values of $d\epsilon/d\alpha$ are decreasing near the maximum lift of the wing for tail locations on or below the chord plane extended, while for tail positions from the chord plane to $0.38\frac{b}{2}$ above, the values of $d\epsilon/d\alpha$ are increasing. The low values of $d\epsilon/d\alpha$ for low tail locations indicate that an increase in stability will probably be obtained as the tail is lowered. Although the values of $d\epsilon/d\alpha$ are decreasing near maximum lift for the tail location on the chord plane extended, the influence of the wake (figs. 18(b) and 19(b)) may be detrimental at this location. The contours of dynamic-pressure ratio indicate that when the flaps are deflected the wake is approximately $0.18\frac{b}{2}$ below the chord plane extended at low angles of attack. At high angles of attack or when the flapped wing is in the presence of the ground the wake has moved up to within $0.10\frac{b}{2}$ of the chord plane extended.

The presence of the ground substantially reduced the values of $d\epsilon/d\alpha$ and at the lowest ground height actually produced slight negative values of $d\epsilon/d\alpha$ near maximum lift for the plain wing. The values of $d\epsilon/d\alpha$ for the flapped wing became even more negative at low ground heights than those for the plain wing, and although negative values of $d\epsilon/d\alpha$ will improve the stability, such variations may be undesirable from the standpoint of trim.

The data obtained for the plain and flapped wing with and without the ground present indicate that from a consideration of downwash and dynamic pressure the most favorable tail location would be below the chord plane extended and with the greater tail length.

Calculated Downwash

The possibility of using lifting-line theory to determine the downwash behind sweptback wings has been briefly investigated. The procedure for the calculations is given in the appendix. Experimental results have been compared with variations of downwash with vertical distance, calculated at the plane of symmetry and at a spanwise station $0.33\frac{b}{2}$ (figs. 20 and 21). The vertical reference point in figure 20 is the 0.25-chord point of the root chord and in figure 21 it is the 0.25-chord point of the chord at spanwise station $0.33\frac{b}{2}$. The spanwise variations of maximum downwash obtained experimentally are presented in figure 22. Also included in this figure are values of downwash calculated at the center of the vortex sheet and as can be seen in figure 20 they do not necessarily represent the maximum values obtained.

It is apparent in figure 20 that the lifting-line theory, as applied in the present calculations, underestimates the experimental downwash in the plane of symmetry. For the angle-of-attack range shown, the value of $d\epsilon/d\alpha$ calculated is approximately 20 percent lower than that obtained experimentally. The results presented in figures 21 and 22 show that the agreement improves outboard of the plane of symmetry. The assumption was made in the calculations that the vortex sheet was shed along the 0.25-chord line and that the wing was at zero degree angle of attack. The calculations were repeated taking into account the tilt of the vortex sheet (extending from the 0.25-chord line) as the angle of attack increased. The results of these calculations were essentially in agreement with the original calculations. In order to evaluate the upwash contributed by the negative vorticity shed over the inboard sections of the wing, calculations were made neglecting the negative vorticity. The downwash angles obtained are shown in figure 20 and the calculated value of $d\epsilon/d\alpha$ is now only 10 percent lower than the experimental value. Neglecting the negative vorticity at the inboard sections had a negligible effect on the downwash calculated at stations outboard of the plane of symmetry.

Reference 2 indicates that for downwash calculations behind straight wings the displacement of the vortex sheet must be accounted for and the distention of the vortex sheet may be neglected. The displacement of the vortex sheet, employing the method of reference 2, appears adequate for sweptback wings (figs. 20 and 21) whereas the distention of the vortex sheet behind a sweptback wing may not be small enough to neglect.

CONCLUDING REMARKS

The results of the investigation to provide flow inclination and wake data behind a 42° sweptback wing both with and without a simulated ground present indicate:

1. The qualitative results of the air-stream survey for the ground-out condition are, in general, consistent with the results which would be expected from a consideration of the span-load curve associated with sweptback wings. It was found also that without the ground present the tip vortices for the plain wing were shed and located at a position that would be expected for a straight tapered wing.

2. The variations of average downwash and average dynamic-pressure ratio with angle of attack indicate that for either model configuration the most preferable tail location would be below the chord plane extended and at the most rearward survey position. In the presence of the ground, negative variations of average downwash with angle of attack were obtained, and though such variations would increase the degree of stability, they may be undesirable from the standpoint of trim.

3. Calculations of downwash by the lifting-line method (as applied) underestimated the experimental downwash at the plane of symmetry but resulted in reasonable estimates of the experimental downwash outboard of the plane of symmetry.

Langley Aeronautical Laboratory
National Advisory Committee for Aeronautics
Langley Field, Va.

APPENDIX

METHOD OF DOWNWASH CALCULATIONS

The reasonable agreement, attained for unswept wings, between values of downwash calculated by the method presented in references 1 and 2 and those obtained by experiment suggests an extension of the method to account for the sweep of the lifting line. Obvious objections or simplifications imposed by the lifting-line method have been discussed rather completely in reference 1 for the case of an unswept wing and it can be assumed that they apply in essence to sweptback wings as well. Although the aspect ratios of sweptback wings are, in general, smaller than those of the unswept wings treated in references 1 and 2, in the region of the tailplane, the lifting-line theory may still be expected to render approximate estimates of the downwash. Little is known of the downward displacement and distention of the vortex sheet behind a sweptback wing; hence, for the present calculations the assumptions made for unswept wings are applied.

The Biot-Savart equation has been expanded, as in reference 2, to determine the induced-downward velocity due to the bound vortex and two trailing vortices, assuming, however, that the bound vortex is swept along the 0.25-chord line. The resulting induced-downward velocity for any point whose coordinates are x, y, z may be expressed in fraction of stream velocity as:

$$\frac{w}{V} = -\int_0^1 \left(\frac{cc_l}{b}\right)(g_1)\,ds + \int_0^{-1} \left(\frac{cc_l}{b}\right)(g_2)\,ds$$

where

$$g_1 = \frac{1}{4\pi}\left(\frac{(s - y)}{\left[(s - y)^2 + z^2\right]}\left[1 + \frac{x - s\tan\Lambda}{\sqrt{(s - y)^2 + (x - s\tan\Lambda)^2 + z^2}}\right]\right.$$

$$+ \frac{(x - y\tan\Lambda)\cos\Lambda}{\left[(x - y\tan\Lambda)^2\cos^2\Lambda + z^2\right]}\left\{\frac{\frac{s}{\cos\Lambda} - \sqrt{y^2 + x^2 - \left[(x - y\tan\Lambda)\cos\Lambda\right]^2}}{\sqrt{(s - y)^2 + (x - s\tan\Lambda)^2 + z^2}}\right.$$

$$\left.\left. + \frac{\sqrt{y^2 + x^2 - \left[(x - y\tan\Lambda)\cos\Lambda\right]^2}}{\sqrt{y^2 + x^2 + z^2}}\right\}\right)$$

$$g_2 = \frac{1}{4\pi}\left(\frac{(s + y)}{\left[(s + y)^2 + z^2\right]} \left[1 + \frac{x - s \tan \Lambda}{\sqrt{(s + y)^2 + (x - s \tan \Lambda)^2 + z^2}} \right] \right.$$

$$+ \frac{(x + y \tan \Lambda) \cos \Lambda}{\left[(x + y \tan \Lambda)^2 \cos^2 \Lambda + z^2\right]} \left\{ \frac{\frac{s}{\cos \Lambda} - \sqrt{y^2 + x^2 - \left[(x + y \tan \Lambda) \cos \Lambda\right]^2}}{\sqrt{(s + y)^2 + (x - s \tan \Lambda)^2 + z^2}} \right.$$

$$\left. \left. + \frac{\sqrt{y^2 + x^2 - \left[(x + y \tan \Lambda) \cos \Lambda\right]^2}}{\sqrt{y^2 + x^2 + z^2}} \right\} \right)$$

and

$$\frac{cc_l}{b} = \frac{2\tau}{Vb}$$

The integration was performed by numerical summation with vorticity shed every $0.1\frac{b}{2}$ outboard of the plane of symmetry. Then the downwash angle can be evaluated:

$$\epsilon' = \frac{w}{V} (57.3)$$

The displacement of the vortex sheet according to reference 2 is

$$h = \int_{T.E.}^{x} \tan \epsilon \, dx$$

For the present calculations the span-load curve was computed by an empirical method which adapts Schrenk's method to sweptback wings (reference 8).

REFERENCES

1. Silverstein, Abe, and Katzoff, S.: Design Charts for Predicting Downwash Angles and Wake Characteristics behind Plain and Flapped Wings. NACA Rep. No. 648, 1939.

2. Silverstein, Abe, Katzoff, S., and Bullivant, W. Kenneth: Downwash and Wake behind Plain and Flapped Airfoils. NACA Rep. No. 651, 1939.

3. Katzoff, S., and Sweberg, Harold H.: Ground Effect on Downwash Angles and Wake Location. NACA Rep. No. 738, 1943.

4. Purser, Paul E., Spearman, M. Leroy, and Bates, William R.: Preliminary Investigation at Low Speed of Downwash Characteristics of Small-Scale Sweptback Wings. NACA TN No. 1378, 1947.

5. Tolhurst, William H., Jr.: An Investigation of the Downwash and Wake behind Large-Scale Swept and Unswept Wings. NACA RM No. A7L05, 1948.

6. Furlong, G. Chester, and Bollech, Thomas V.: Effect of Ground Interference on the Aerodynamic Characteristics of a 42° Sweptback Wing. NACA RM No. L8F04, 1948.

7. Recant, Isidore G.: Wind-Tunnel Investigation of Ground Effect on Wings with Flaps. NACA TN No. 705, 1939.

8. Diederick, Franklin W.: A Simple Approximate Method for Obtaining Spanwise Lift Distributions over Swept Wings. NACA RM No. L7I07, 1948.

9. Spooner, Stanley H., and Martina, Albert P.: Longitudinal Stability Characteristics of a 42° Sweptback Wing and Tail Combination at a Reynolds Number of 6.8×10^6. NACA RM No. L8E12, 1948.

TABLE I

LIST OF DOWNWASH ANGLE, SIDEWASH ANGLE, AND DYNAMIC-PRESSURE RATIO CONTOUR CHARTS PRESENTED

Figure no.	Flaps	Plane of survey (M.A.C.)	Ground distance (M.A.C.)	Angle of attack and lift coefficient
6	Off	2.0	∞	(a) $\alpha = 7.9^\circ$; $C_L = 0.51$. (b) $\alpha = 13.1^\circ$; $C_L = 0.81$. (c) $\alpha = 16.0^\circ$; $C_L = 0.97$.
10	Off	2.0	0.92	(a) $\alpha = 6.7^\circ$; $C_L = 0.48$. (b) $\alpha = 11.9^\circ$; $C_L = 0.80$. (c) $\alpha = 14.6^\circ$; $C_L = 0.95$.
14	Off	2.0	0.68	(a) $\alpha = 6.7^\circ$; $C_L = 0.51$. (b) $\alpha = 11.9^\circ$; $C_L = 0.83$. (c) $\alpha = 14.6^\circ$; $C_L = 0.98$.
7	Off	2.8	∞	(a) $\alpha = 7.9^\circ$; $C_L = 0.51$. (b) $\alpha = 13.1^\circ$; $C_L = 0.81$. (c) $\alpha = 16.0^\circ$; $C_L = 0.97$.
11	Off	2.8	0.92	(a) $\alpha = 6.7^\circ$; $C_L = 0.48$. (b) $\alpha = 11.9^\circ$; $C_L = 0.80$. (c) $\alpha = 14.6^\circ$; $C_L = 0.95$.
15	Off	2.8	0.68	(a) $\alpha = 6.7^\circ$; $C_L = 0.51$. (b) $\alpha = 11.9^\circ$; $C_L = 0.83$. (c) $\alpha = 14.6^\circ$; $C_L = 0.98$.
8	Deflected	2.0	∞	(a) $\alpha = 3.6^\circ$; $C_L = 0.61$. (b) $\alpha = 8.5^\circ$; $C_L = 0.91$. (c) $\alpha = 13.5^\circ$; $C_L = 1.20$. (d) $\alpha = 16.8^\circ$; $C_L = 1.35$.
12	Deflected	2.0	0.92	(a) $\alpha = 2.4^\circ$; $C_L = 0.59$. (b) $\alpha = 7.1^\circ$; $C_L = 0.89$. (c) $\alpha = 9.7^\circ$; $C_L = 1.04$. (d) $\alpha = 12.5^\circ$; $C_L = 1.18$.
16	Deflected	2.0	0.68	(a) $\alpha = 2.4^\circ$; $C_L = 0.62$. (b) $\alpha = 7.3^\circ$; $C_L = 0.91$. (c) $\alpha = 10.0^\circ$; $C_L = 1.00$. (d) $\alpha = 13.6^\circ$; $C_L = 1.20$.
9	Deflected	2.8	∞	(a) $\alpha = 3.6^\circ$; $C_L = 0.61$. (b) $\alpha = 8.5^\circ$; $C_L = 0.91$. (c) $\alpha = 13.5^\circ$; $C_L = 1.20$. (d) $\alpha = 16.8^\circ$; $C_L = 1.35$.
13	Deflected	2.8	0.92	(a) $\alpha = 3.4^\circ$; $C_L = 0.59$. (b) $\alpha = 7.1^\circ$; $C_L = 0.89$. (c) $\alpha = 9.7^\circ$; $C_L = 1.04$. (d) $\alpha = 12.5^\circ$; $C_L = 1.18$.
17	Deflected	2.8	0.68	(a) $\alpha = 2.4^\circ$; $C_L = 0.62$. (b) $\alpha = 7.3^\circ$; $C_L = 0.91$. (c) $\alpha = 10.0^\circ$; $C_L = 1.00$. (d) $\alpha = 13.6^\circ$; $C_L = 1.20$.

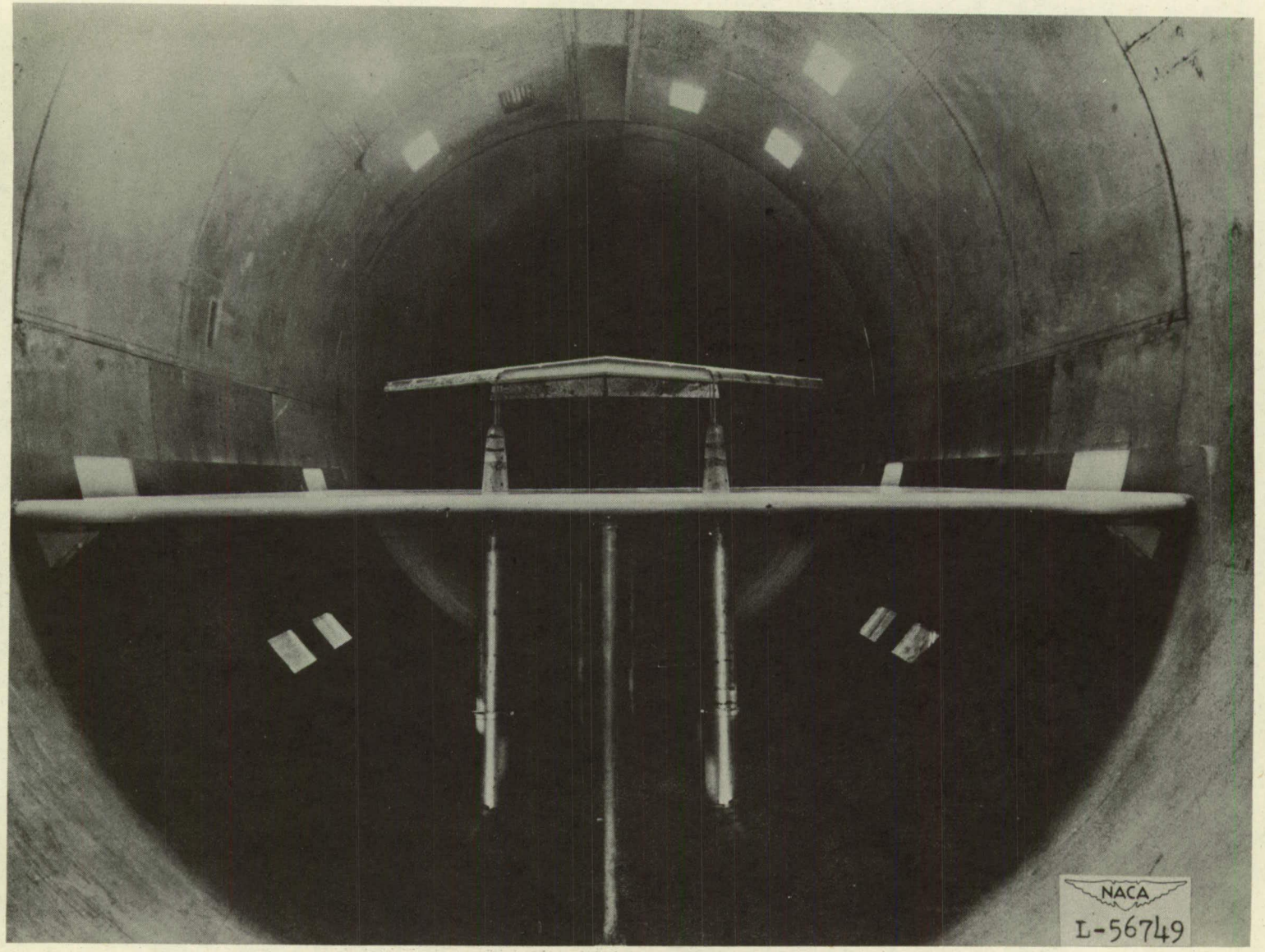

(a) Front view.

Figure 1.- A 42° sweptback wing mounted in the Langley 19-foot pressure tunnel. Flaps deflected; ground board in. Ground distance 0.92 M.A.C.

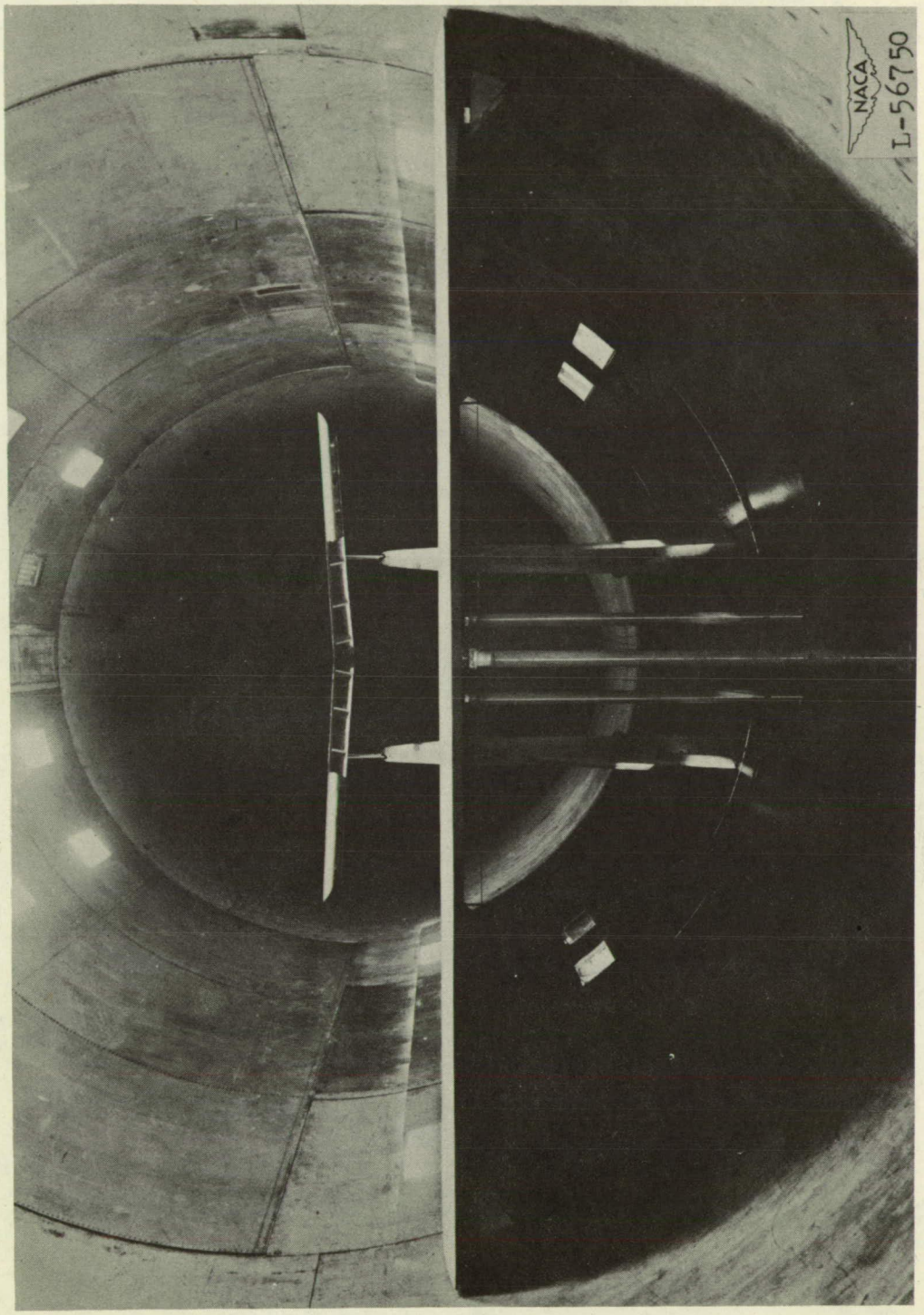

(b) Rear view.

Figure 1.- Concluded.

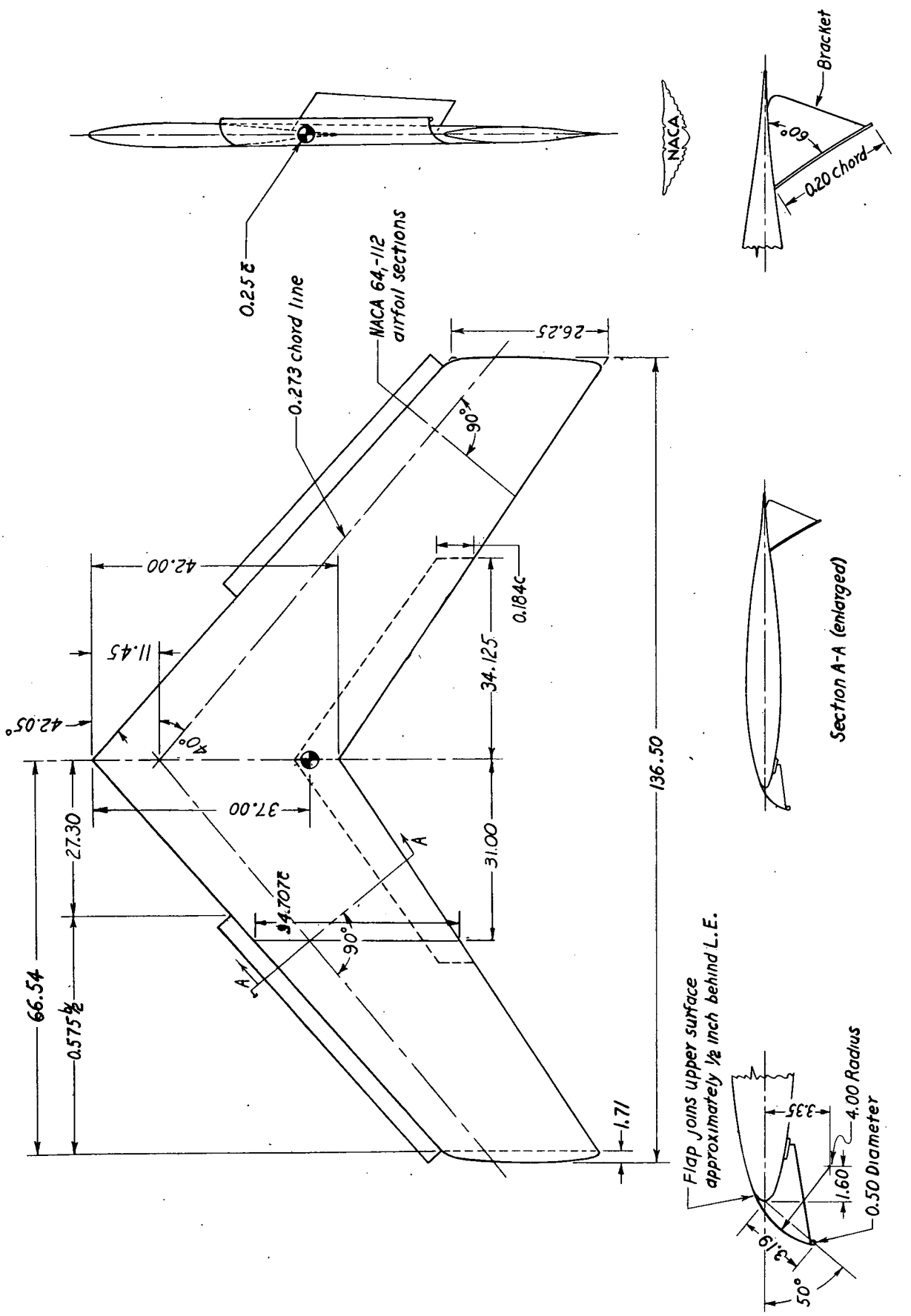

Figure 2.- Layout of 42° sweptback wing. All dimensions in inches.

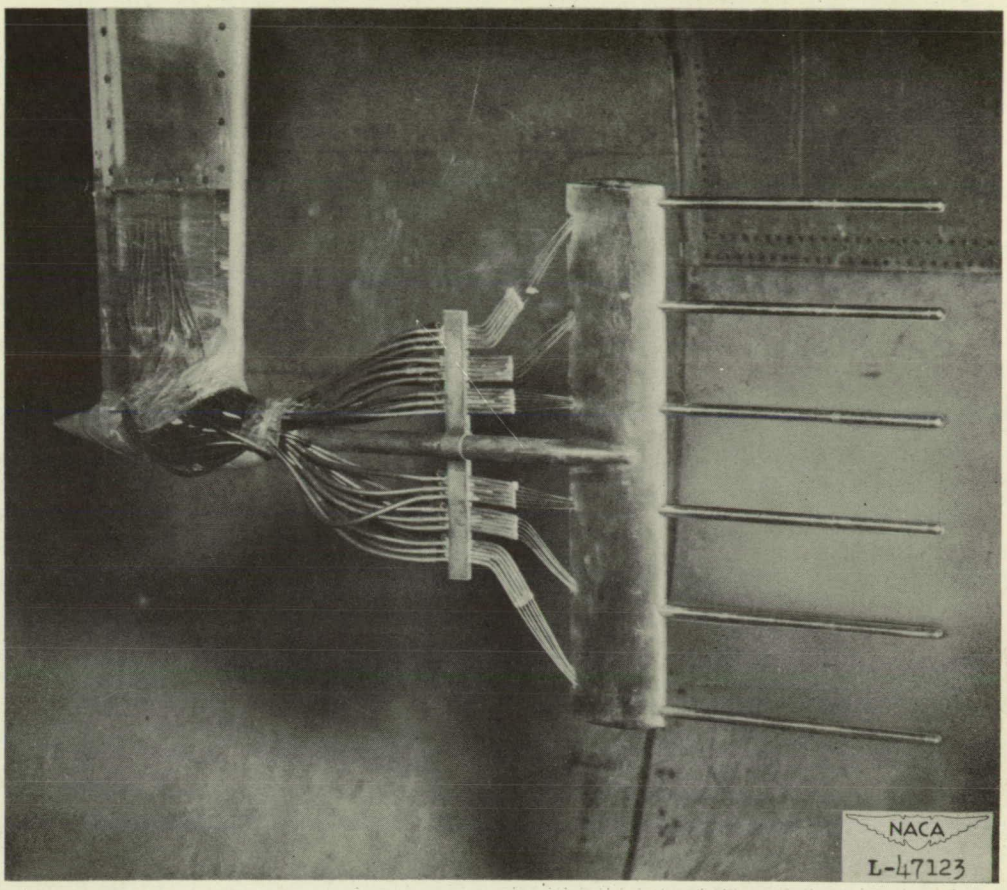

(a) Photograph of rake head.

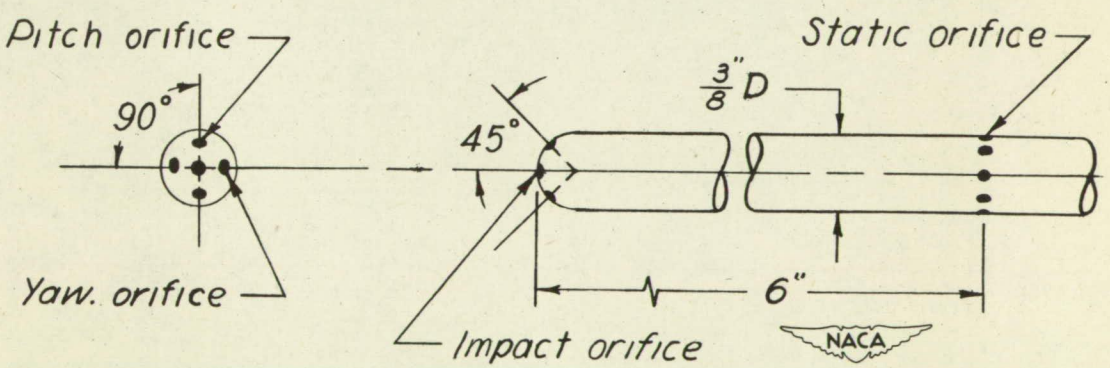

(b) Sketch of tube head.

Figure 3.- Langley 19-foot pressure tunnel air-stream survey rake.

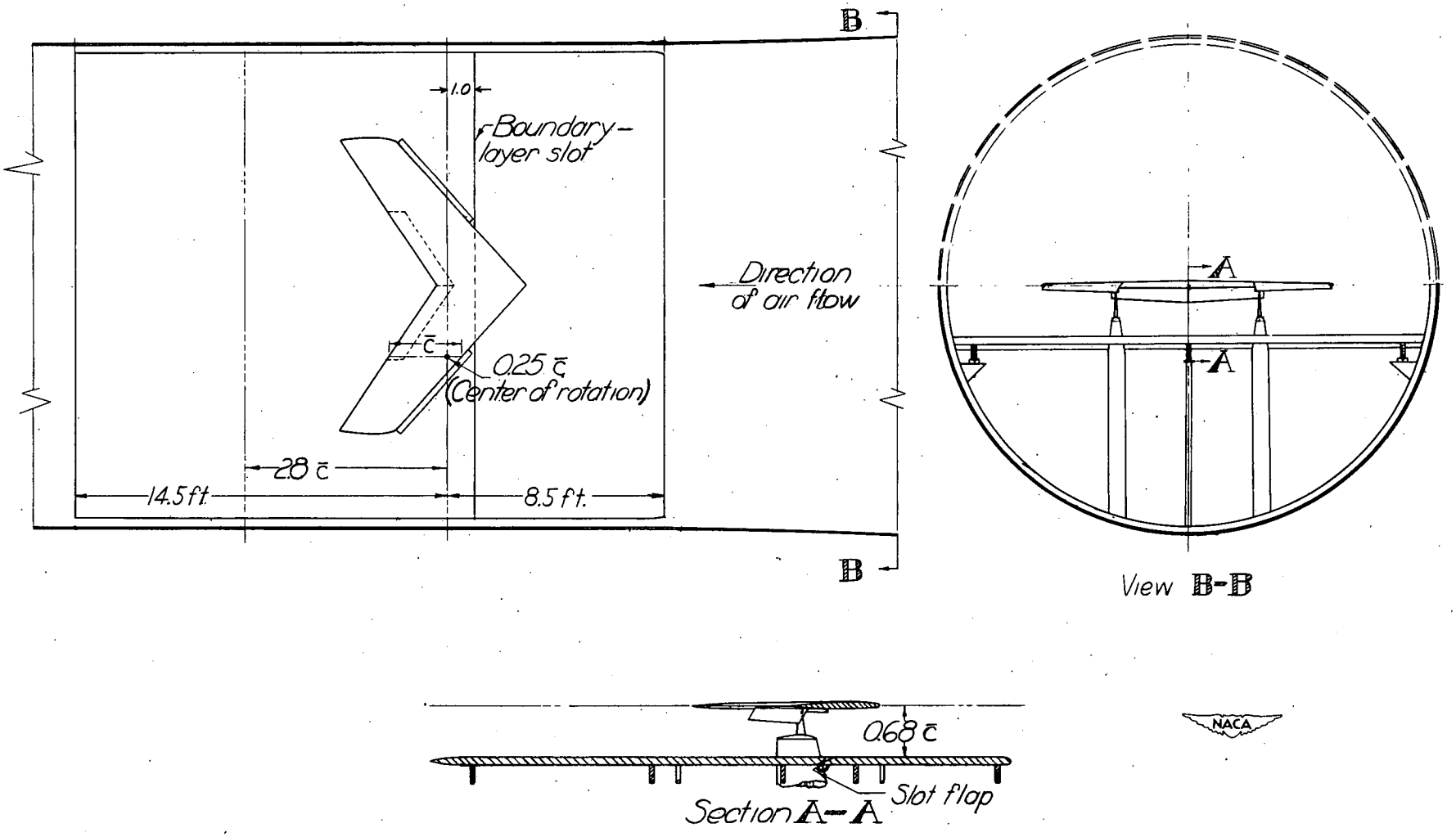

Figure 4.- Sketch of 42° sweptback wing and ground board used in the 19-foot pressure tunnel. Ground distance 0.68 M.A.C.

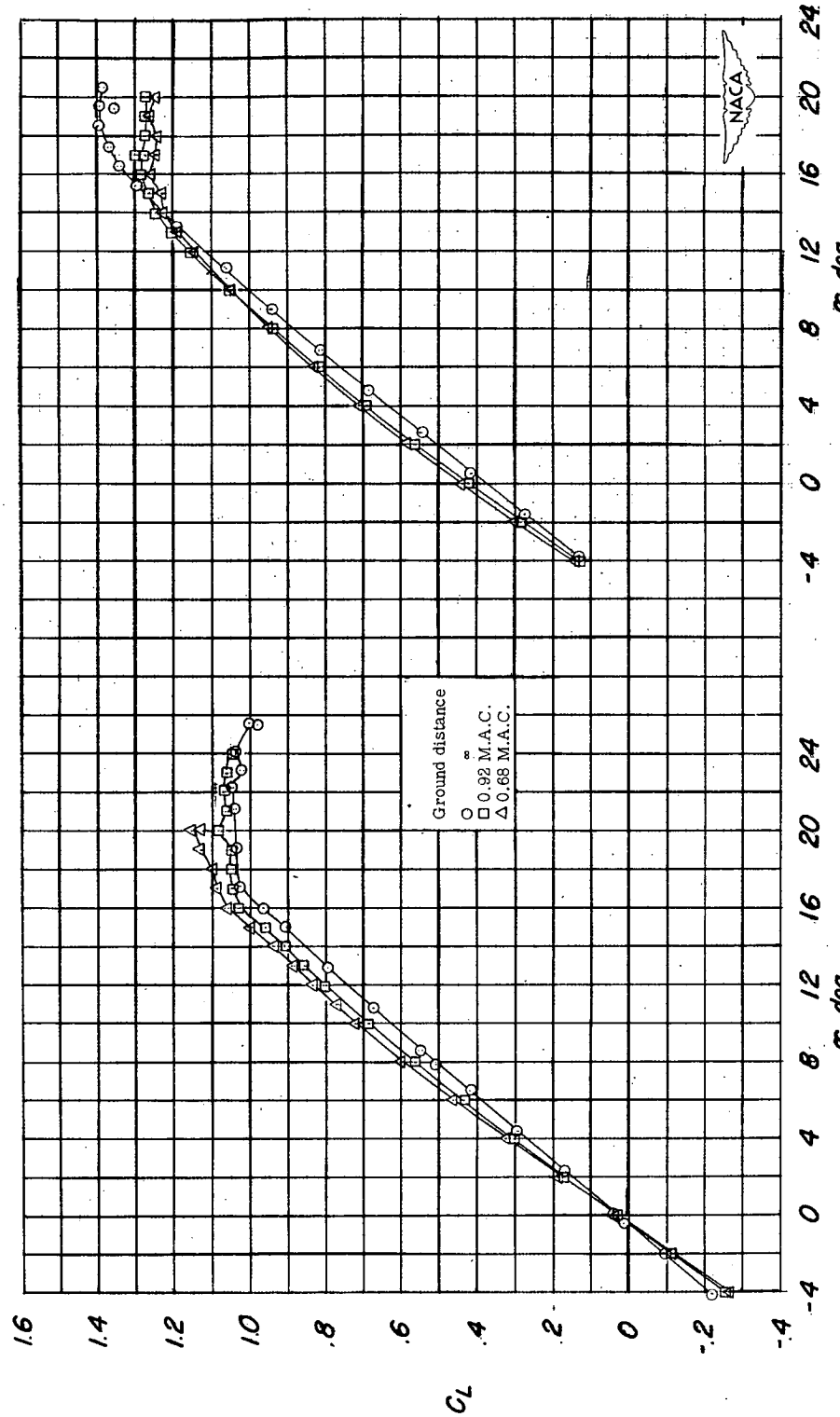

(a) Flaps neutral. (b) Flaps deflected.

Figure 5.- Variations of lift coefficient with angle of attack for various ground distances. Flaps neutral and flaps deflected; R = 6.8 × 10^6.

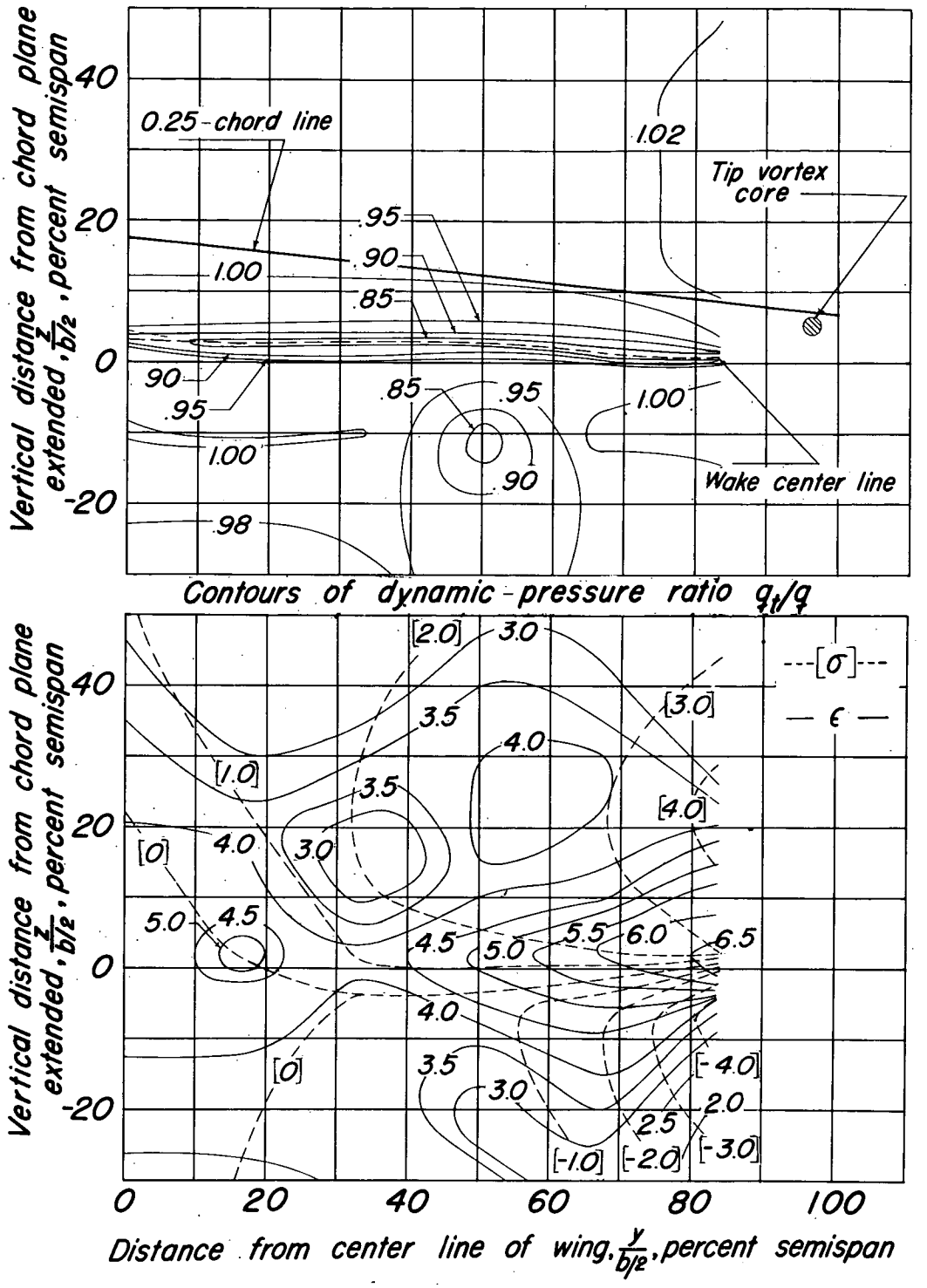

Contours of downwash angle ϵ and sidewash angle σ in degrees

(a) $\alpha = 7.9°$; $C_L = 0.51$.

NACA

Figure 6.— Downwash angle, sidewash angle, and dynamic-pressure ratios behind a 42° swept back wing. Longitudinal plane of survey at 2.0 M.A.C.; flaps neutral; ground distance ∞.

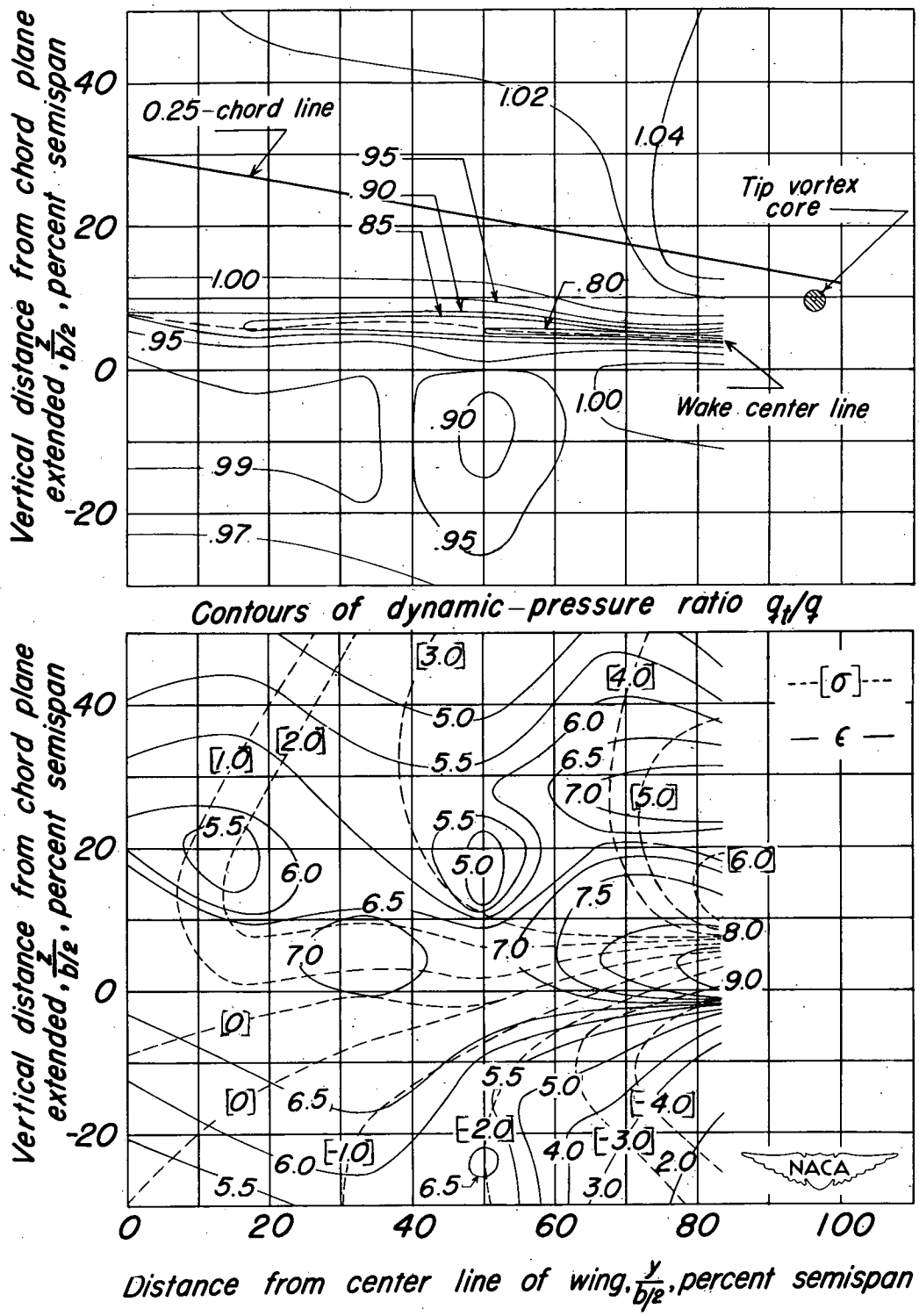

Contours of downwash angle ϵ and sidewash angle σ in degrees

(b) $\alpha = 13.1°$; $C_L = 0.81$.

Figure 6.- Continued.

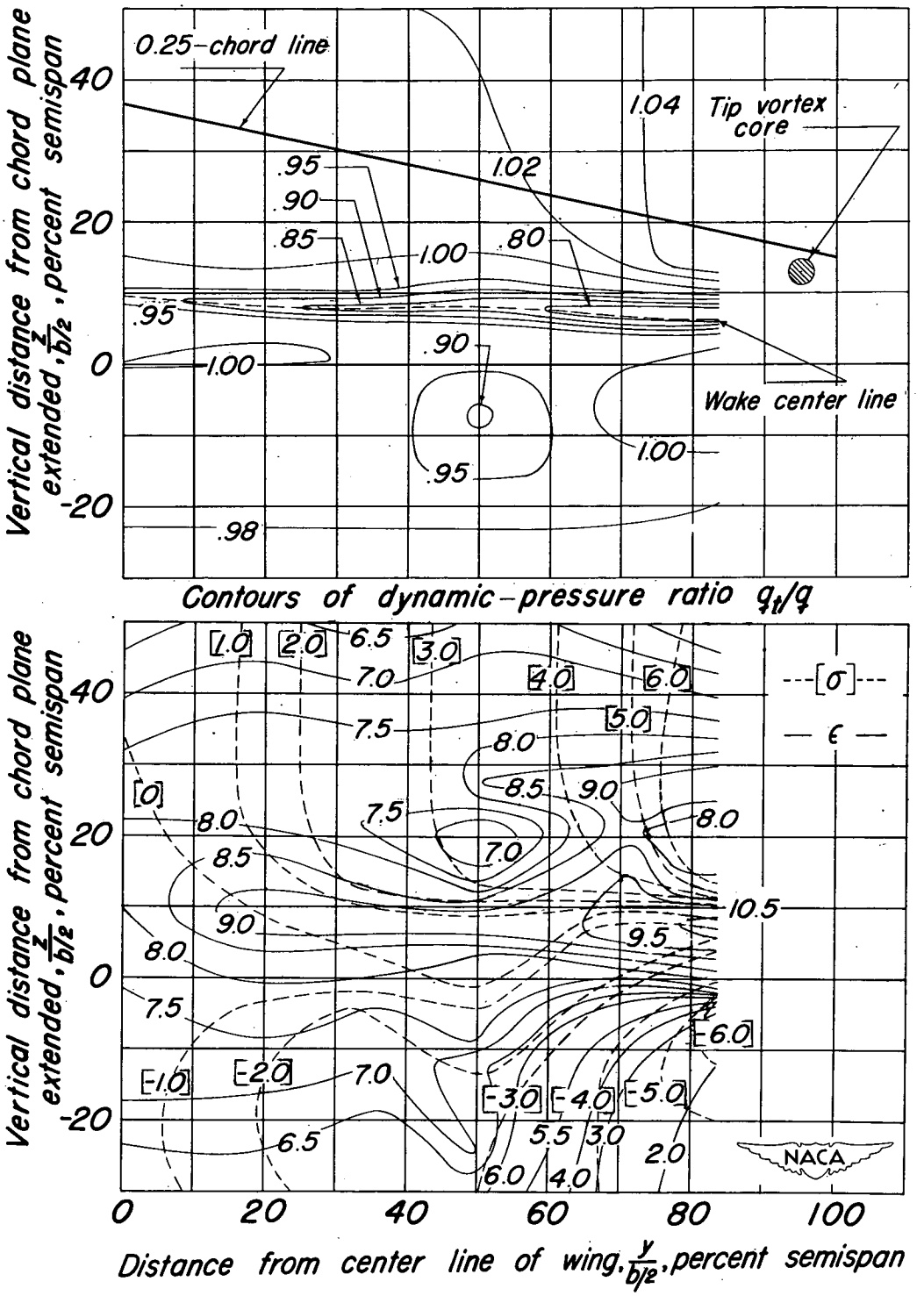

Contours of downwash angle ϵ and sidewash angle σ in degrees

(c) $\alpha = 16.0°$; $C_L = 0.97$

Figure 6. – Concluded.

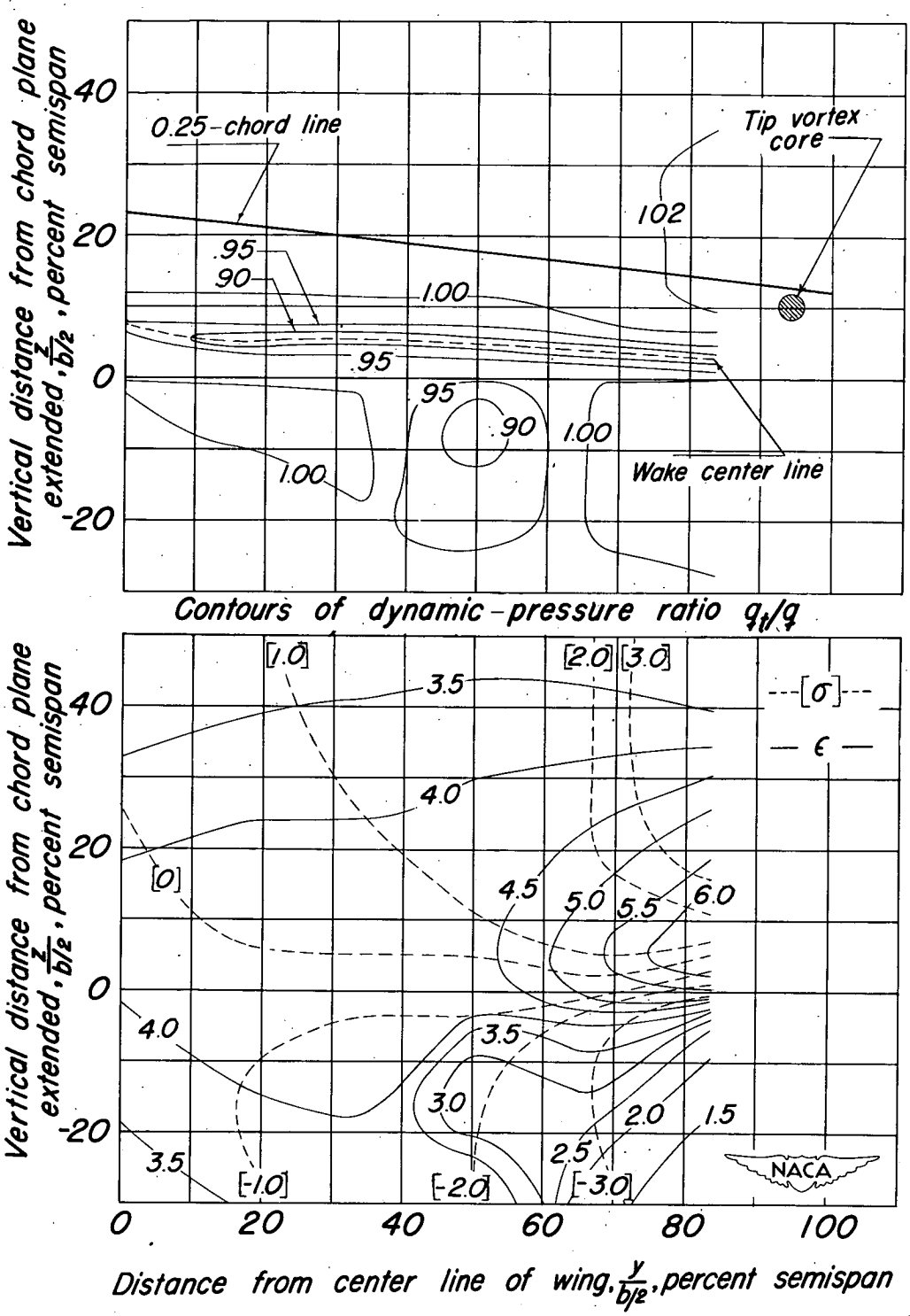

Contours of downwash angle ϵ and sidewash angle σ in degrees

(a) $\alpha = 7.9°$; $C_L = 0.51$.

Figure 7. — Downwash angle, sidewash angle, and dynamic-pressure ratios behind a 42° sweptback wing. Longitudinal plane of survey at 2.8 M.A.C.; flaps neutral; ground distance ∞.

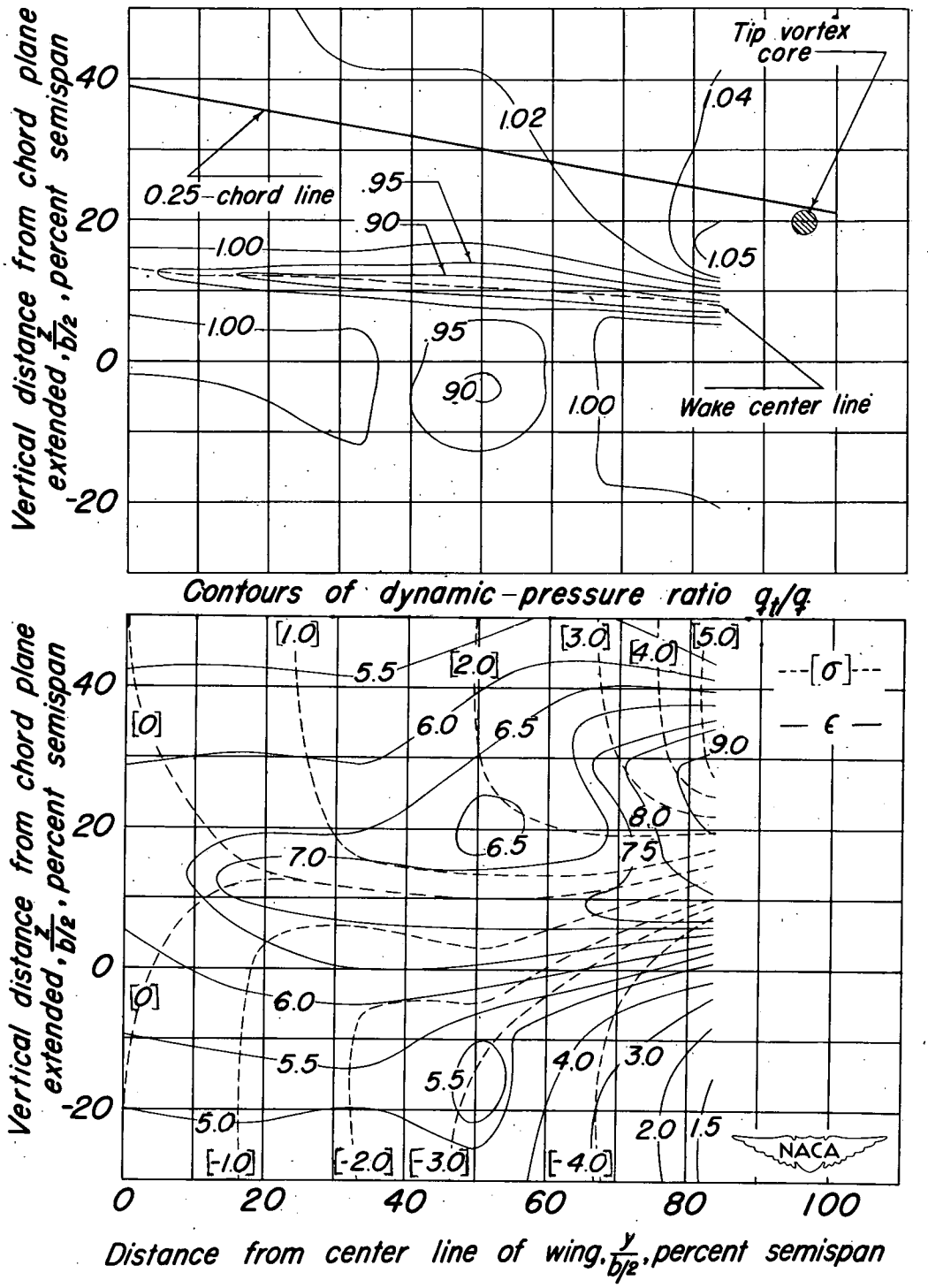

Contours of downwash angle ϵ and sidewash angle σ in degrees

(b) $\alpha = 13.1^\circ$; $C_L = 0.81$

Figure 7. – Continued.

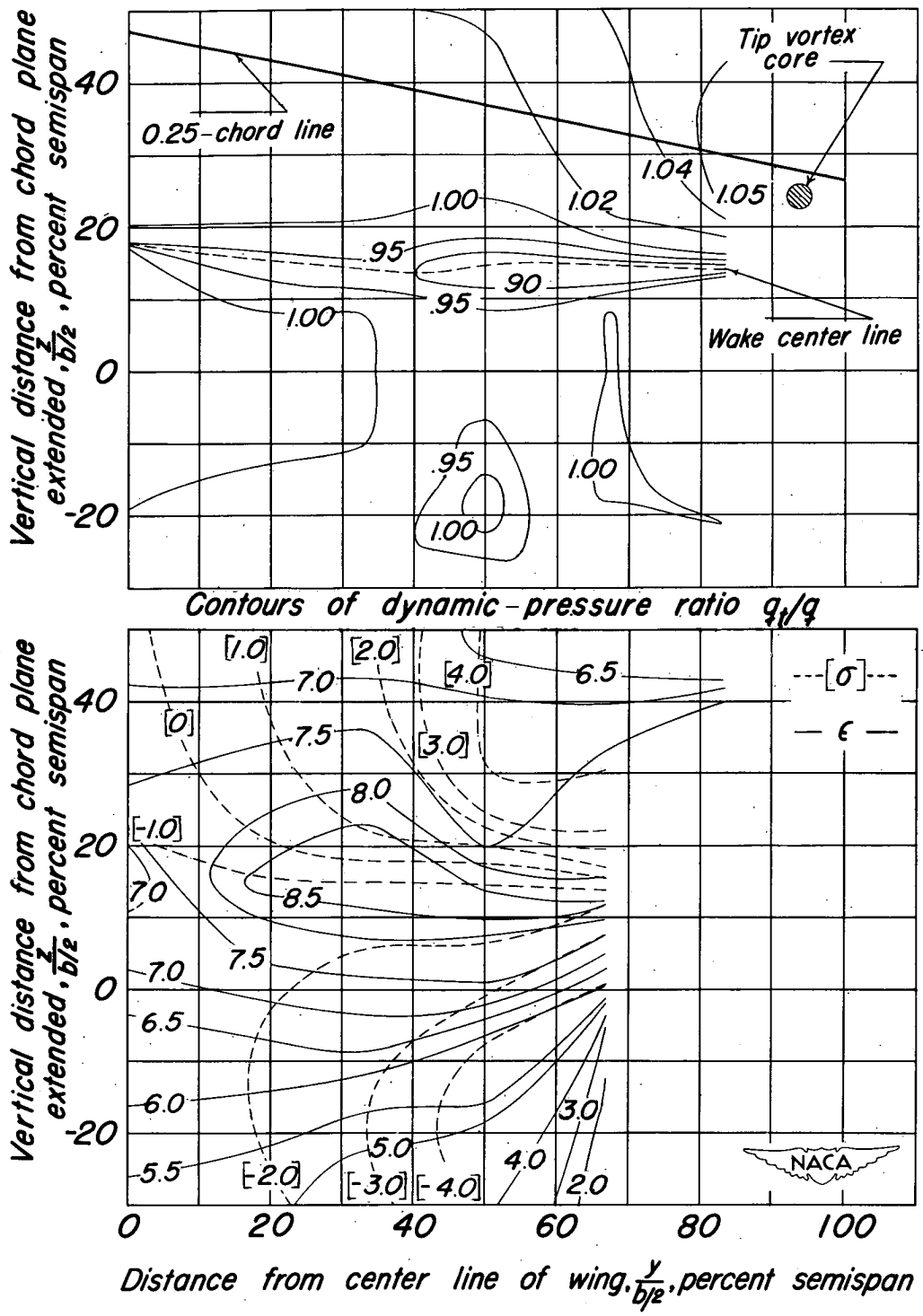

Contours of downwash angle ϵ and sidewash angle σ in degrees

(c) $\alpha = 16.0°$; $C_L = 0.97$

Figure 7 – Concluded.

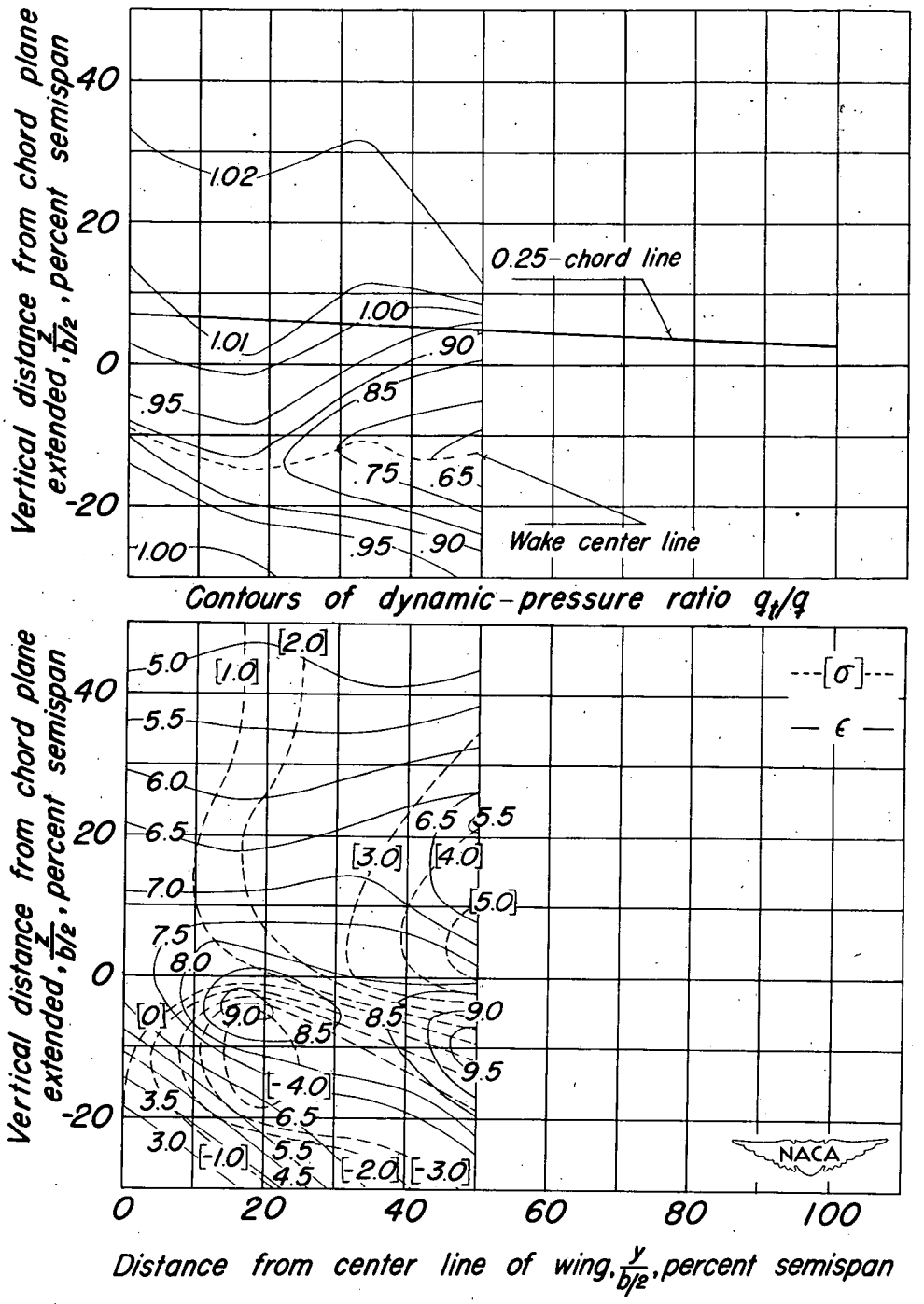

Contours of downwash angle ϵ and sidewash angle σ in degrees

(a) $\alpha = 3.6°$; $C_L = 0.61$

Figure 8. – Downwash angle, sidewash angle, and dynamic-pressure ratios behind a 42° sweptback wing. Longitudinal plane of survey at 2.0 M.A.C.; flaps deflected; ground distance ∞.

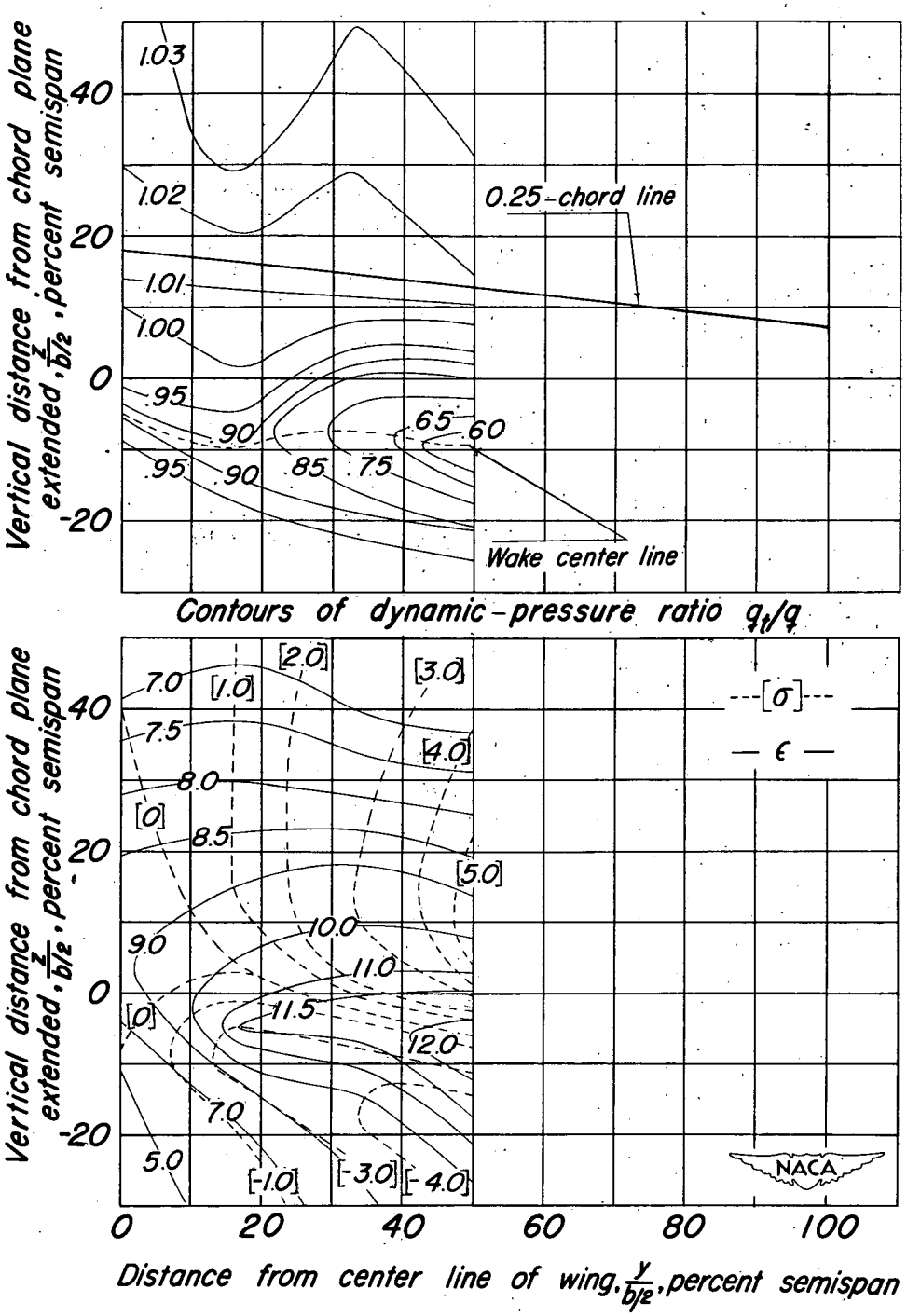

Contours of downwash angle ϵ and sidewash angle σ in degrees

(b) $\alpha = 8.5°$; $C_L = 0.91$.

Figure 8. – Continued.

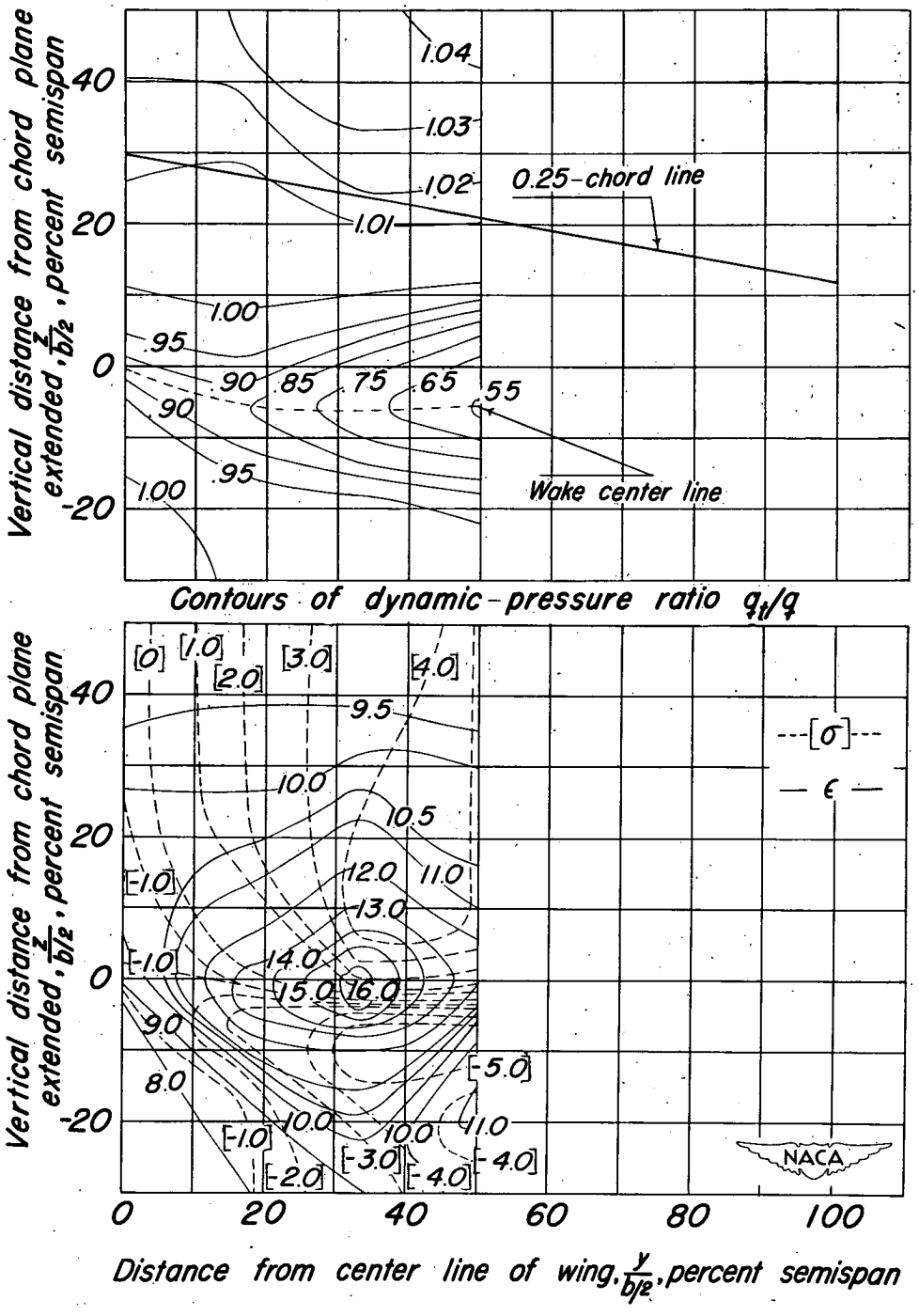

Contours of downwash angle ϵ and sidewash angle σ in degrees

(c) $\alpha = 13.5°$; $C_L = 1.20$

Figure 8. – Continued.

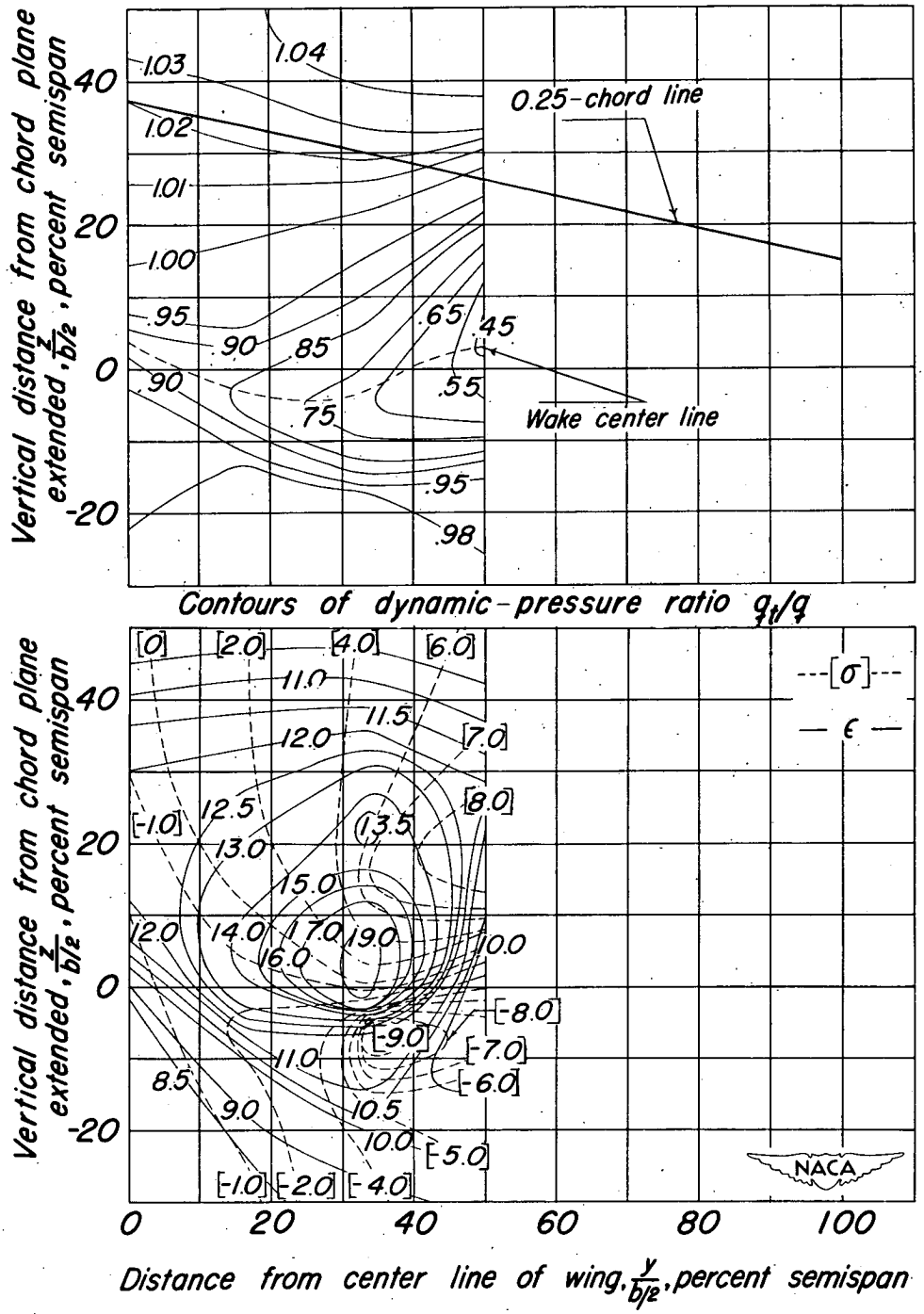

Contours of downwash angle ϵ and sidewash angle σ in degrees

(d) $\alpha = 16.8^\circ$; $C_L = 1.35$

Figure 8. – Concluded.

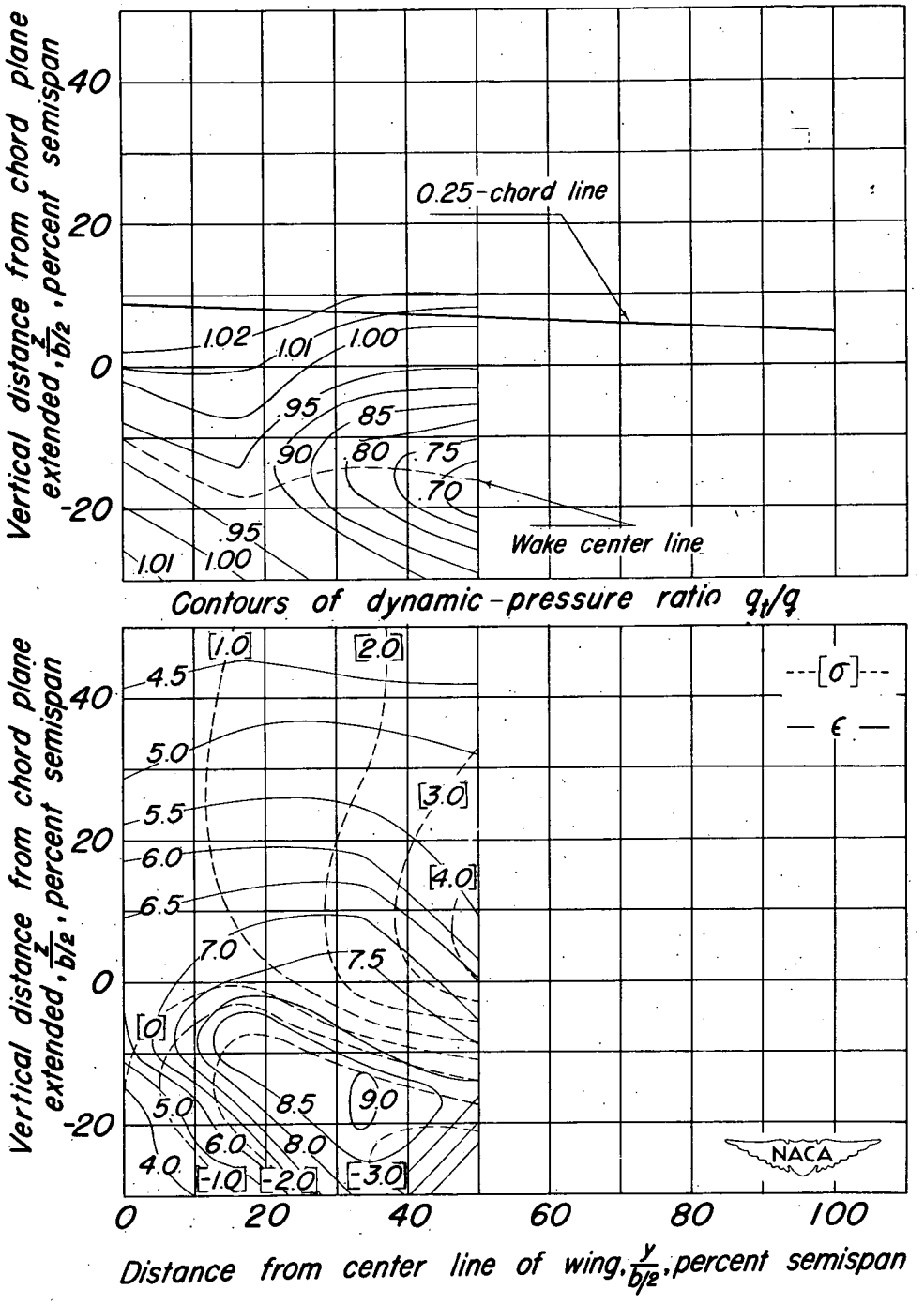

Contours of downwash angle ϵ and sidewash angle σ in degrees

(a) $\alpha = 3.6°$; $C_L = 0.61$

Figure 9. – Downwash angle, sidewash angle, and dynamic-pressure ratios behind a 42° sweptback wing. Longitudinal plane of survey at 2.8 M.A.C.; flaps deflected; ground distance ∞

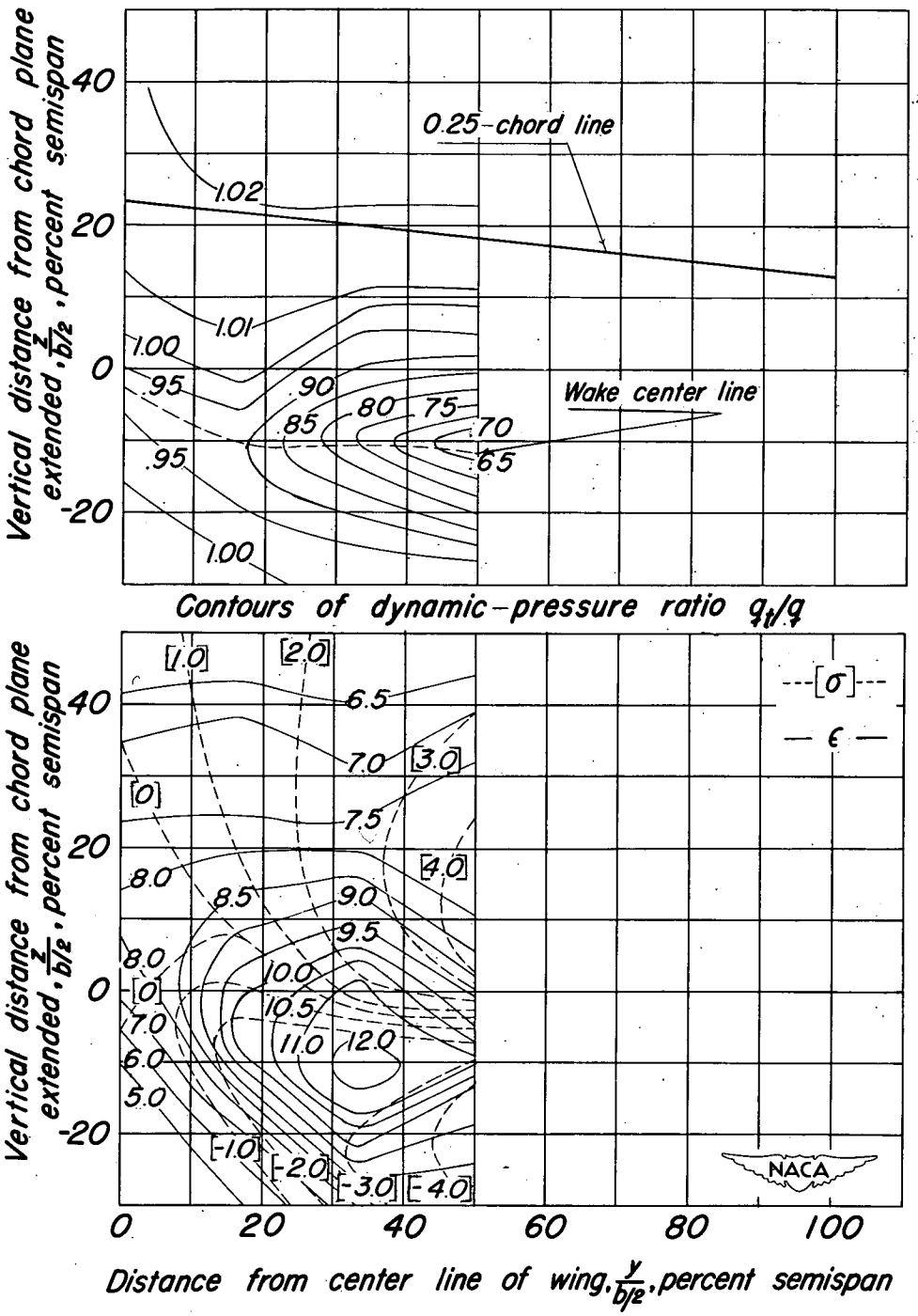

Contours of downwash angle ϵ and sidewash angle σ in degrees

(b) $\alpha = 8.5°$; $C_L = 0.91$.

Figure 9.- Continued.

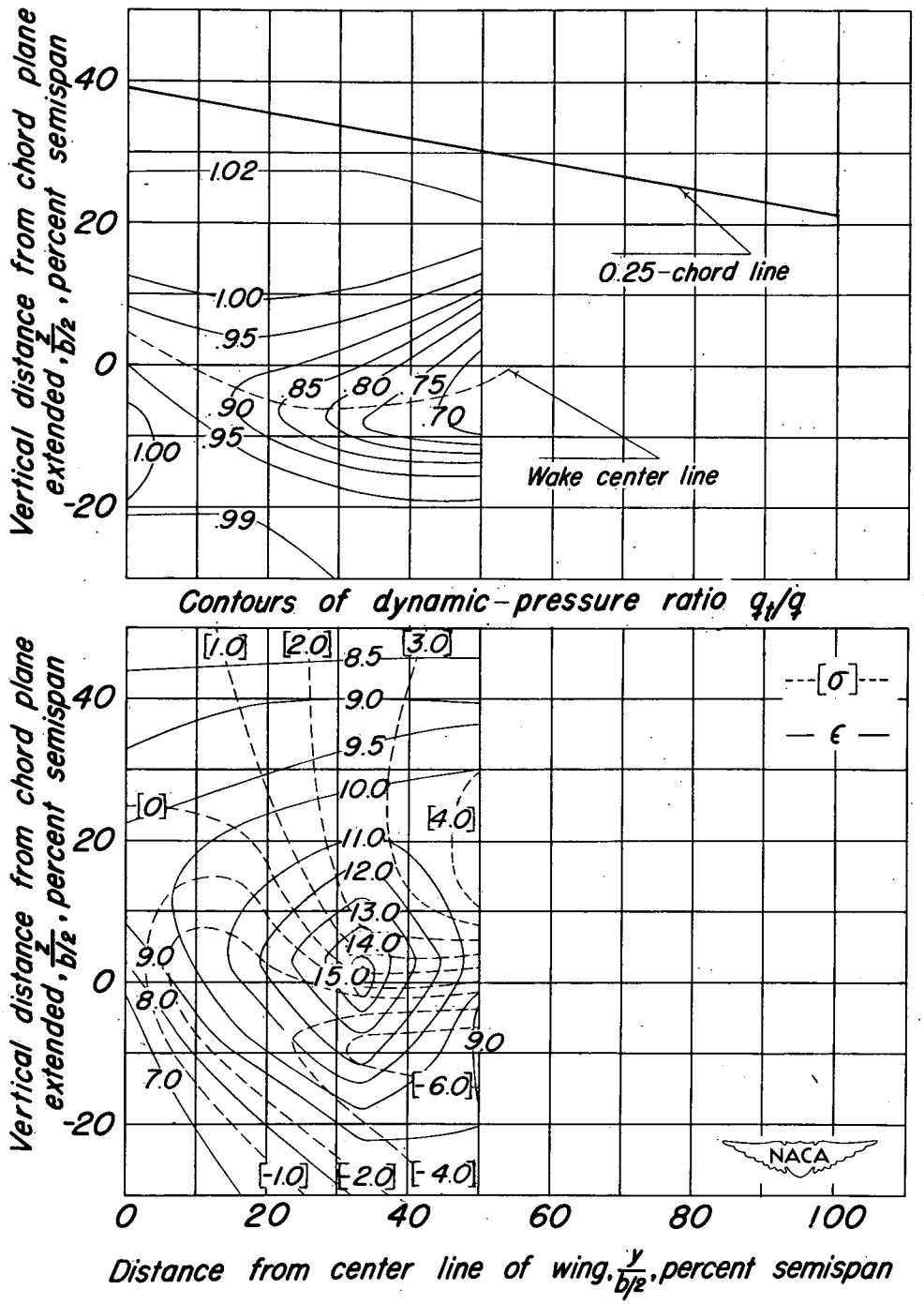

Contours of downwash angle ϵ and sidewash angle σ in degrees

(c) $\alpha = 13.5°$; $C_L = 1.20$

Figure 9 — Continued.

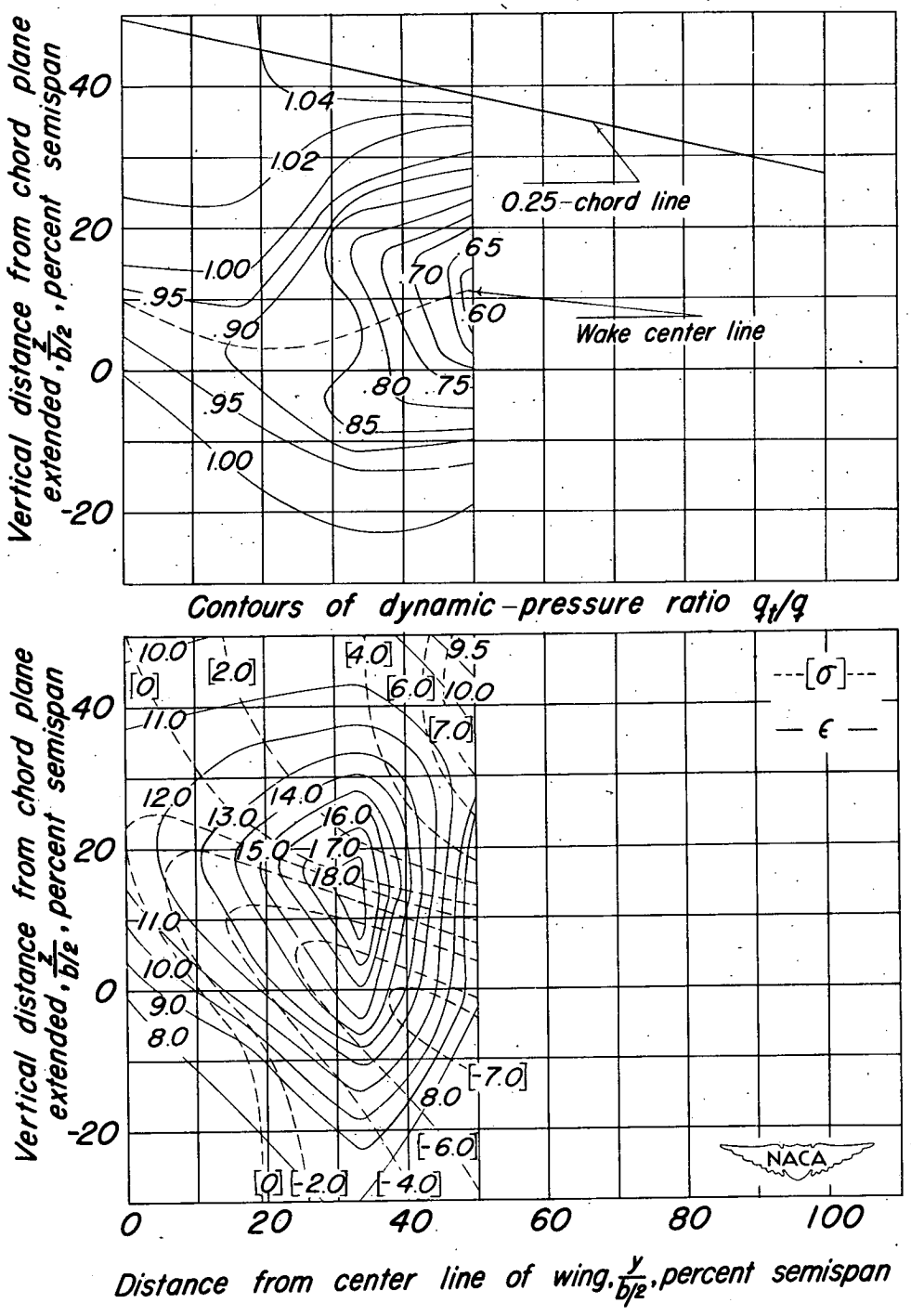

Contours of downwash angle ϵ and sidewash angle σ in degrees

(d) $\alpha = 16.8^\circ$; $C_L = 1.35$.

Figure 9. – Concluded.

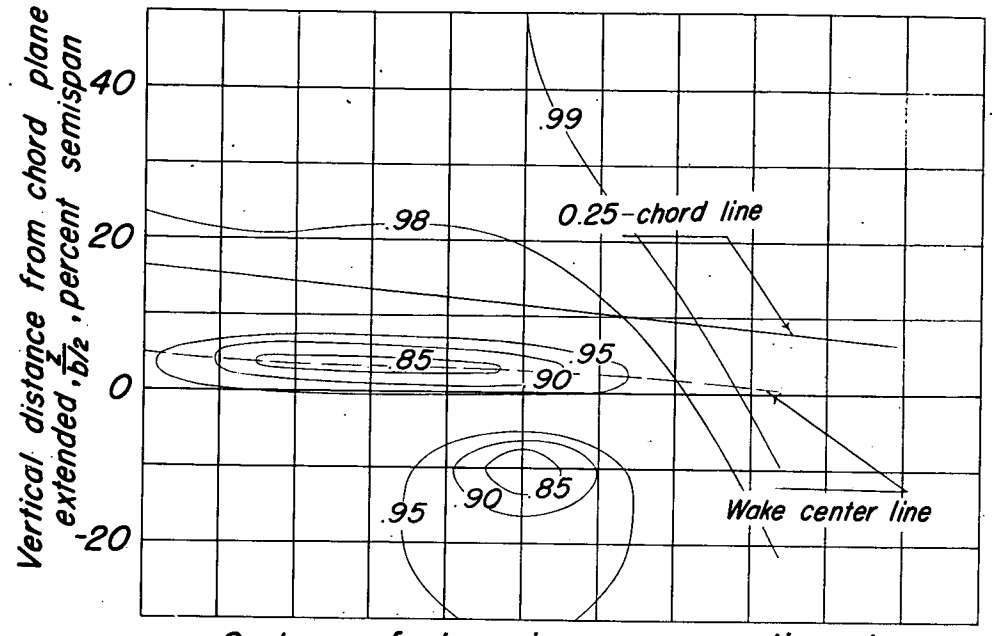

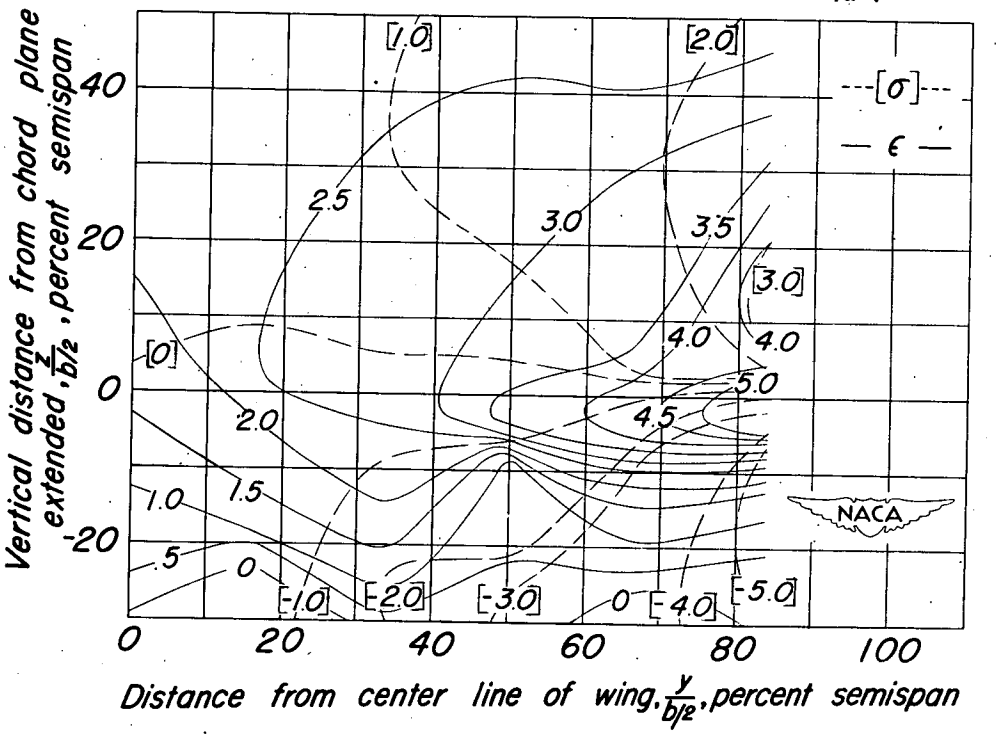

Contours of downwash angle ϵ and sidewash angle σ in degrees

(a) $\alpha = 6.7°$; $C_L = 0.48$.

Figure 10.— Downwash angle, sidewash angle, and dynamic-pressure ratios behind a 42° sweptback wing. Longitudinal plane of survey at 2.0 M.A.C.; flaps neutral; ground distance 0.92 M.A.C.

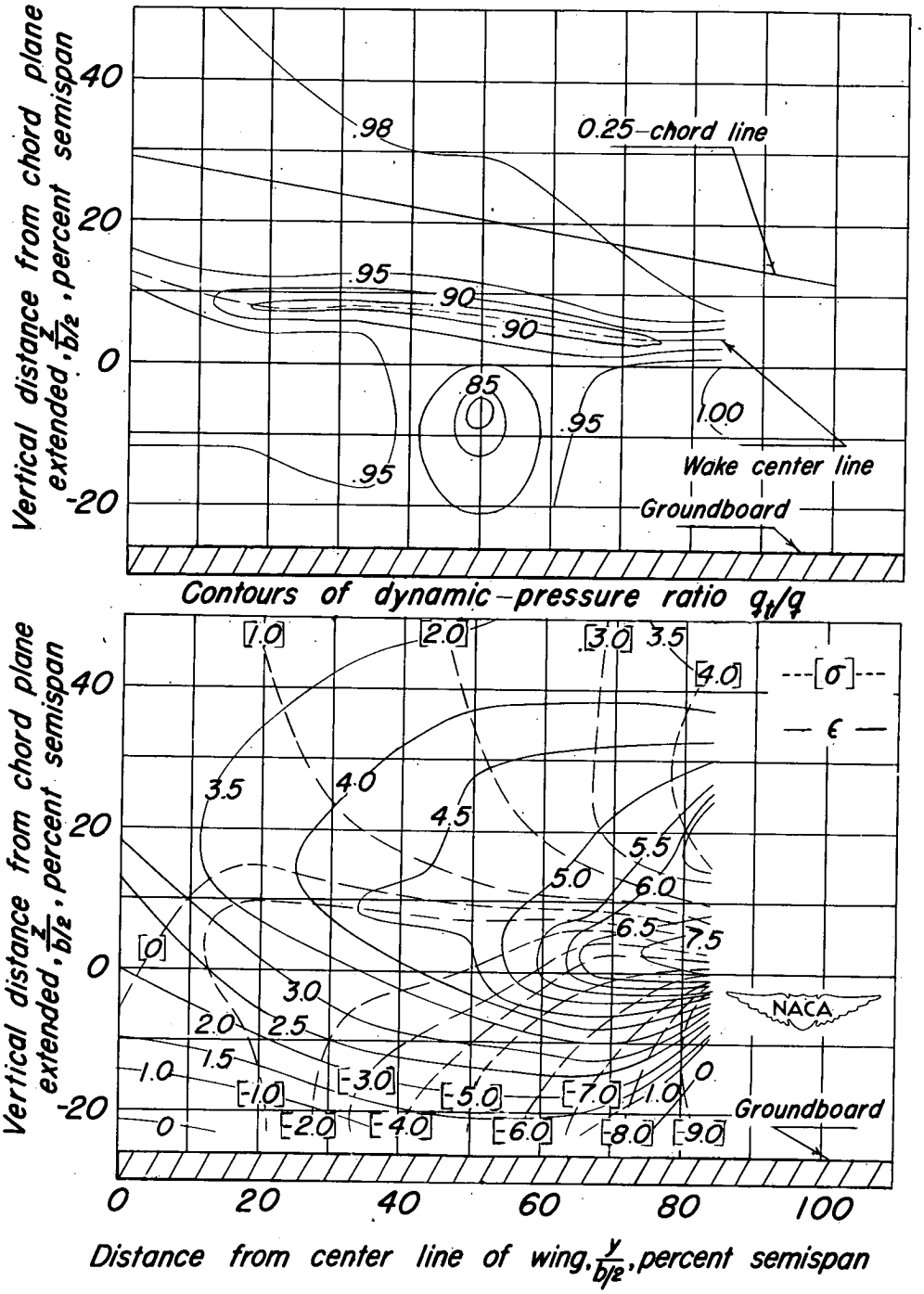

Contours of downwash angle ϵ and sidewash angle σ in degrees

(b) $\alpha = 11.9°$; $C_L = 0.80$.

Figure 10.– Continued.

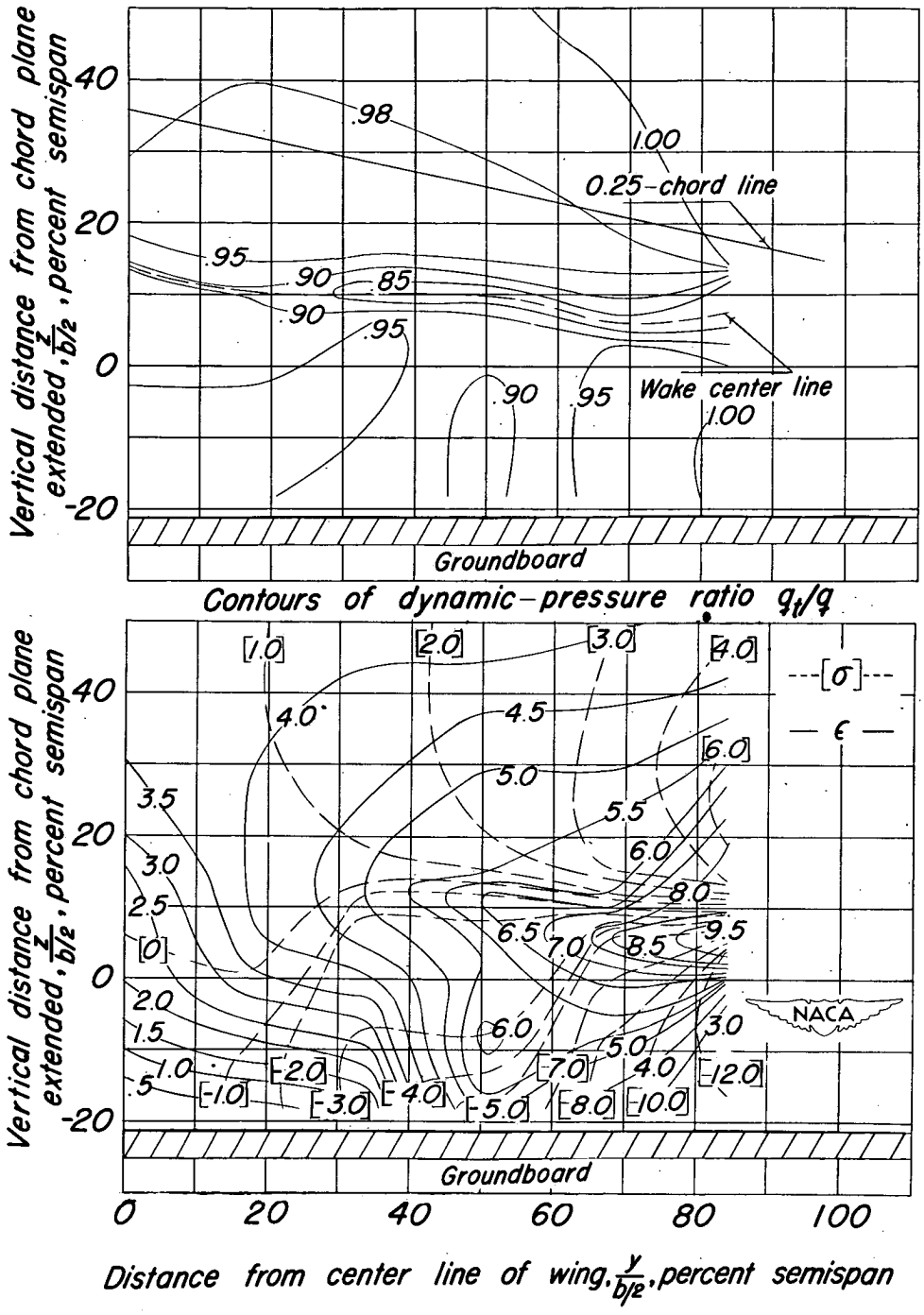

Contours of downwash angle ϵ and sidewash angle σ in degrees

(c) $\alpha = 14.6°$; $C_L = 0.95$.

Figure 10. – Concluded.

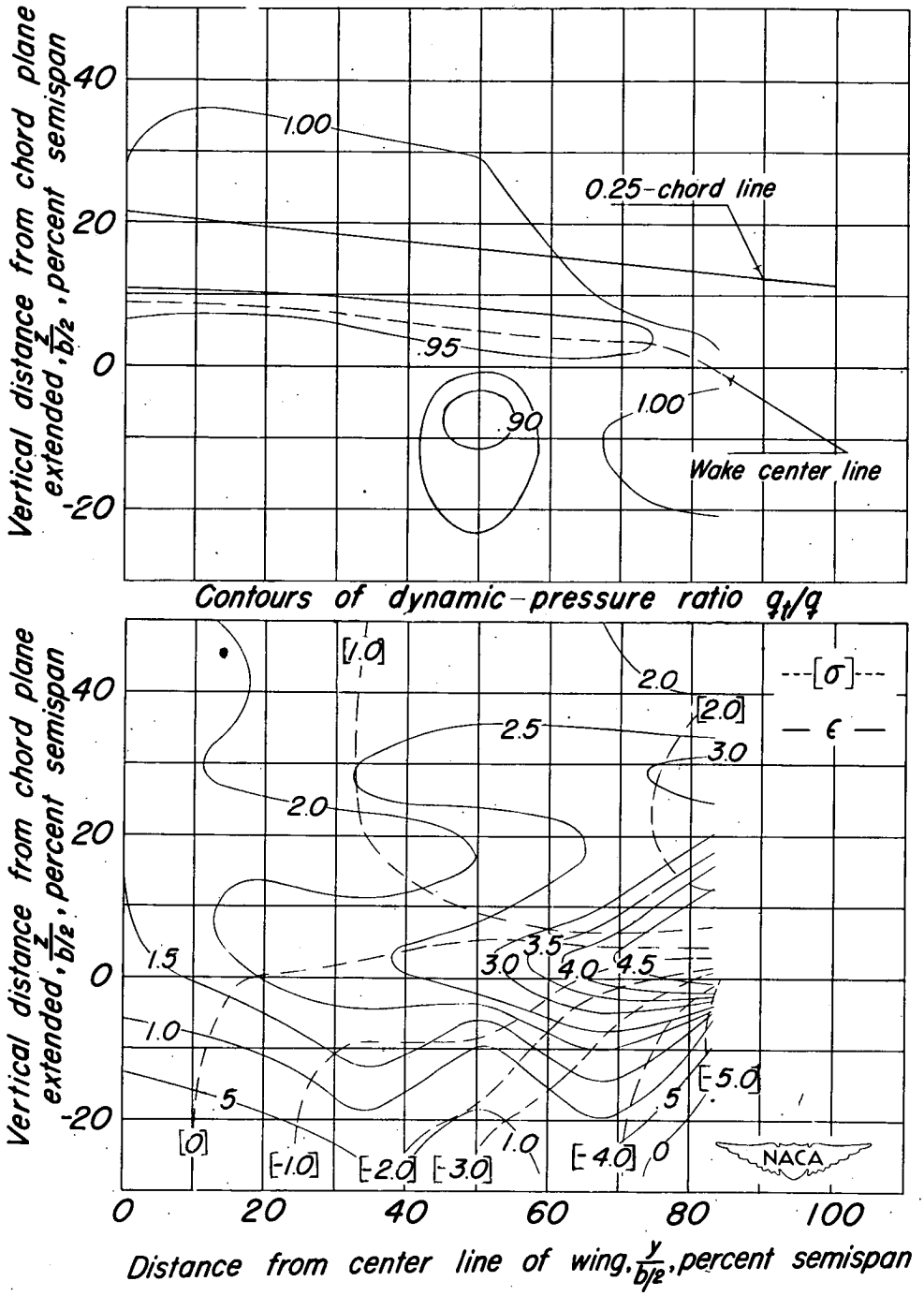

Contours of downwash angle ε and sidewash angle σ in degrees

(a) $\alpha = 6.7°$; $C_L = 0.48$.

Figure 11. — Downwash angle, sidewash angle, and dynamic pressure ratios behind a 42° sweptback wing. Longitudinal plane of survey at 2.8 M.A.C.; flaps neutral; ground distance 0.92 M.A.C.

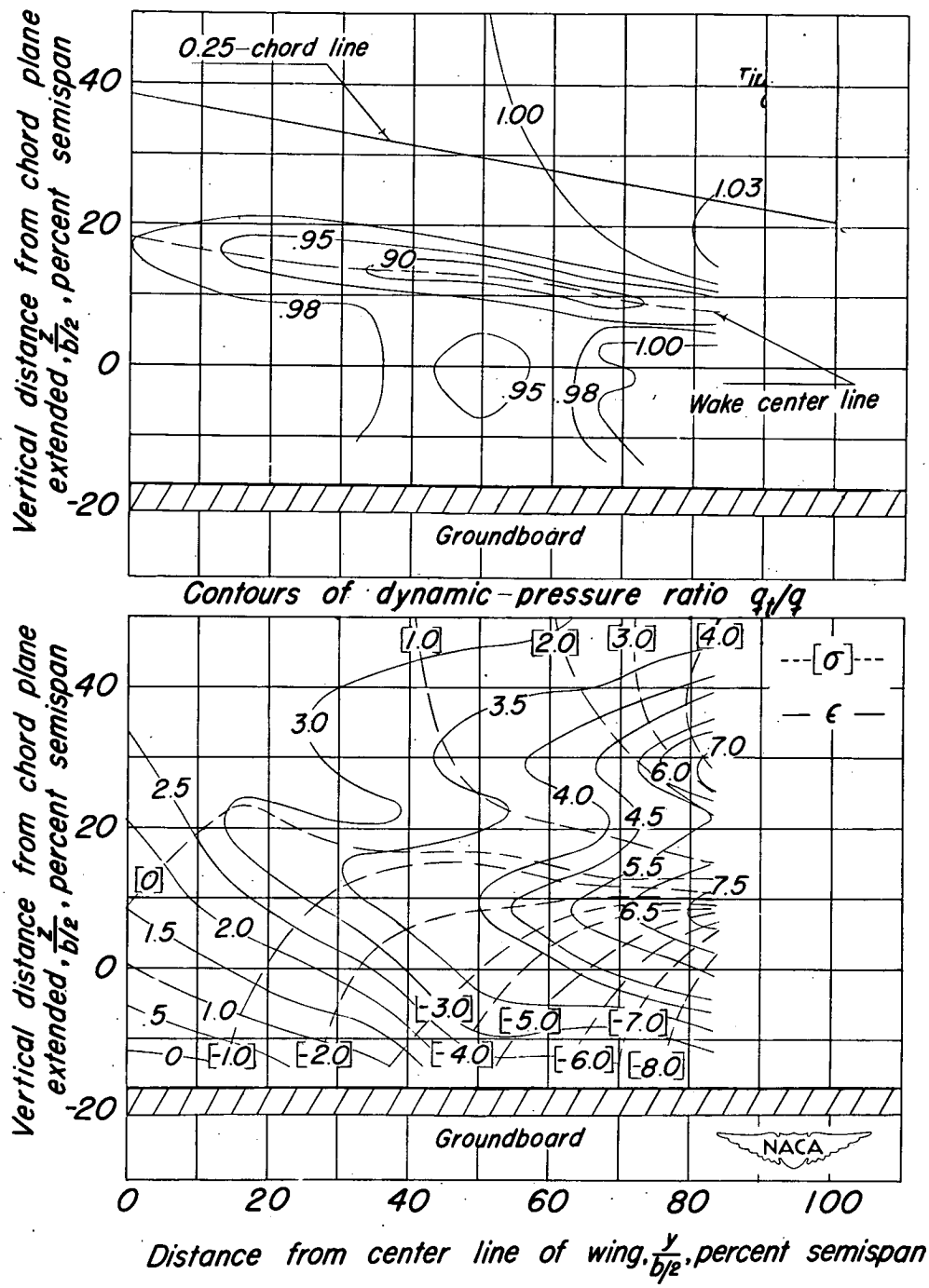

Contours of downwash angle ϵ and sidewash angle σ in degrees

(b) $\alpha = 11.9°$; $C_L = 0.80$.

Figure 11. — Continued.

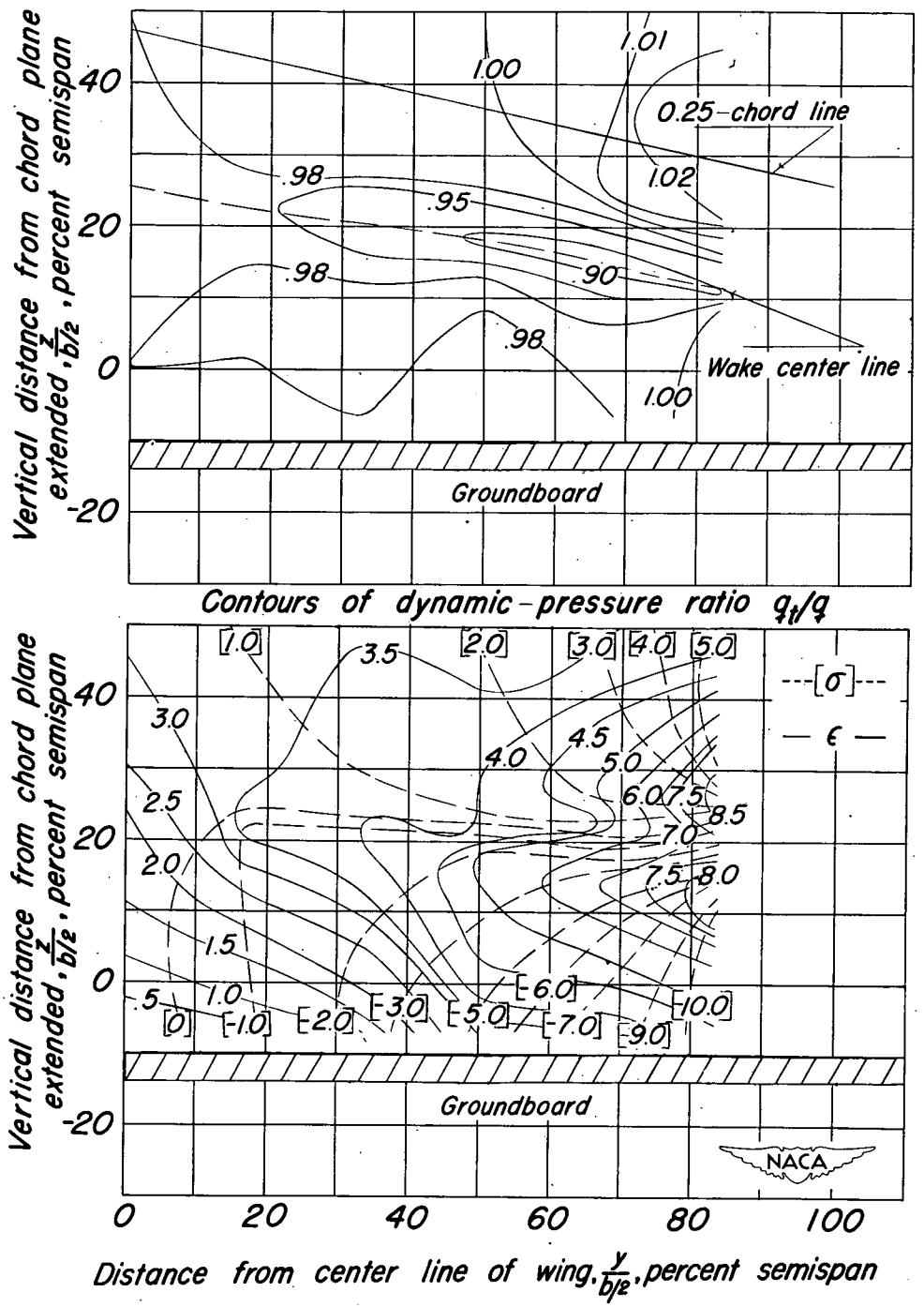

Contours of downwash angle ϵ and sidewash angle σ in degrees

(c) $\alpha = 14.6°$; $C_L = 0.95$.

Figure 11 – Concluded.

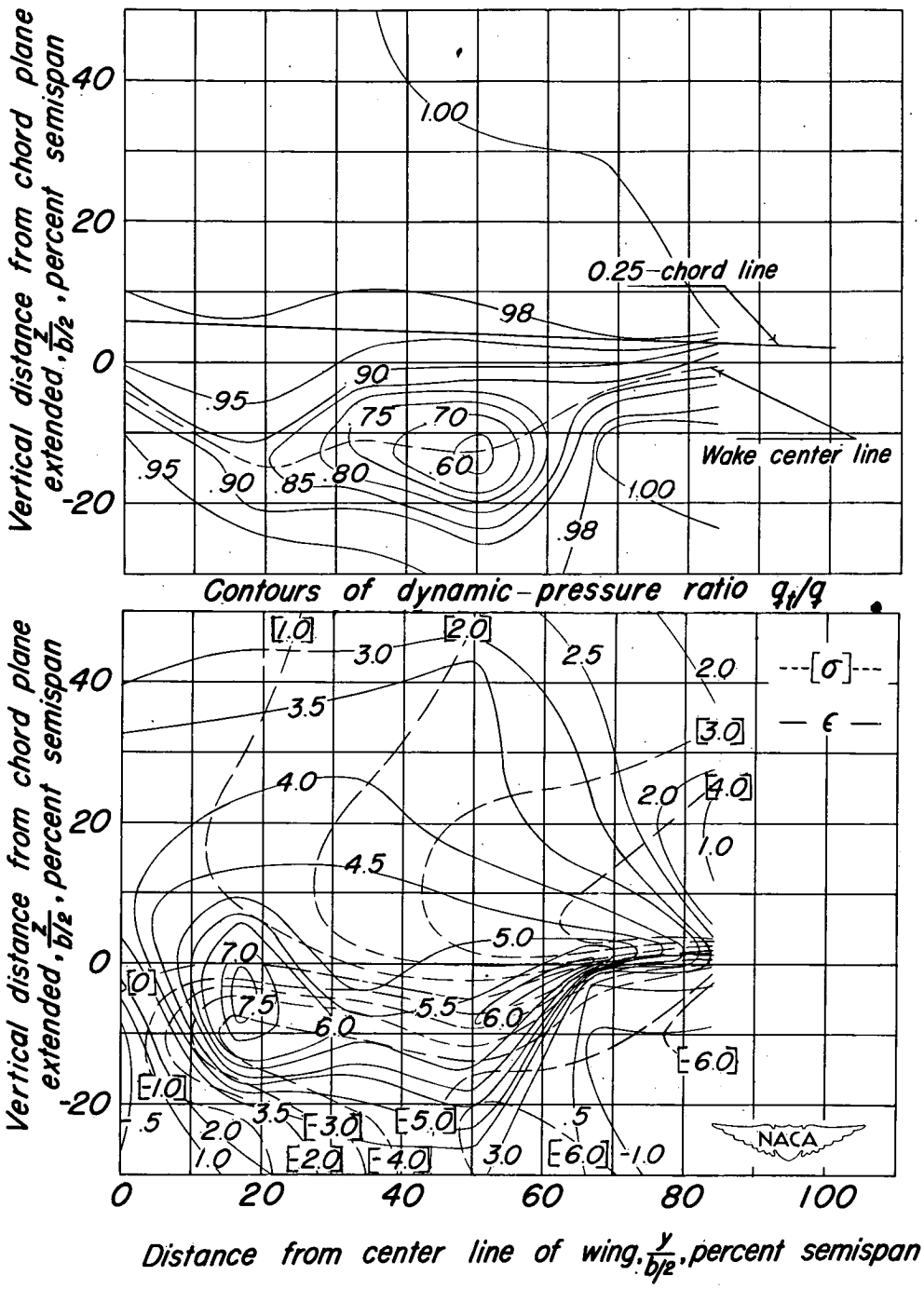

Contours of downwash angle ϵ and sidewash angle σ in degrees

(a) $\alpha = 2.4°$; $C_L = 0.59$.

Figure 12.— Downwash angle, sidewash angle, and dynamic-pressure ratios behind a 42° sweptback wing. Longitudinal plane of survey at 2.0 M.A.C.; flaps deflected; ground distance 0.92 M.A.C.

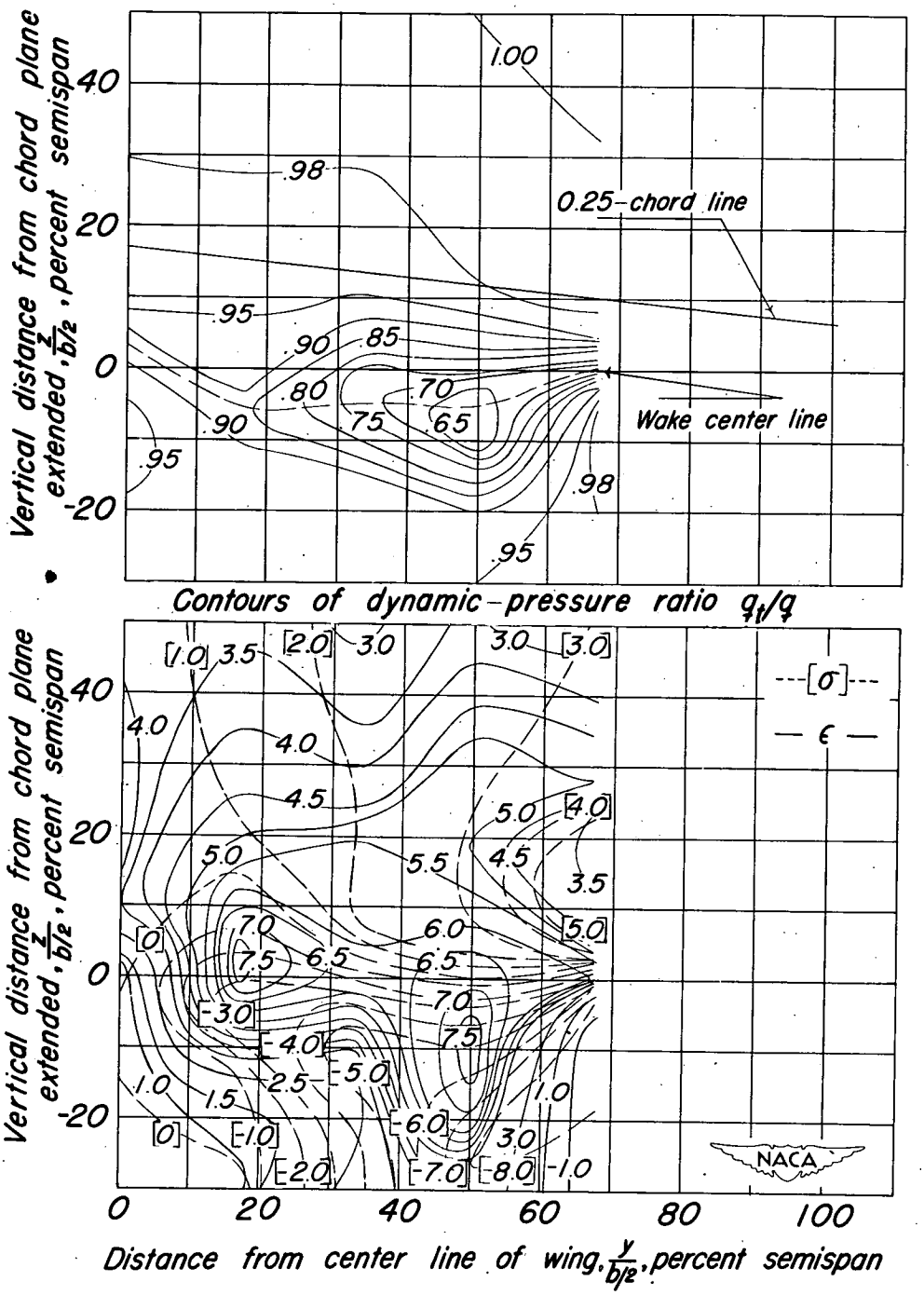

Contours of downwash angle ϵ and sidewash angle σ in degrees

(b) $\alpha = 7.1°$; $C_L = 0.89$.

Figure 12. – Continued.

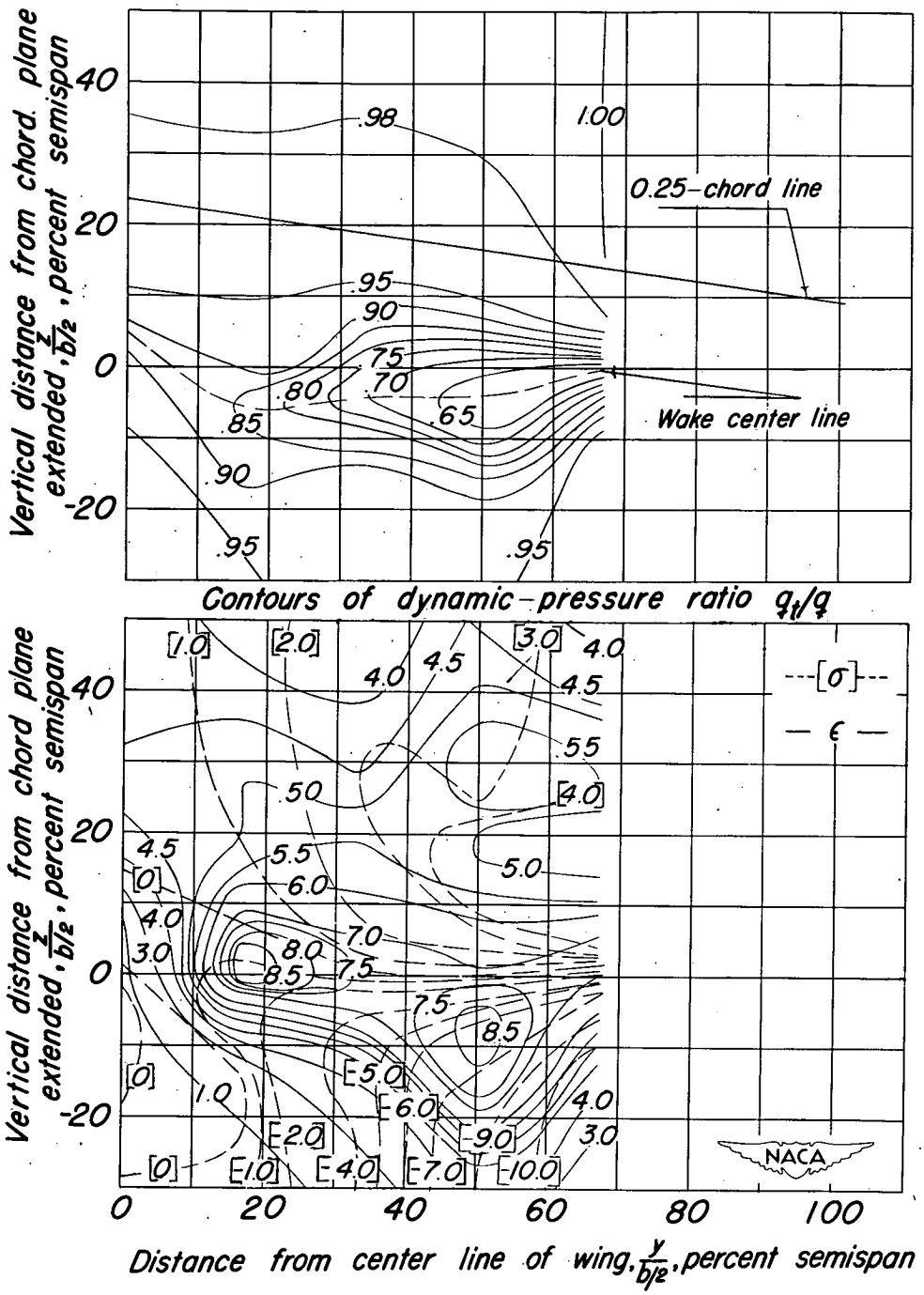

Contours of downwash angle ε and sidewash angle σ in degrees

(c) $\alpha = 9.7°$; $C_L = 1.04$.

Figure 12 – Continued.

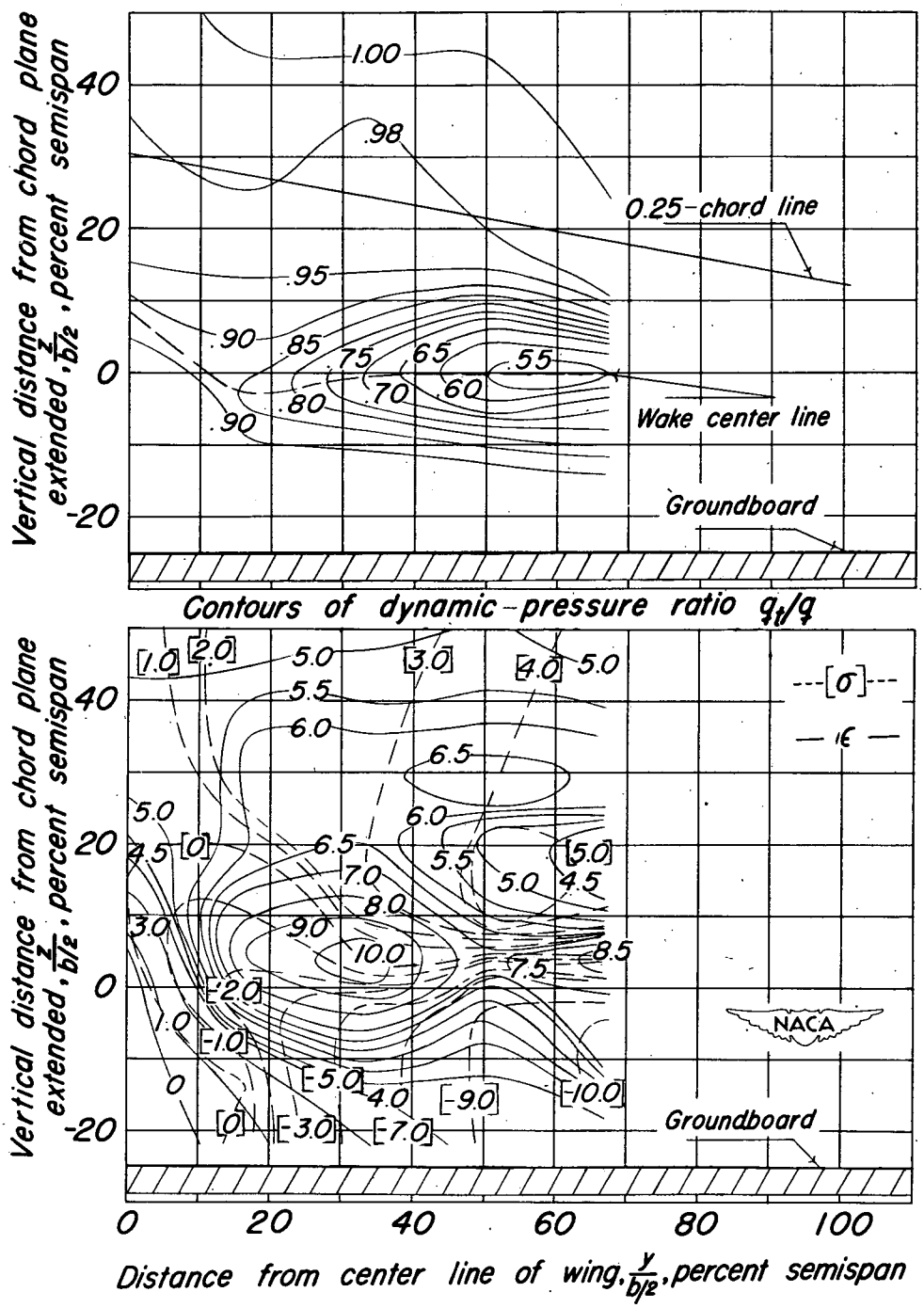

Contours of downwash angle ϵ and sidewash angle σ in degrees

(d) $\alpha = 12.5°$; $C_L = 1.18$.

Figure 12. – Concluded.

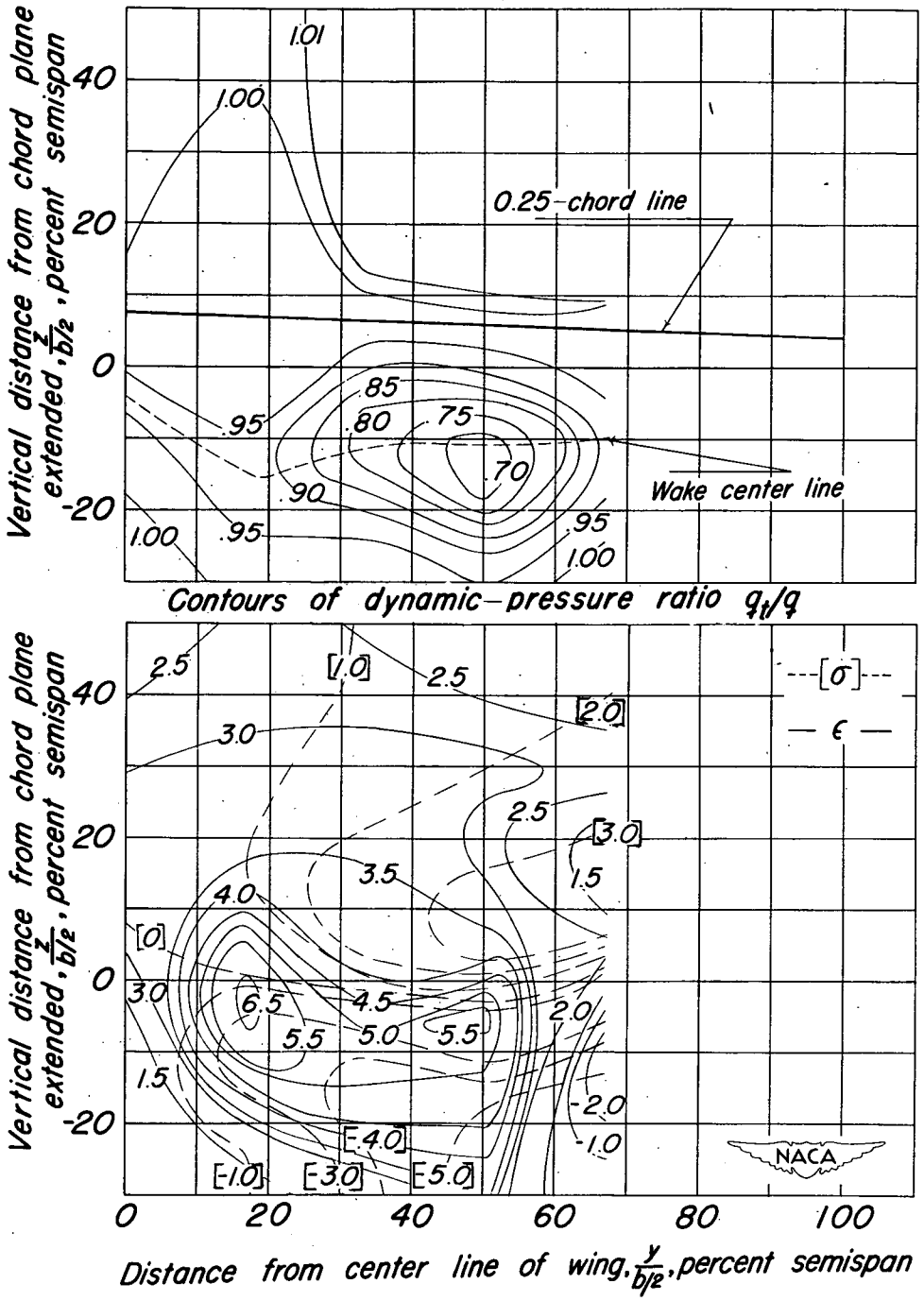

Contours of downwash angle ϵ and sidewash angle σ in degrees

(a) $\alpha = 2.4°$; $C_L = 0.59$.

Figure 13. – Downwash angle, sidewash angle, and dynamic-pressure ratios behind a 42° sweptback wing. Longitudinal plane of survey at 2.8 M.A.C.; flaps deflected; ground distance 0.92 M.A.C.

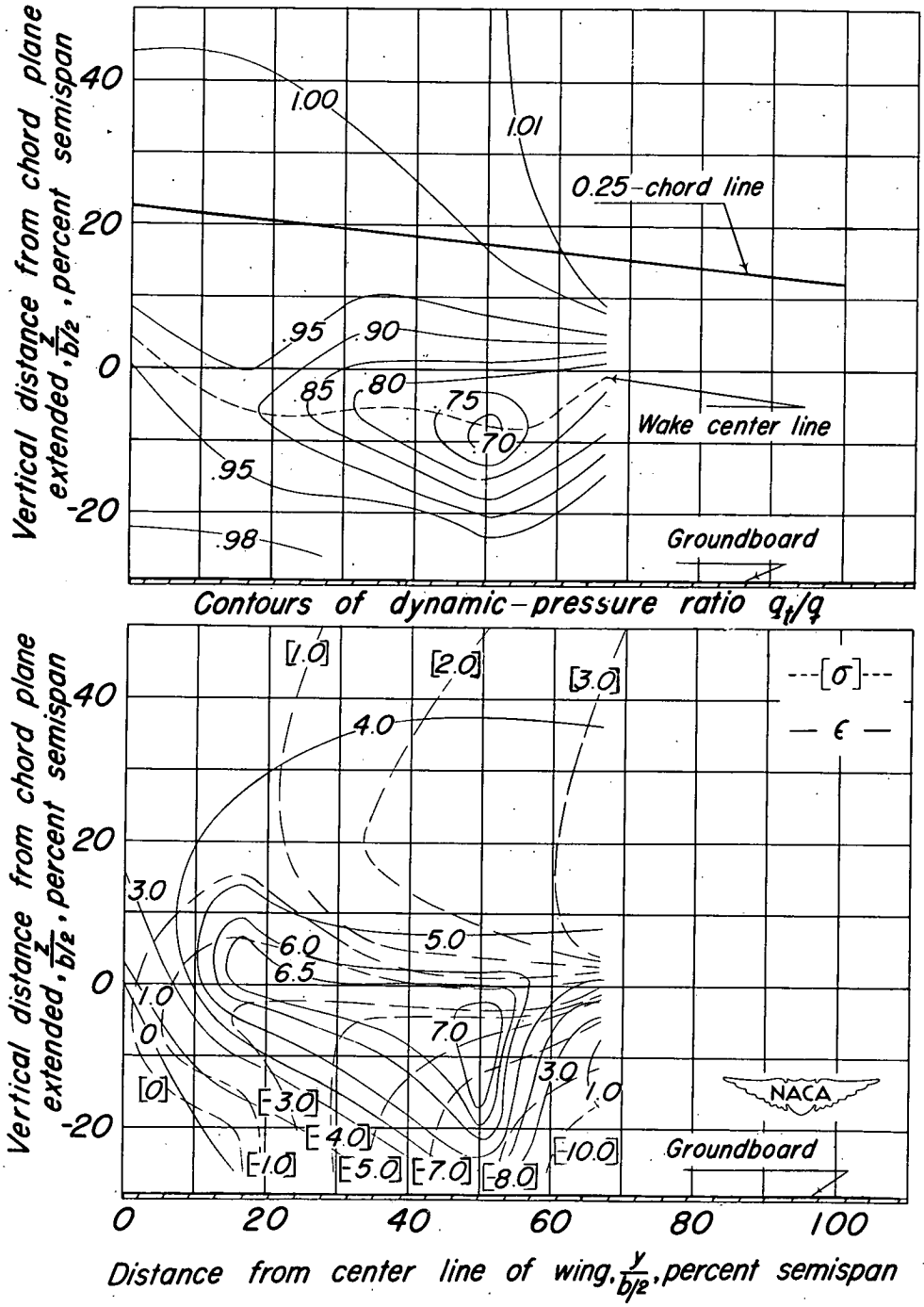

Contours of downwash angle ε and sidewash angle σ in degrees

(b) $\alpha = 7.1°$; $C_L = 0.89$.

Figure 13.– Continued.

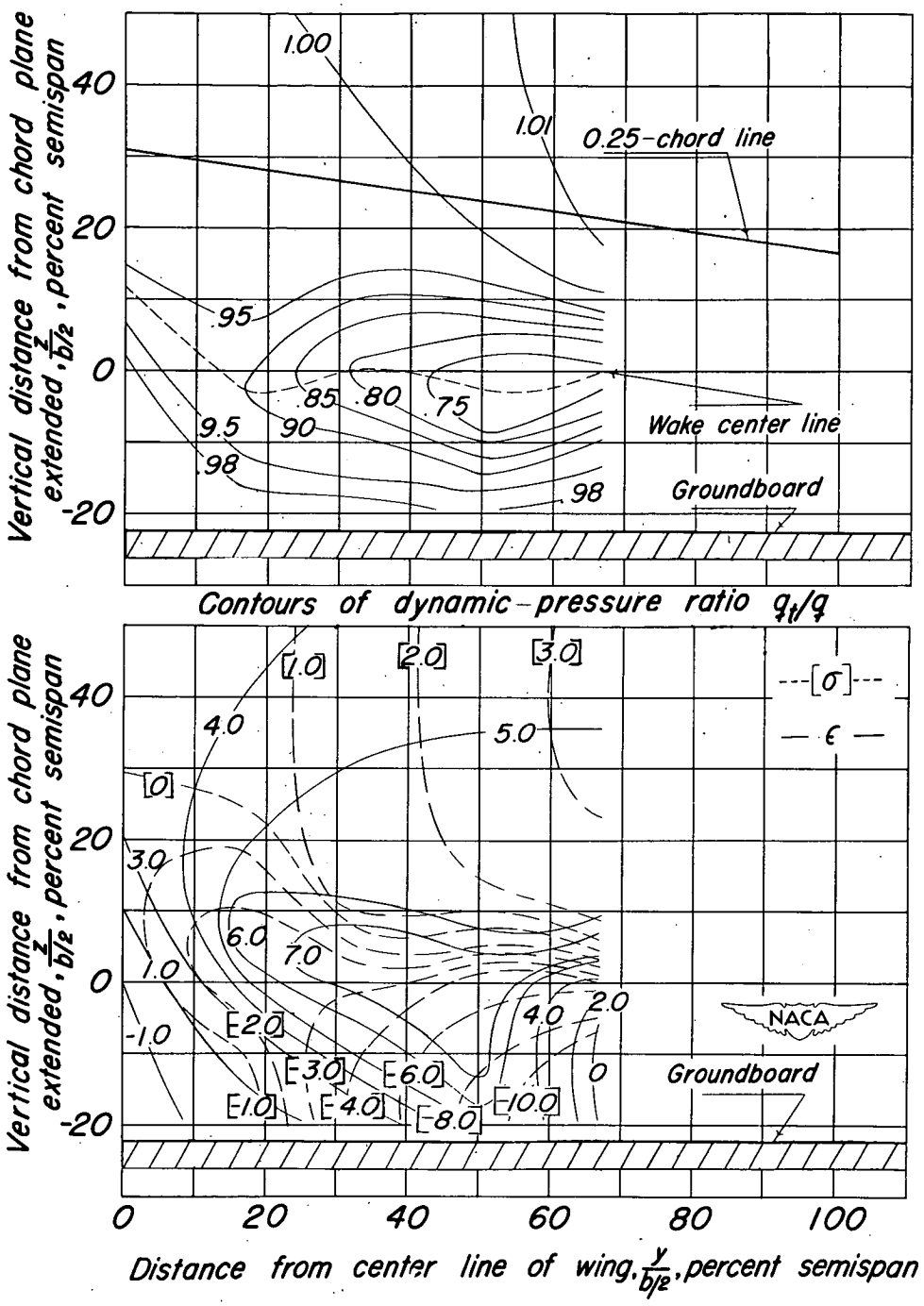

Contours of downwash angle ϵ and sidewash angle σ in degrees

(c) $\alpha = 9.7°$; $C_L = 1.04$.

Figure 13.– Continued.

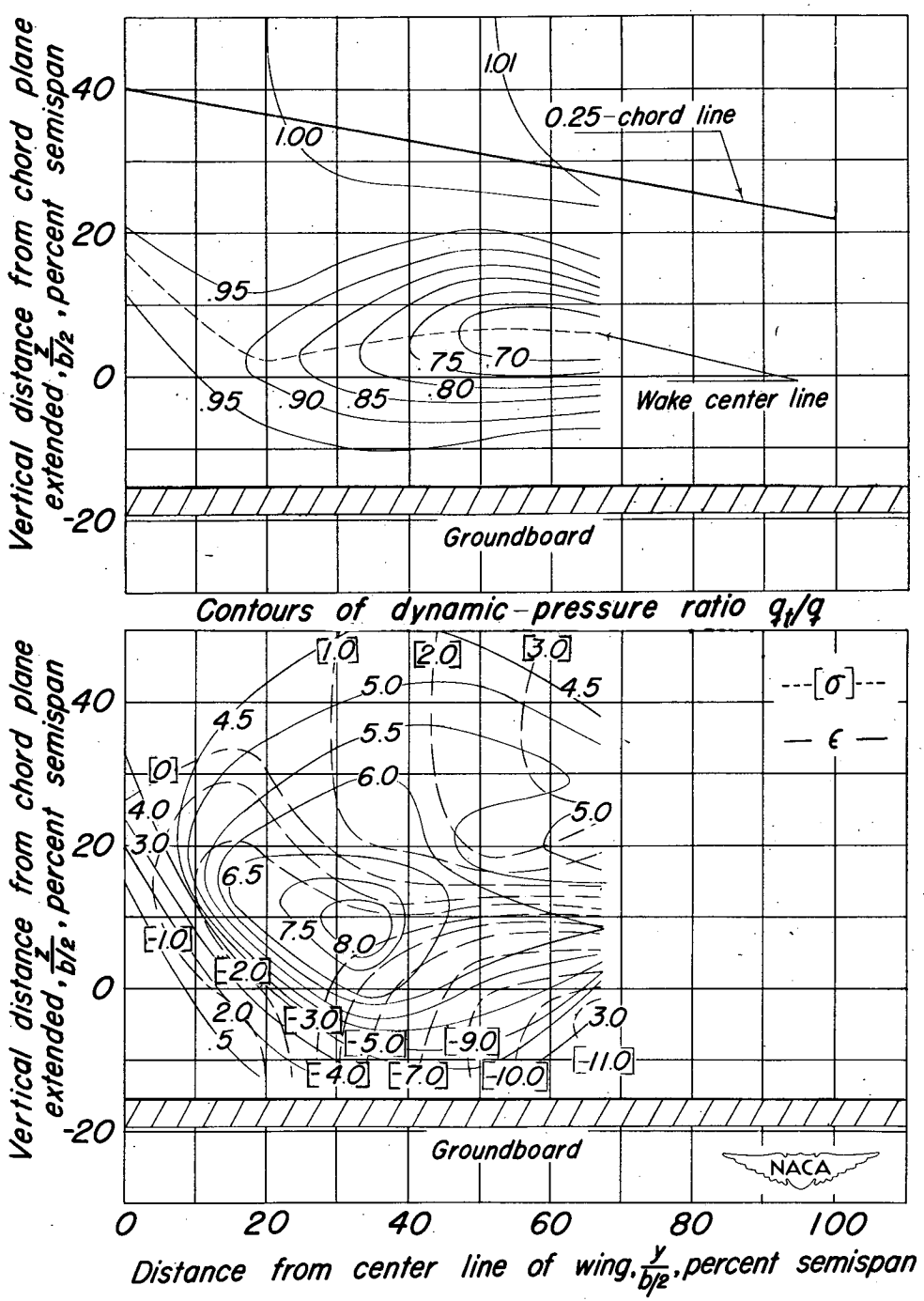

Contours of downwash angle ϵ and sidewash angle σ in degrees

(d) $\alpha = 12.5°$; $C_L = 1.18$.

Figure 13.- Concluded.

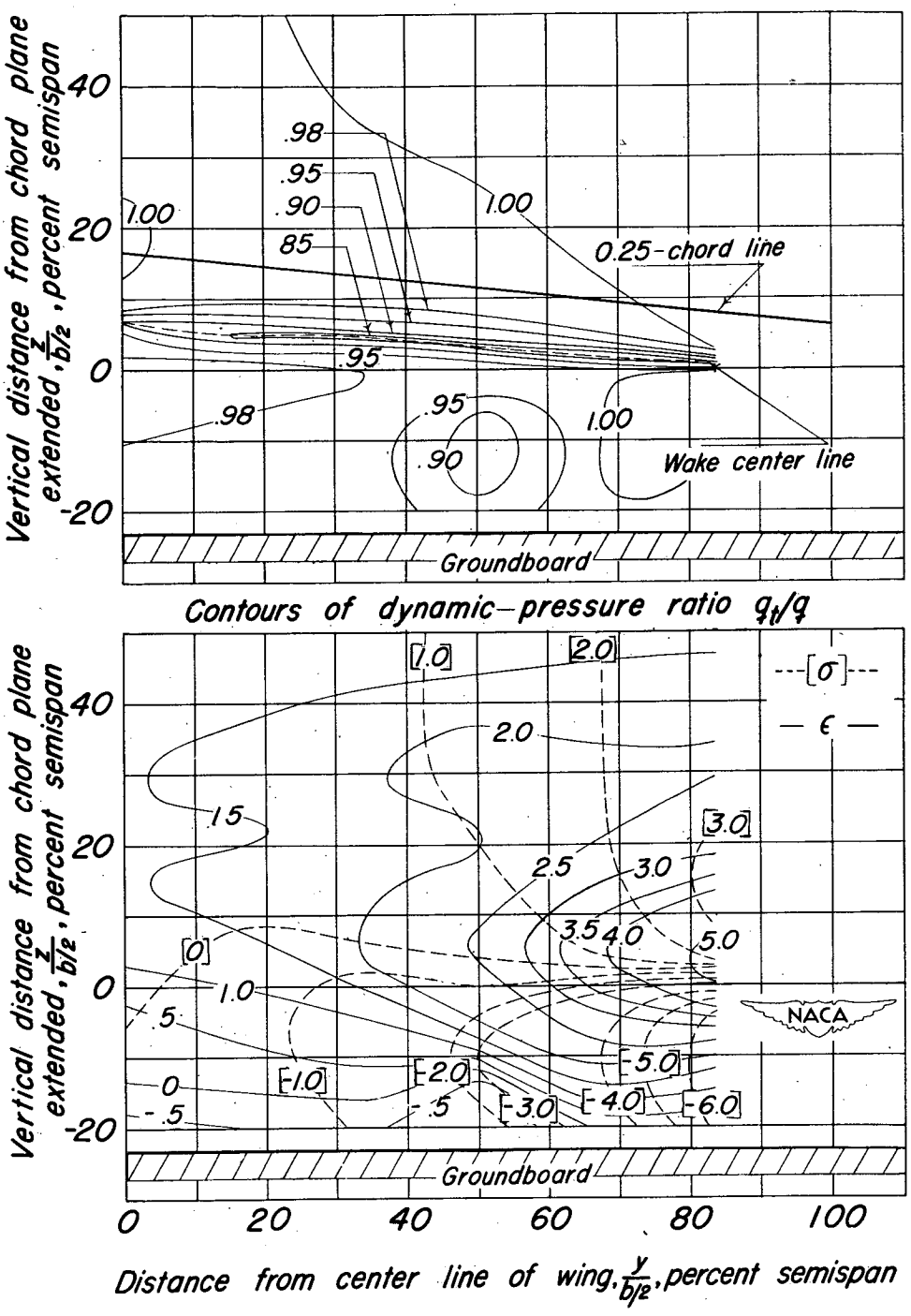

Contours of downwash angle ϵ and sidewash angle σ in degrees

(a) $\alpha = 6.7°$; $C_L = 0.51$

Figure 14.— Downwash angle, sidewash angle, and dynamic-pressure ratios behind a 42° sweptback wing. Longitudinal plane of survey at 2.0 M.A.C.; flaps neutral; ground distance 0.68 M.A.C.

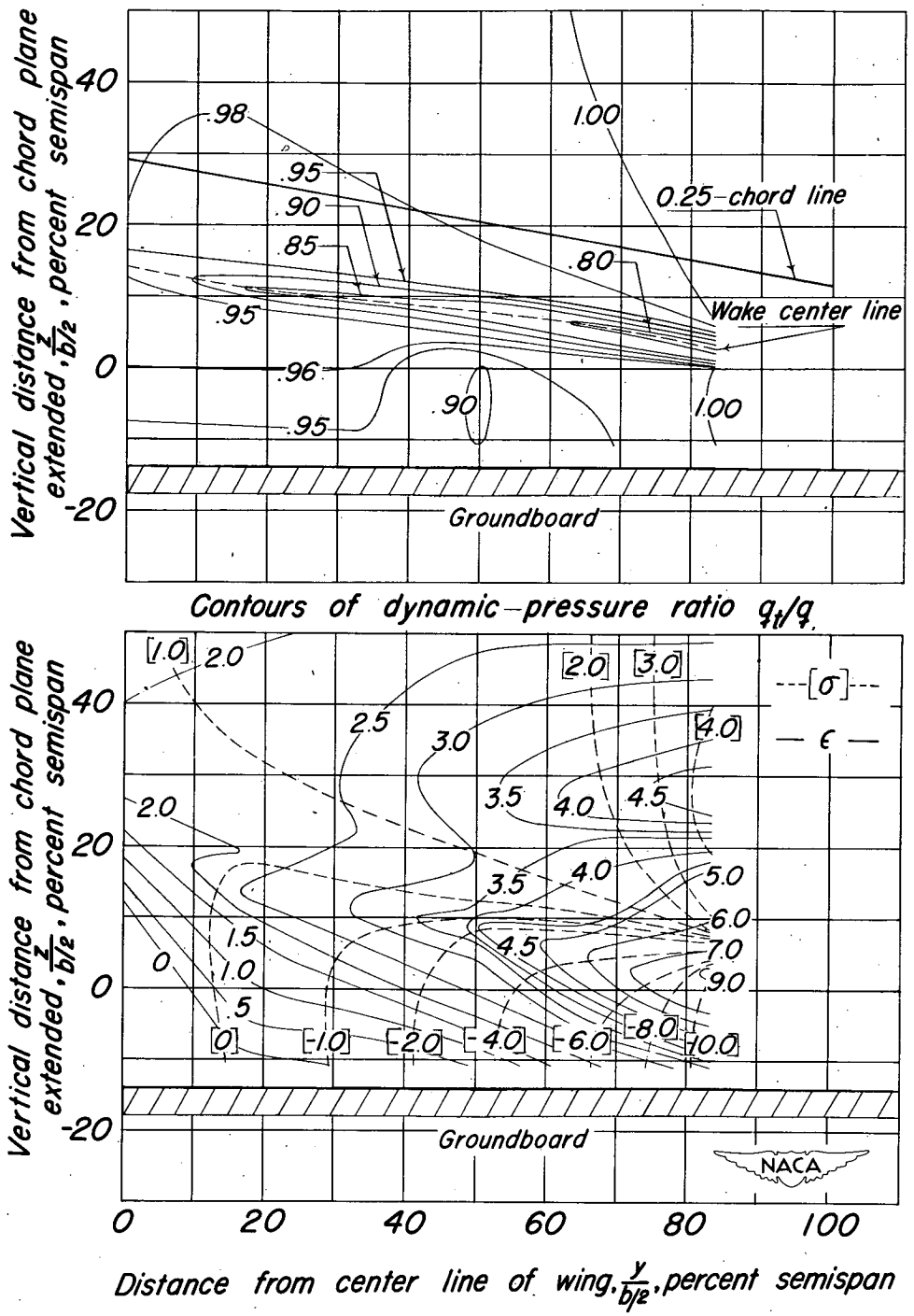

Contours of downwash angle ϵ and sidewash angle σ in degrees

(b) $\alpha = 11.9°$; $C_L = 0.83$

Figure 14.– Continued.

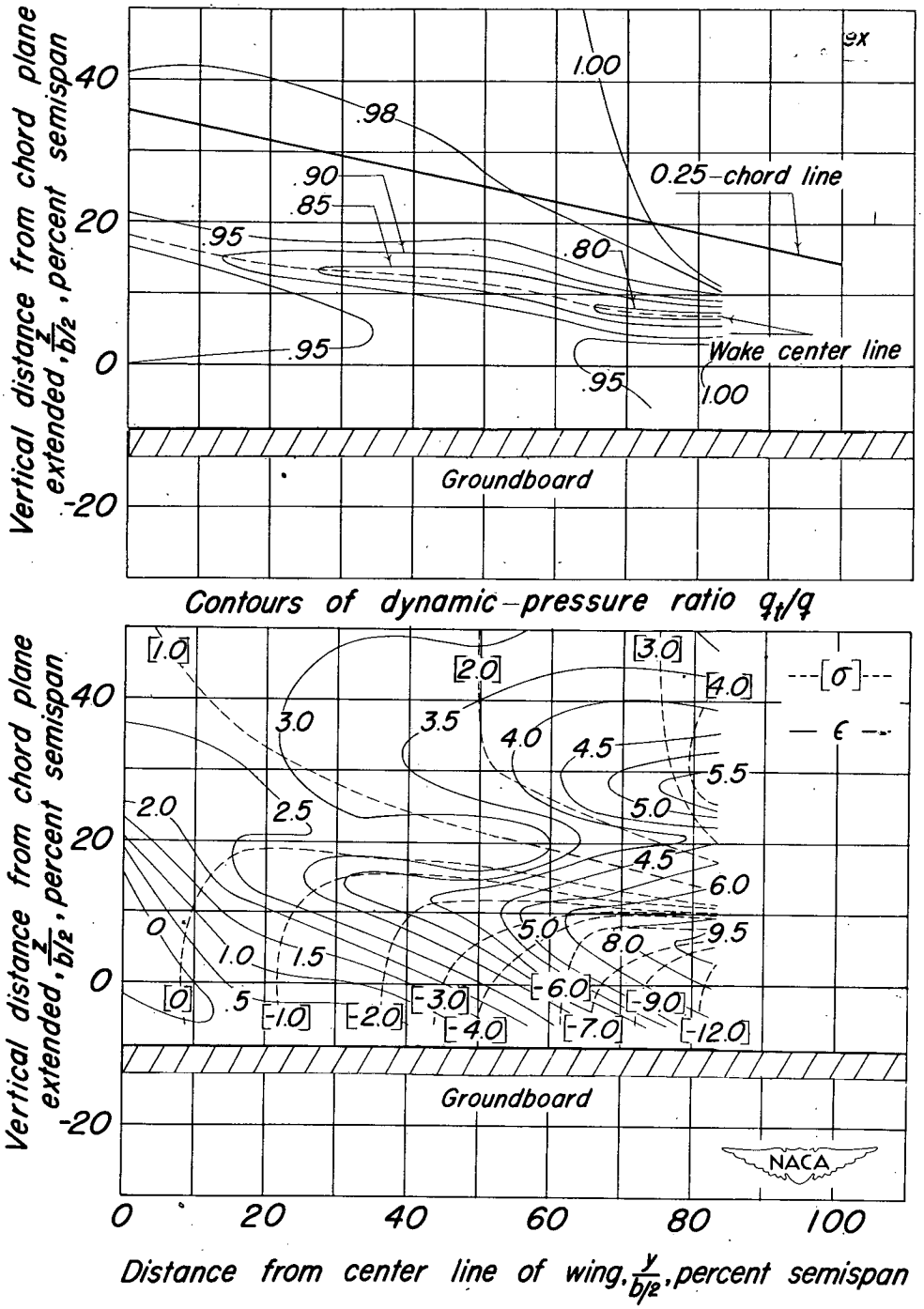

Contours of downwash angle ϵ and sidewash angle σ in degrees

(c) $\alpha = 14.6°$; $C_L = 0.98$

Figure 14.- Concluded.

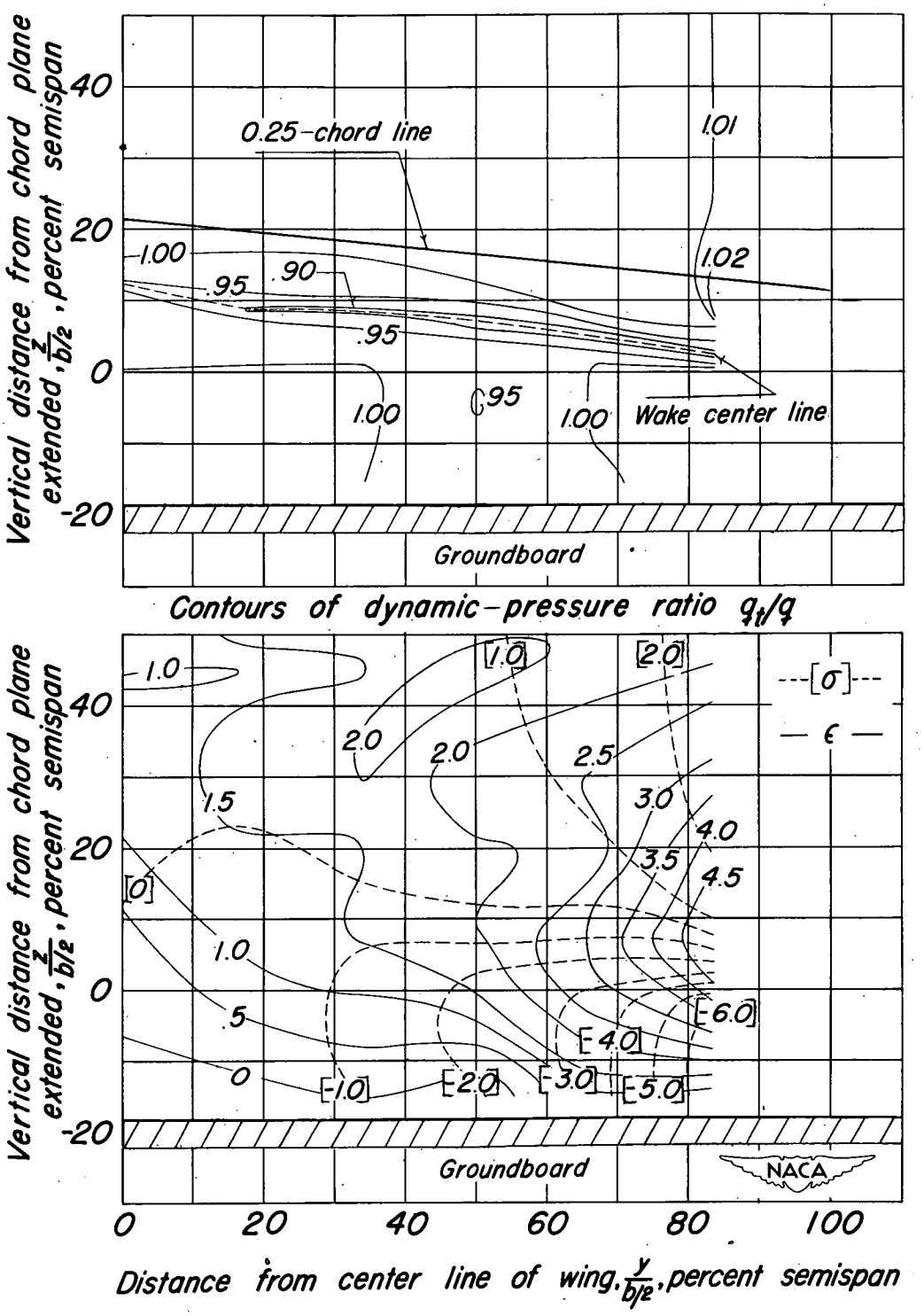

Contours of downwash angle ϵ and sidewash angle σ in degrees

(a) $\alpha = 6.7°$; $C_L = 0.51$.

Figure 15. – Downwash angle, sidewash angle, and dynamic-pressure ratios behind a 42° sweptback wing. Longitudinal plane of survey at 2.8 M.A.C.; flaps neutral; ground distance 0.68 M.A.C.

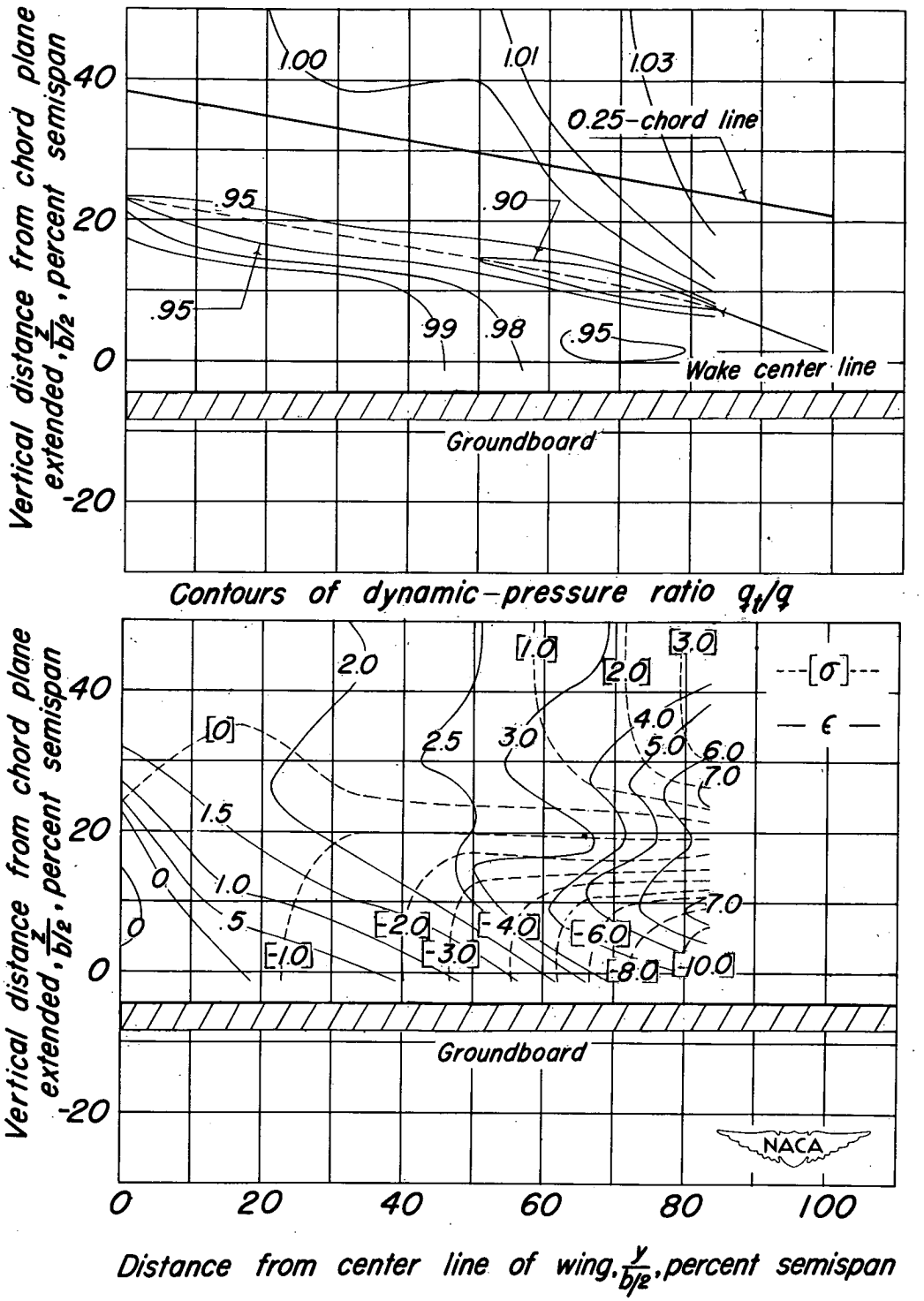

Contours of downwash angle ϵ and sidewash angle σ in degrees

(b) $\alpha = 11.9°$; $C_L = 0.83$.

Figure 15.– Continued.

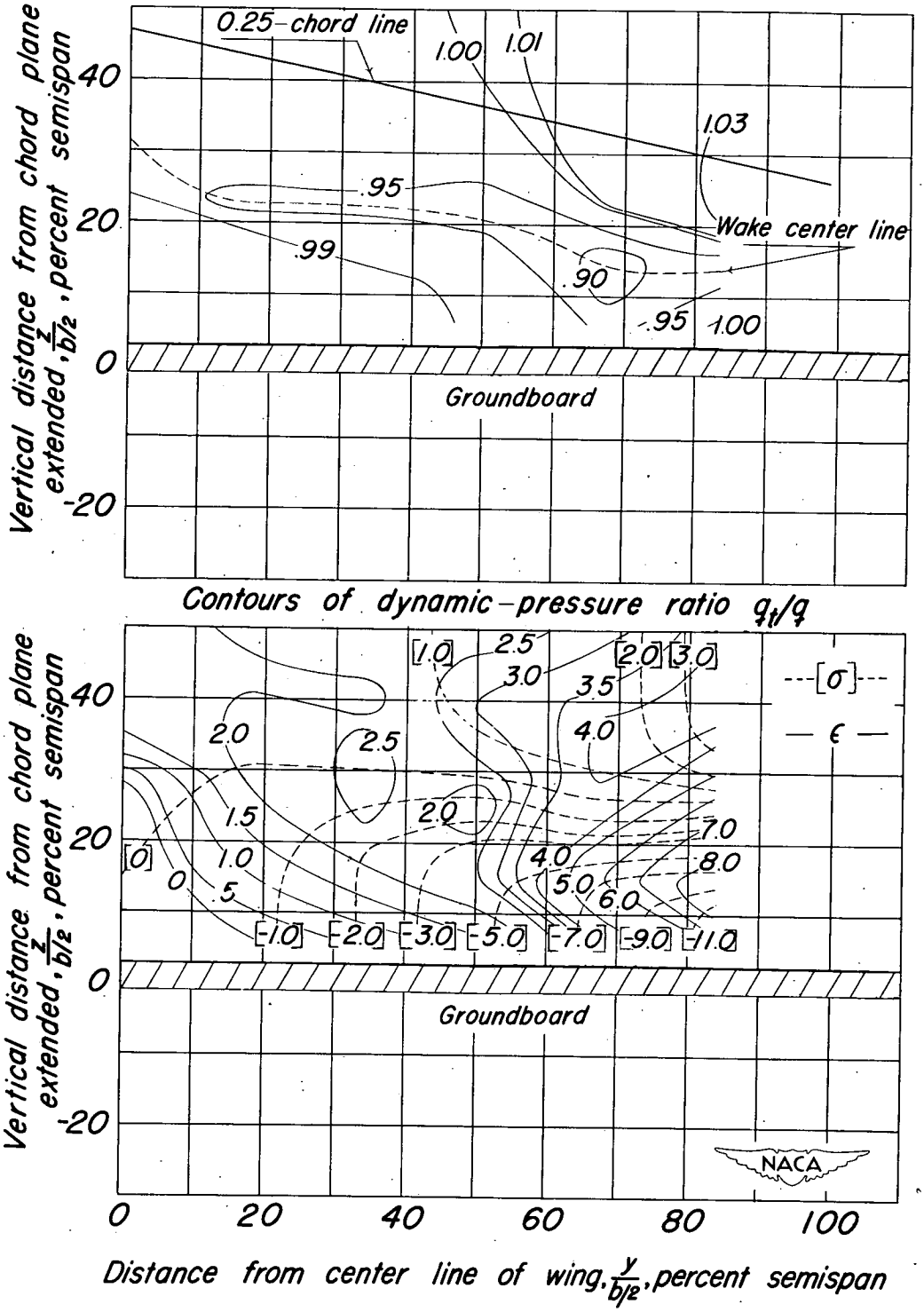

Contours of downwash angle ϵ and sidewash angle σ in degrees

(c) $\alpha = 14.6°$; $C_L = 0.98$.

Figure 15.- Concluded.

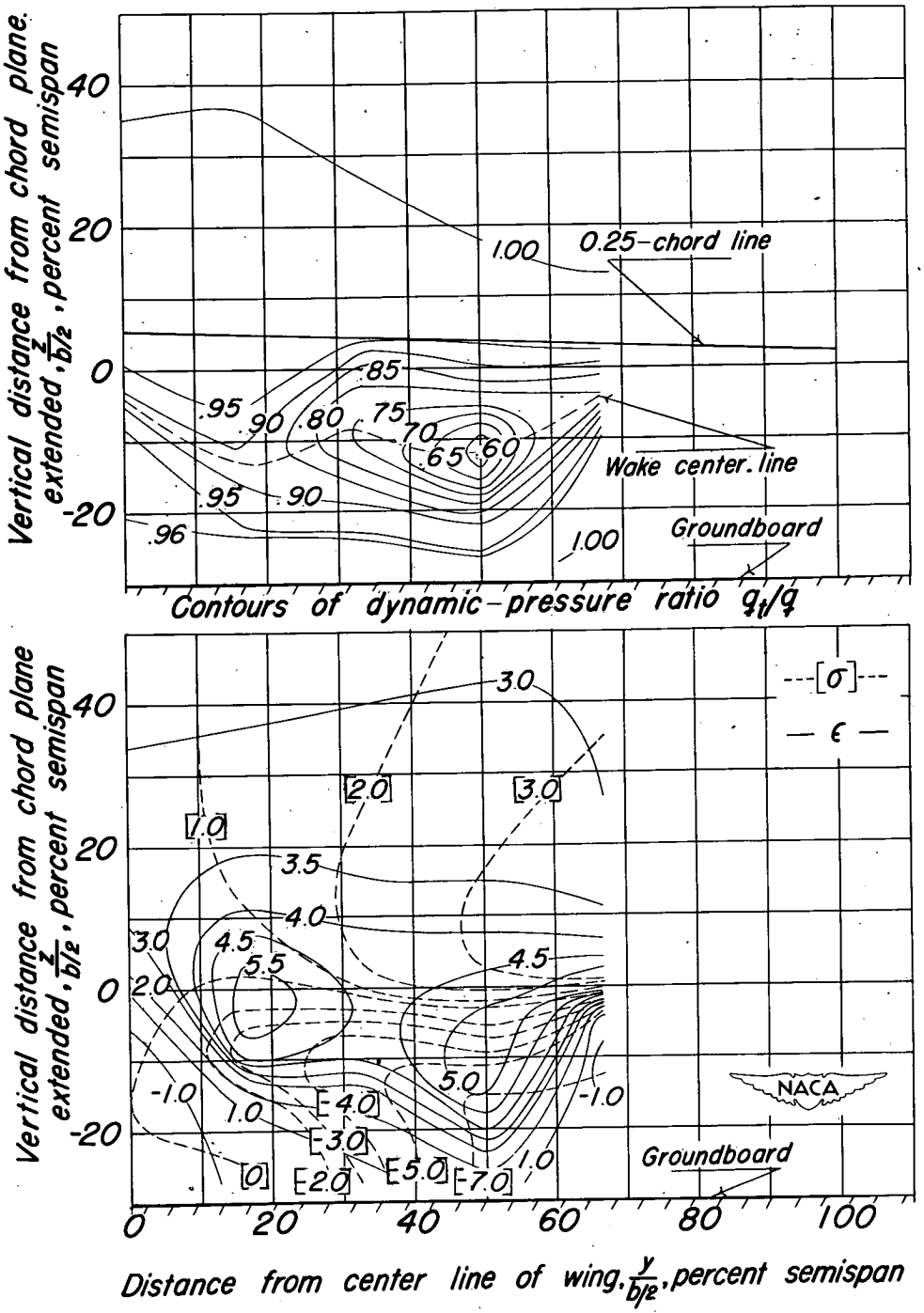

Contours of downwash angle ϵ and sidewash angle σ in degrees
(a) $\alpha = 2.4°$; $C_L = 0.62$.

Figure 16.— Downwash angle, sidewash angle, and dynamic-pressure ratios behind a 42° sweptback wing. Longitudinal plane of survey at 2.0 M.A.C.; flaps deflected; ground distance 0.68 M.A.C.

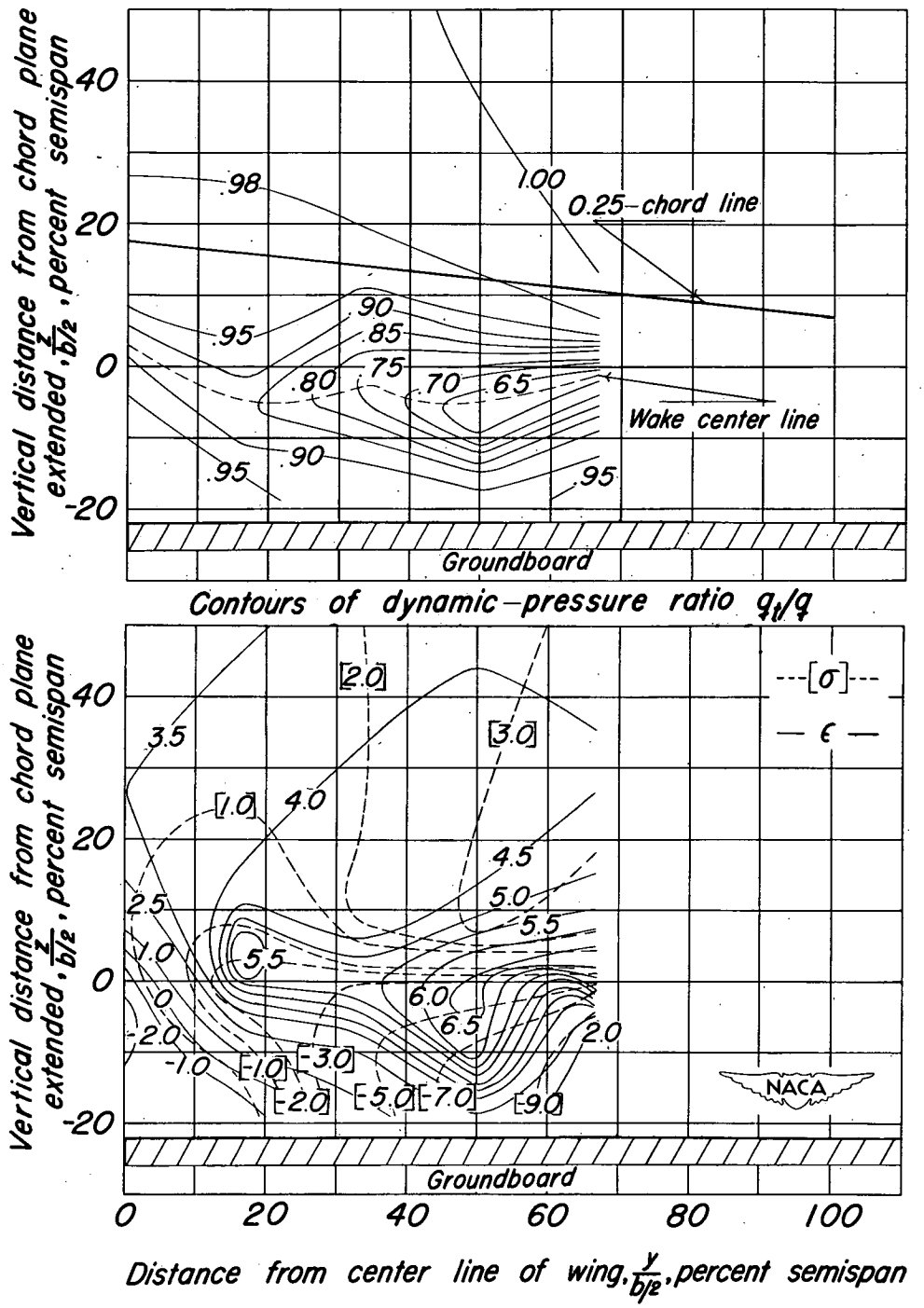

Contours of downwash angle ϵ and sidewash angle σ in degrees

(b) $\alpha = 7.3°$; $C_L = 0.91$

Figure 16.—Continued.

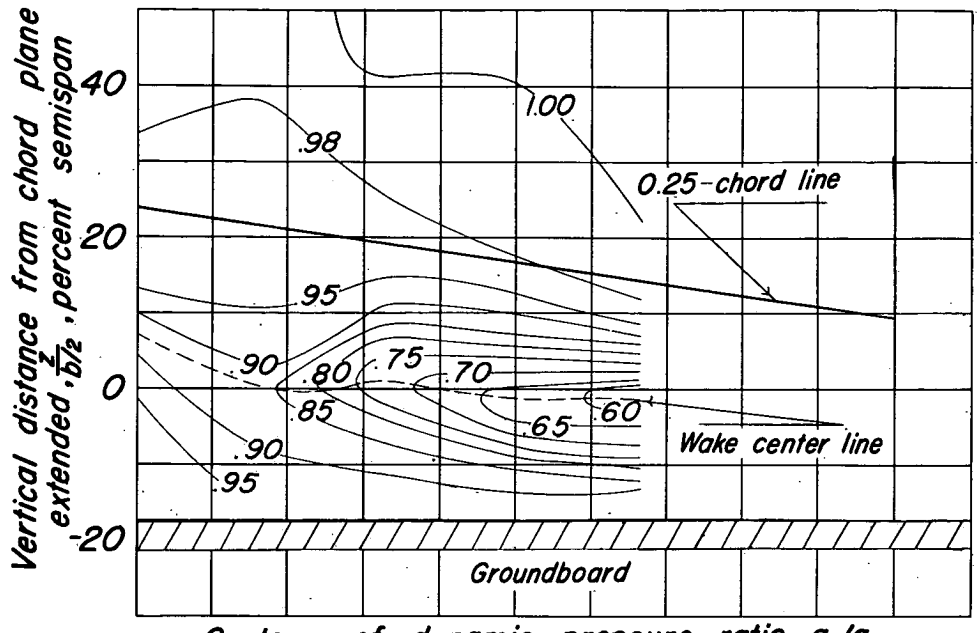

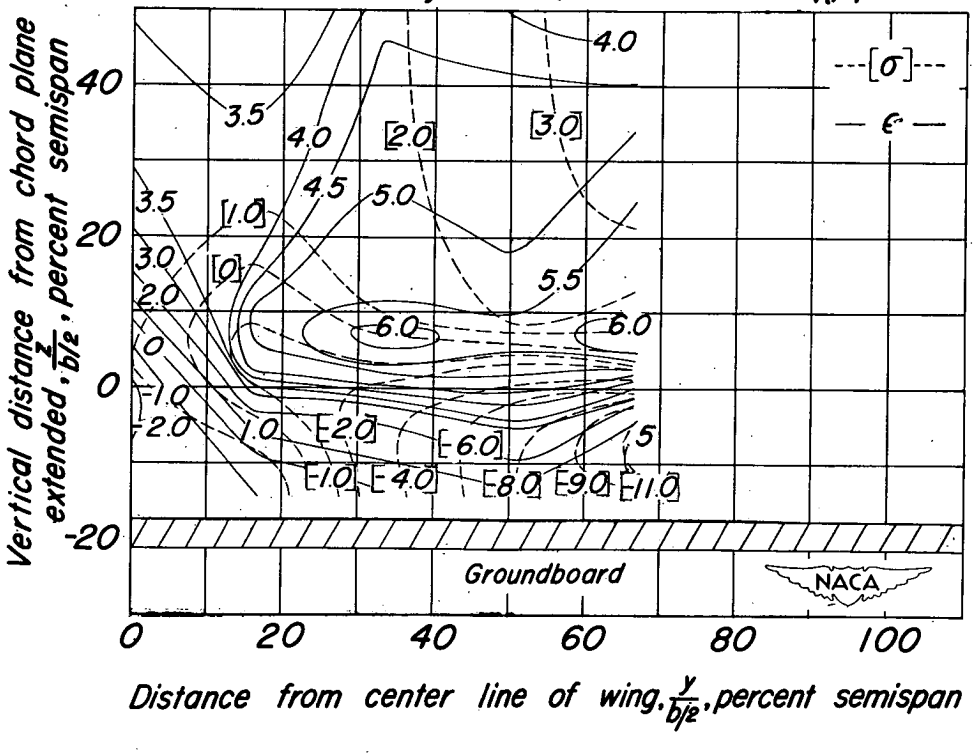

Contours of downwash angle ϵ and sidewash angle σ in degrees

(c) $\alpha = 10.0°$; $C_L = 1.00$

Figure 16.- Continued.

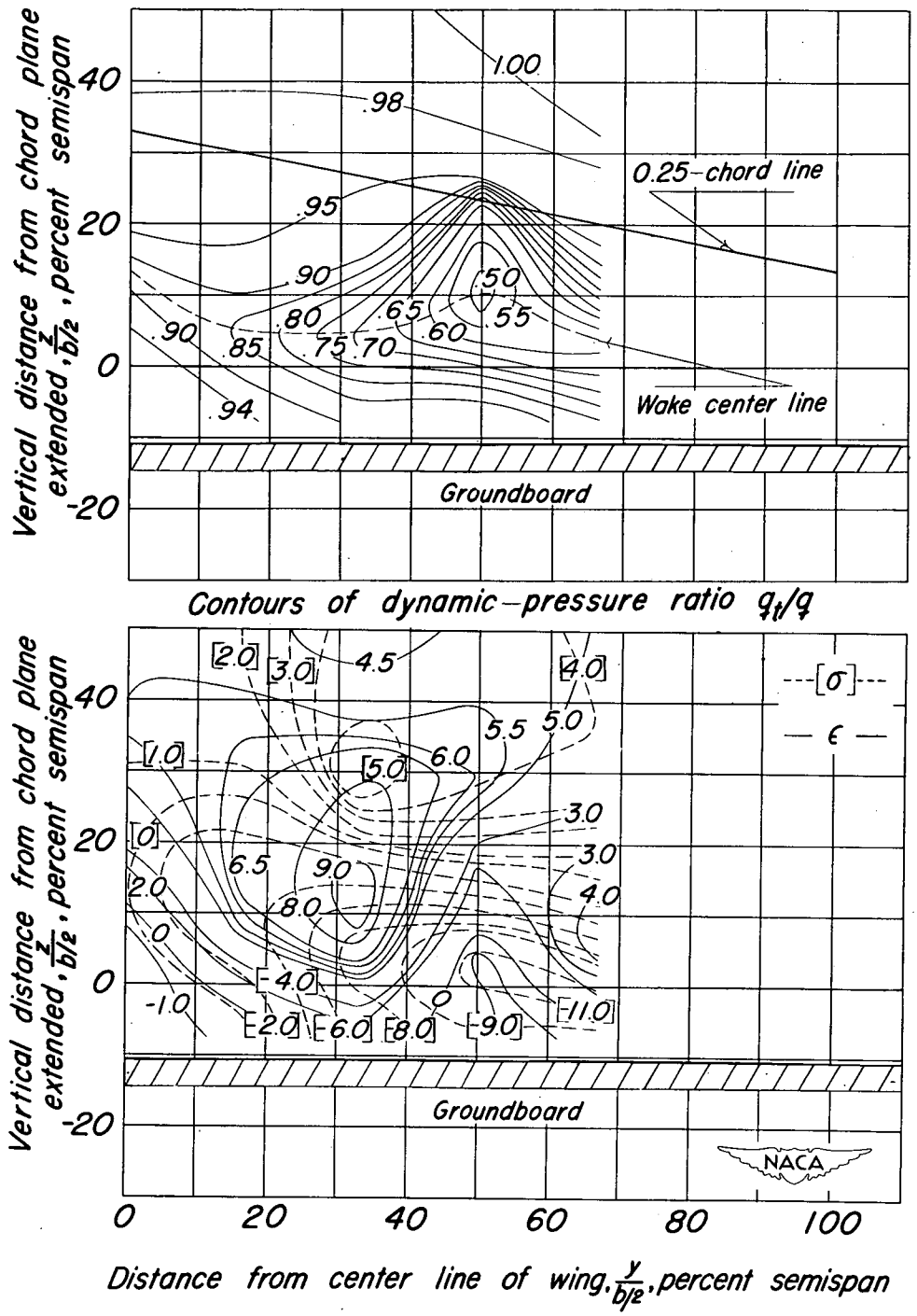

Contours of downwash angle ϵ and sidewash angle σ in degrees
(d) $\alpha = 13.6°$; $C_L = 1.20$.

Figure 16. – Concluded.

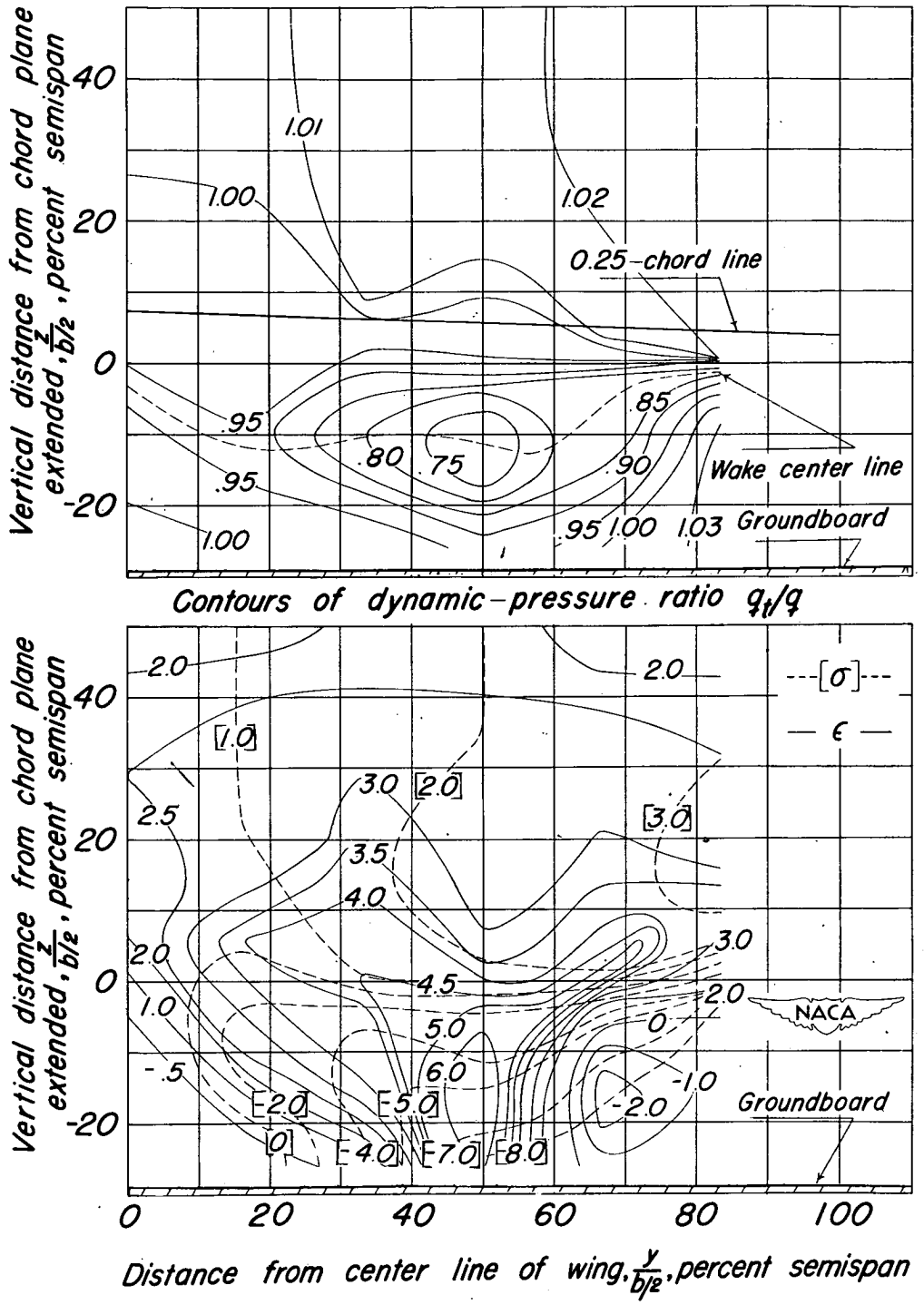

Contours of downwash angle ϵ and sidewash angle σ in degrees
(a) $\alpha = 2.4°$; $C_L = 0.62$.

Figure 17.- Downwash angle, sidewash angle, and dynamic-pressure ratios behind a 42° sweptback wing. Longitudinal plane of survey at 2.8 M.A.C.; flaps deflected; ground distance 0.68 M.A.C.

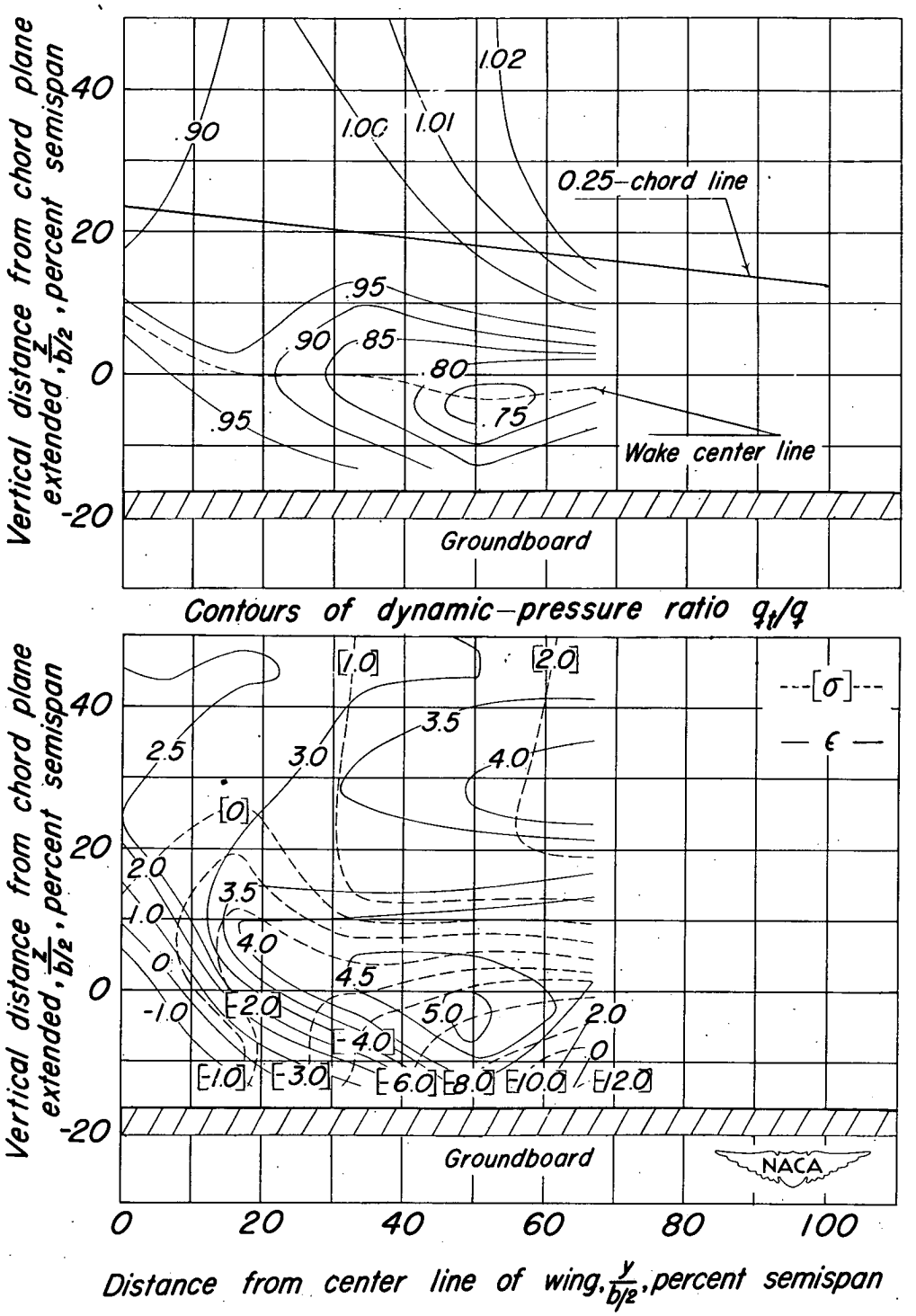

Contours of downwash angle ϵ and sidewash angle σ in degrees

(b) $\alpha = 7.3°$; $C_L = 0.91$

Figure 17.– Continued.

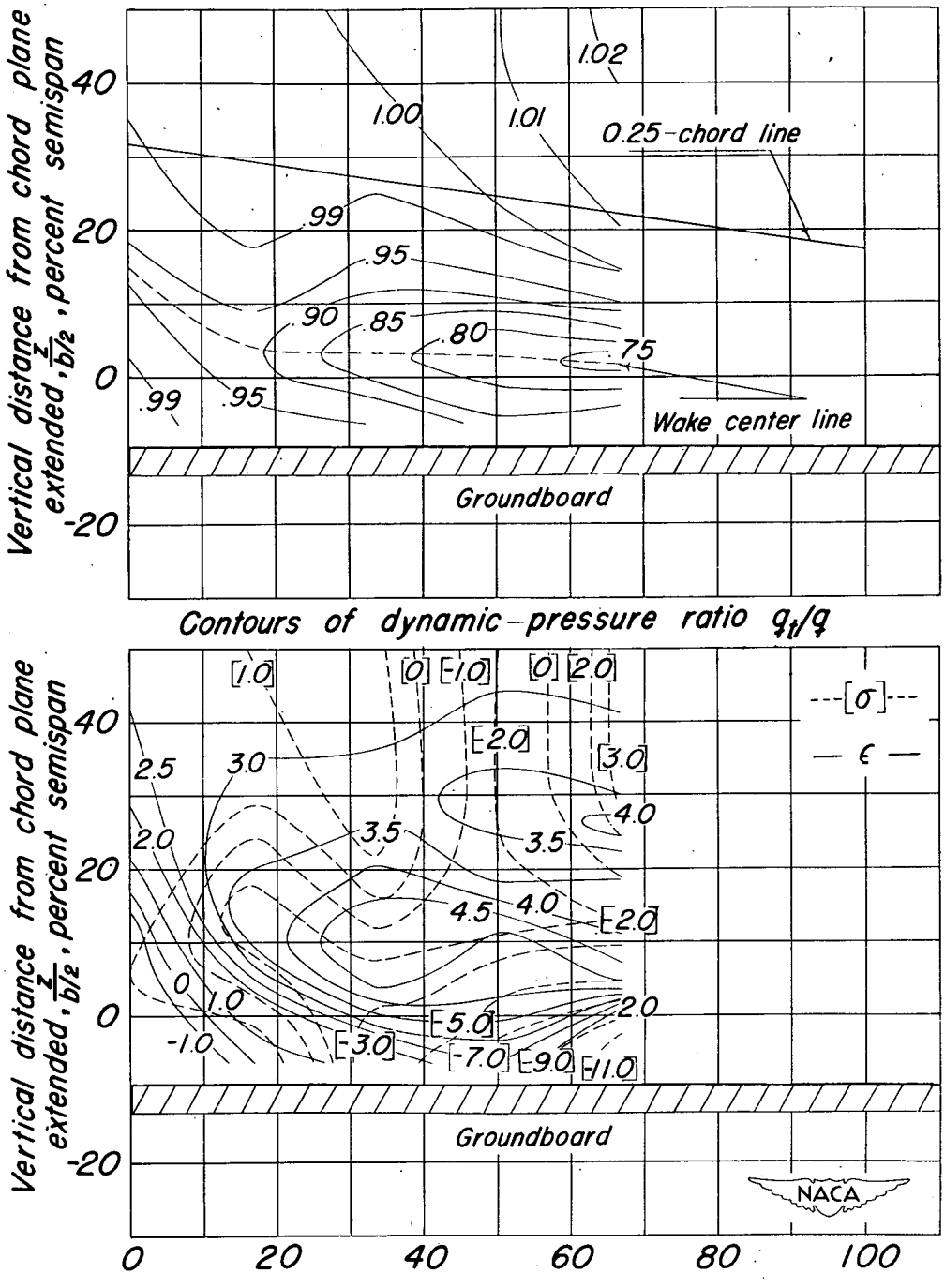

Contours of downwash angle ϵ and sidewash angle σ in degrees

(c) $\alpha = 10.0°$; $C_L = 1.00$

Figure 17.– Continued.

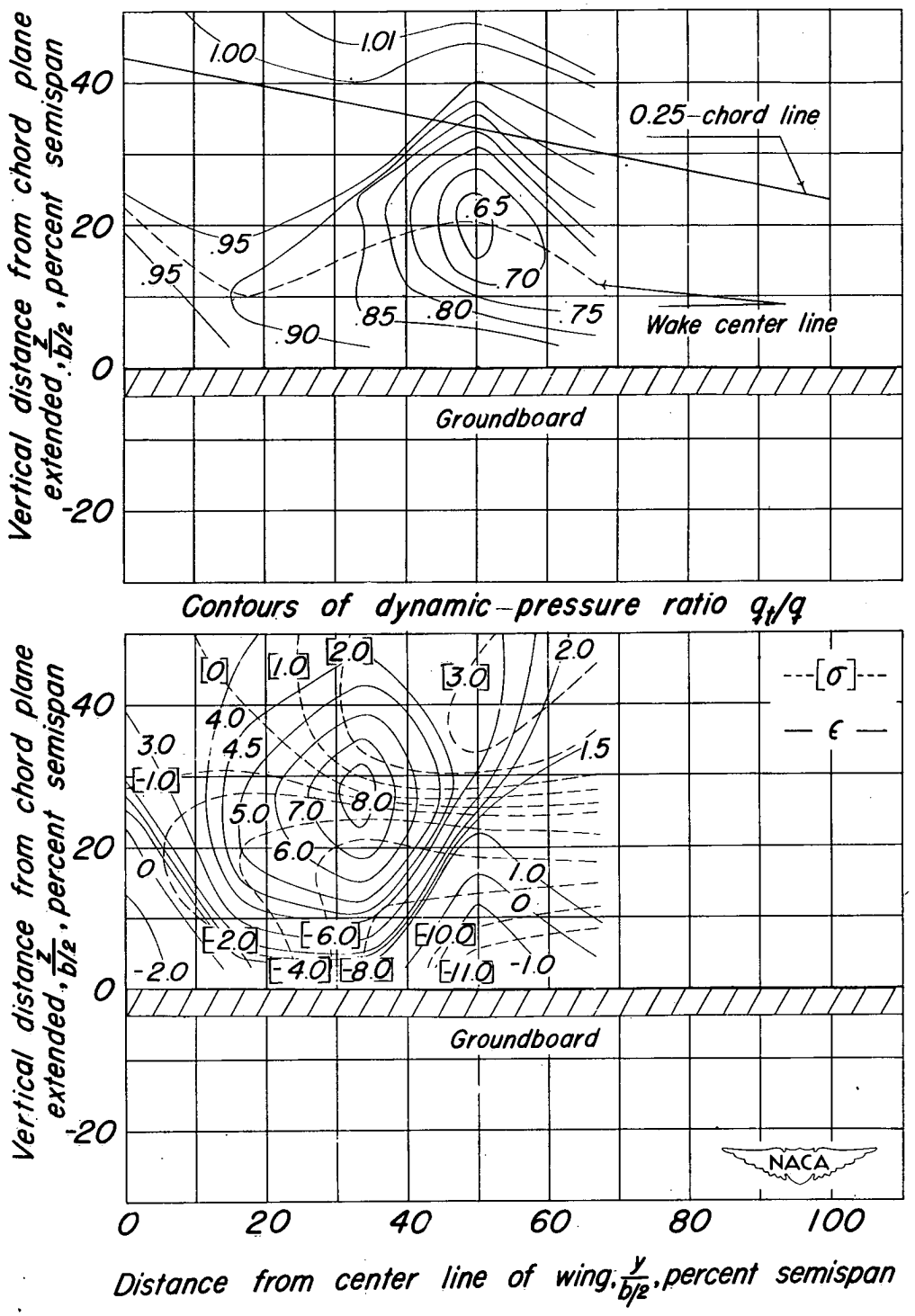

Contours of downwash angle ϵ and sidewash angle σ in degrees

(d) $\alpha = 13.6^\circ$; $C_L = 1.20$

Figure 17.— Concluded.

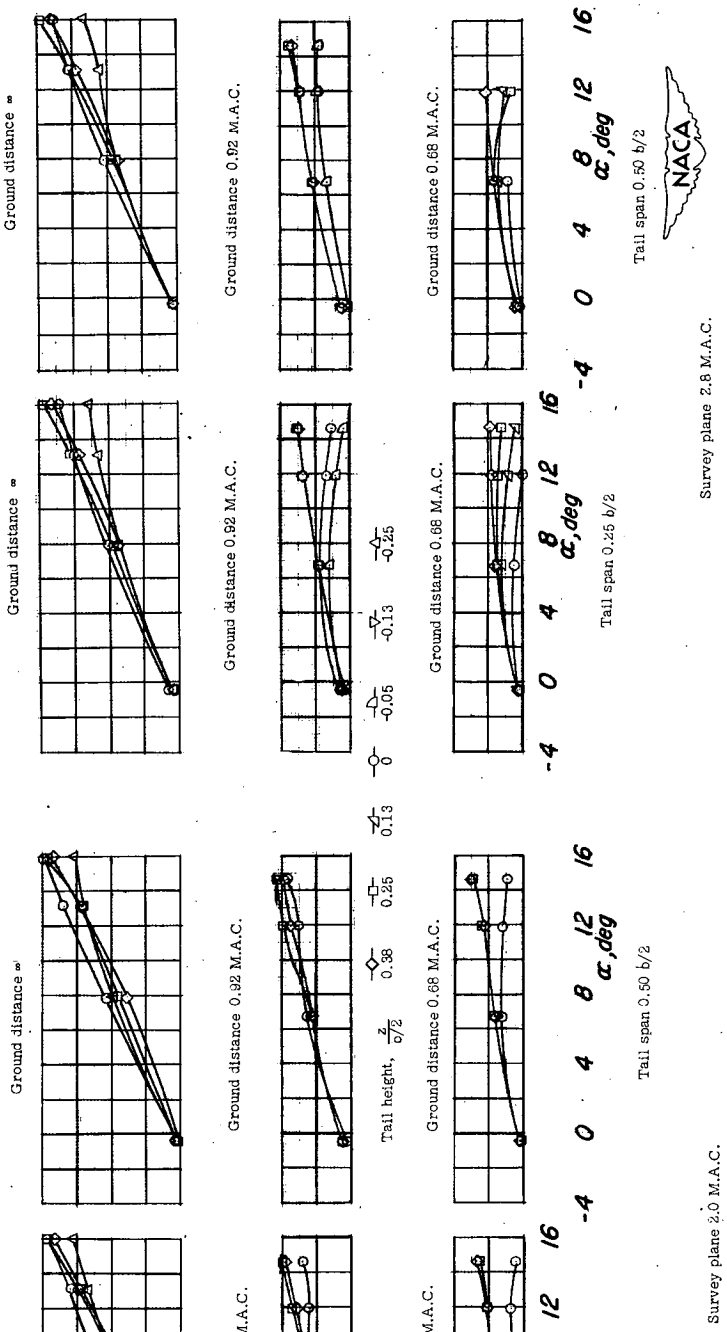

(a) Average downwash angle, ϵ_{av}, degrees.

Figure 18.- The variation of average downwash angle and dynamic-pressure ratios with angle of attack for various ground distances, tail lengths, and tail spans. Flaps neutral.

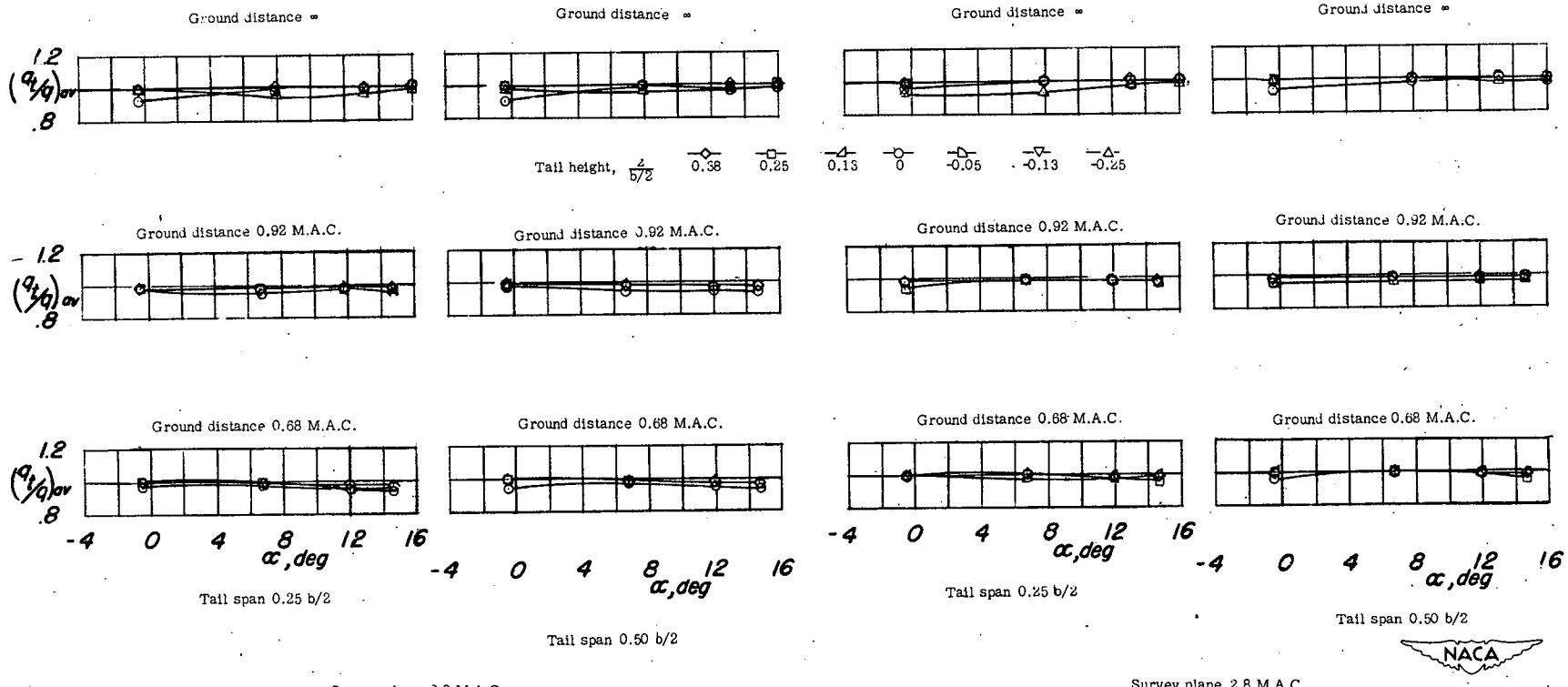

(b) Average dynamic-pressure ratio, $(q_t/q)_{av}$.

Figure 18.- Concluded.

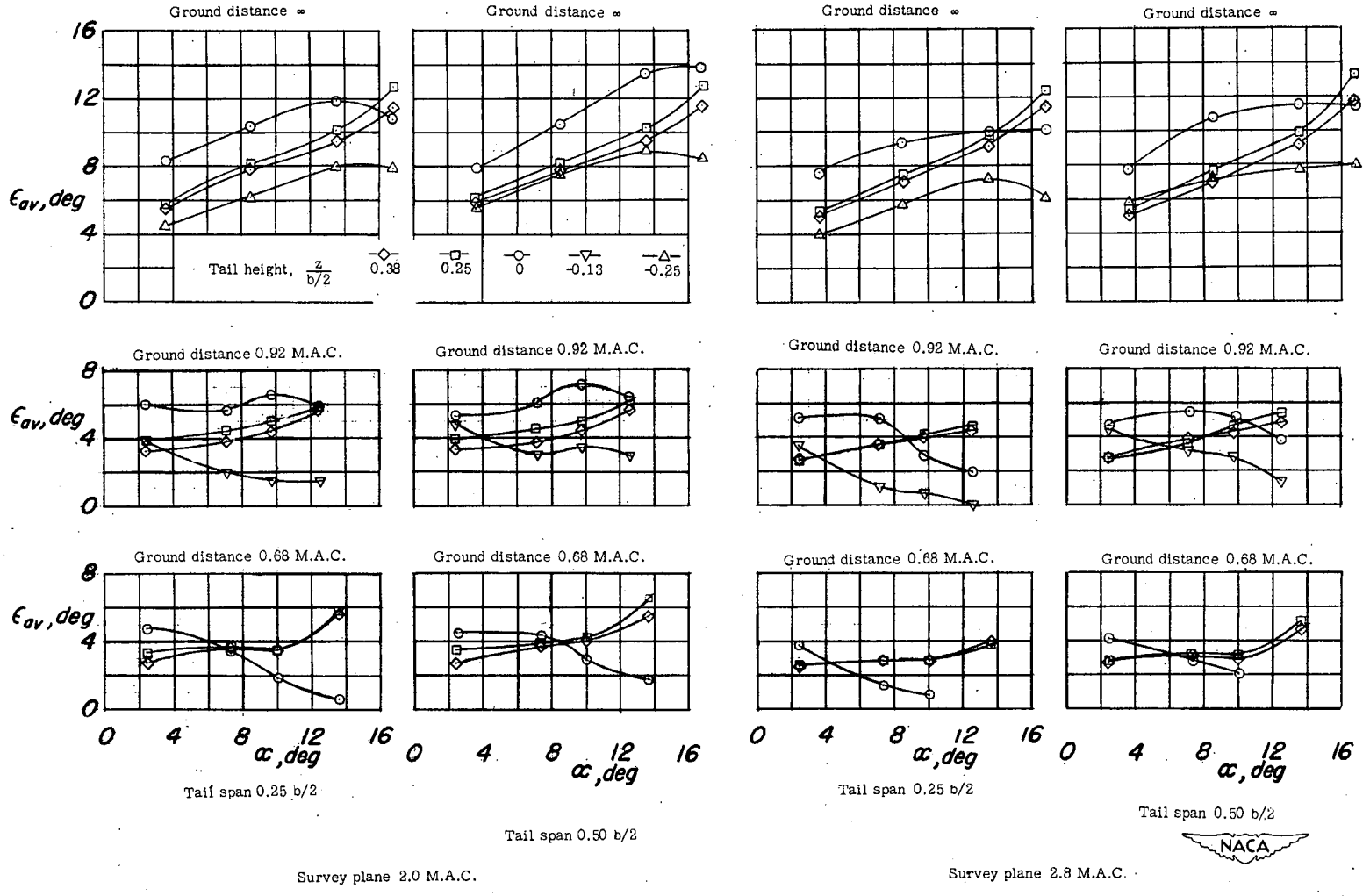

(a) Average downwash angle, ϵ_{av}, degrees.

Figure 19.- The variation of average downwash angle and dynamic-pressure ratios with angle of attack for various grounds distances, tail lengths, and tail spans. Flaps deflected.

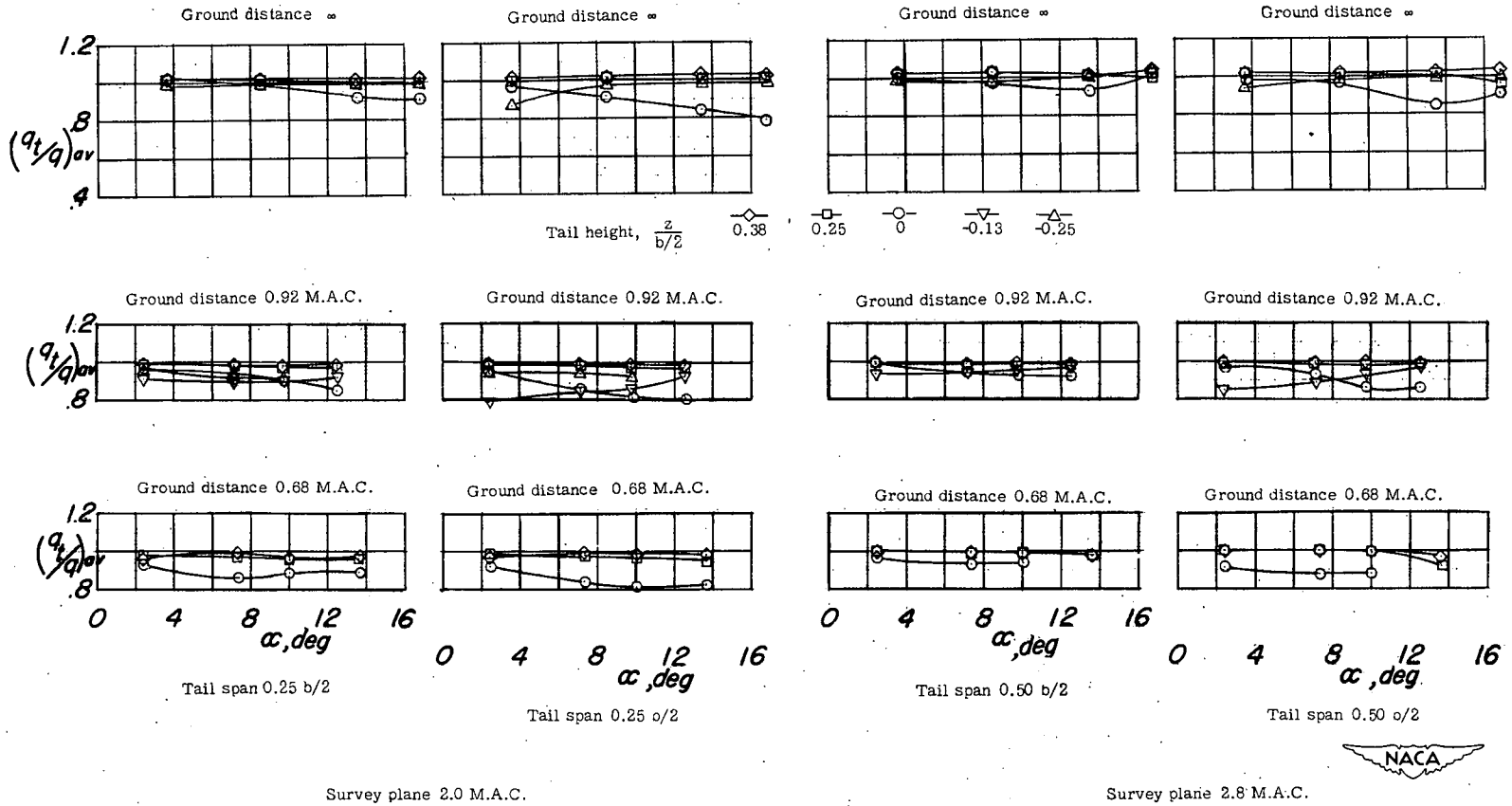

(b) Average dynamic-pressure ratio, $(q_t/q)_{av}$.

Figure 19.- Concluded.

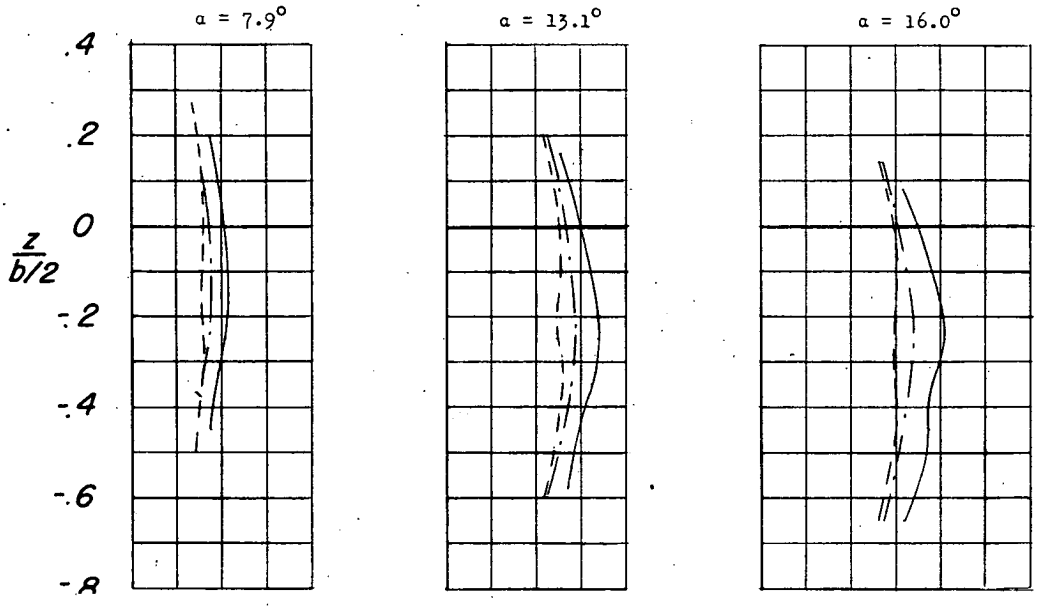

(a) Survey plane 2.0 M.A.C.

——— experimental

— — — — calculated

——— · ——— calculated (neglecting negative vorticity at inboard sections)

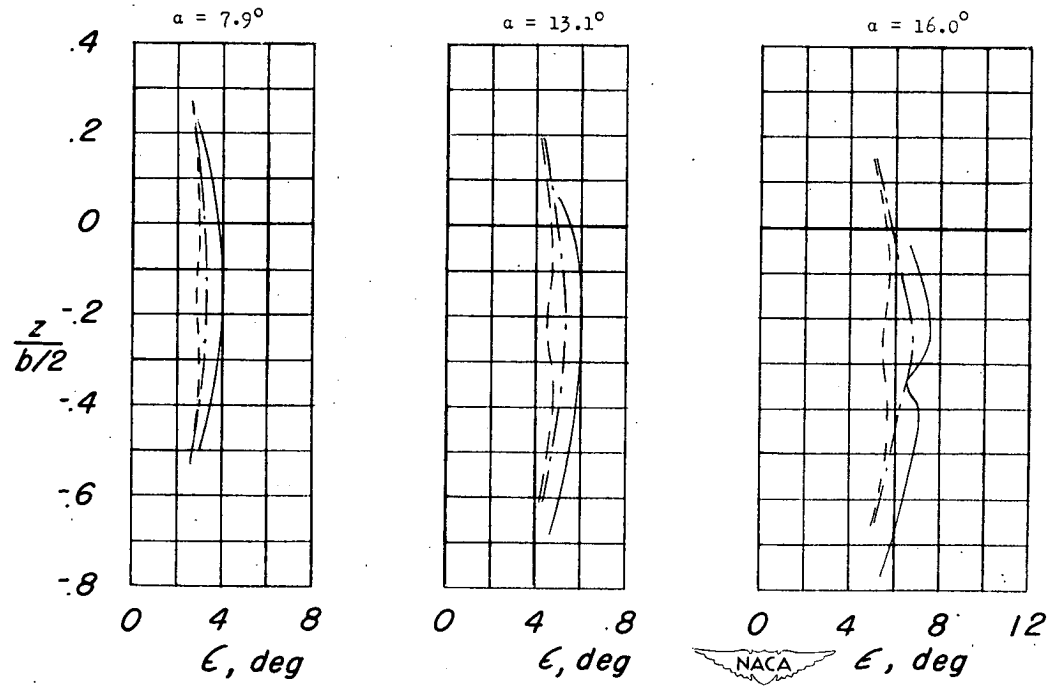

(b) Survey plane 2.8 M.A.C.

Figure 20.- Variation of calculated and experimental values of downwash with vertical distance at the plane of symmetry. (Vertical reference point 0.25 chord at plane of symmetry.)

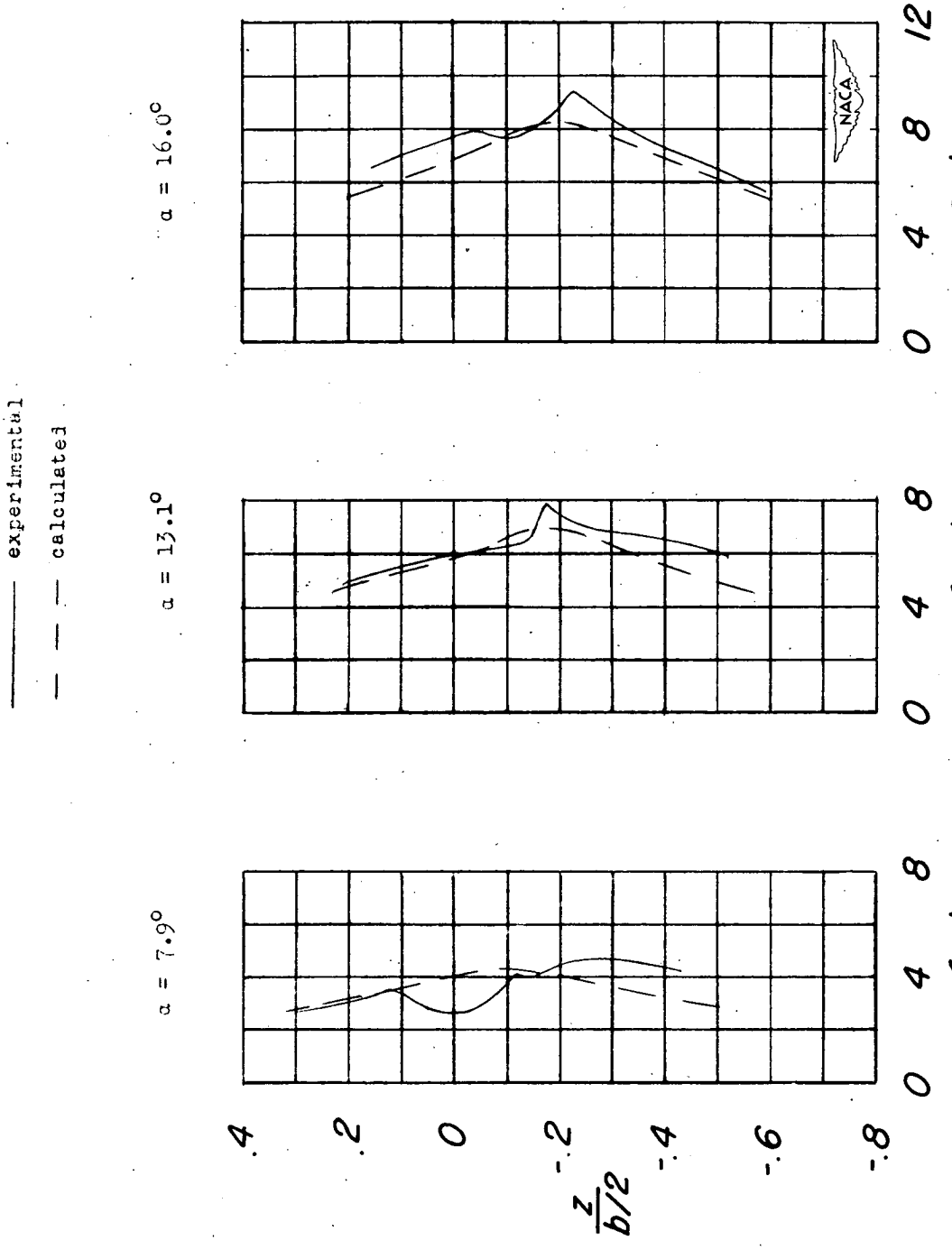

Figure 21.- Variation of calculated and experimental values of downwash with vertical distance at a spanwise station 0.33b/2. (Vertical reference point 0.25 chord at spanwise station 0.33b/2.) Survey plane 2.0 M.A.C.

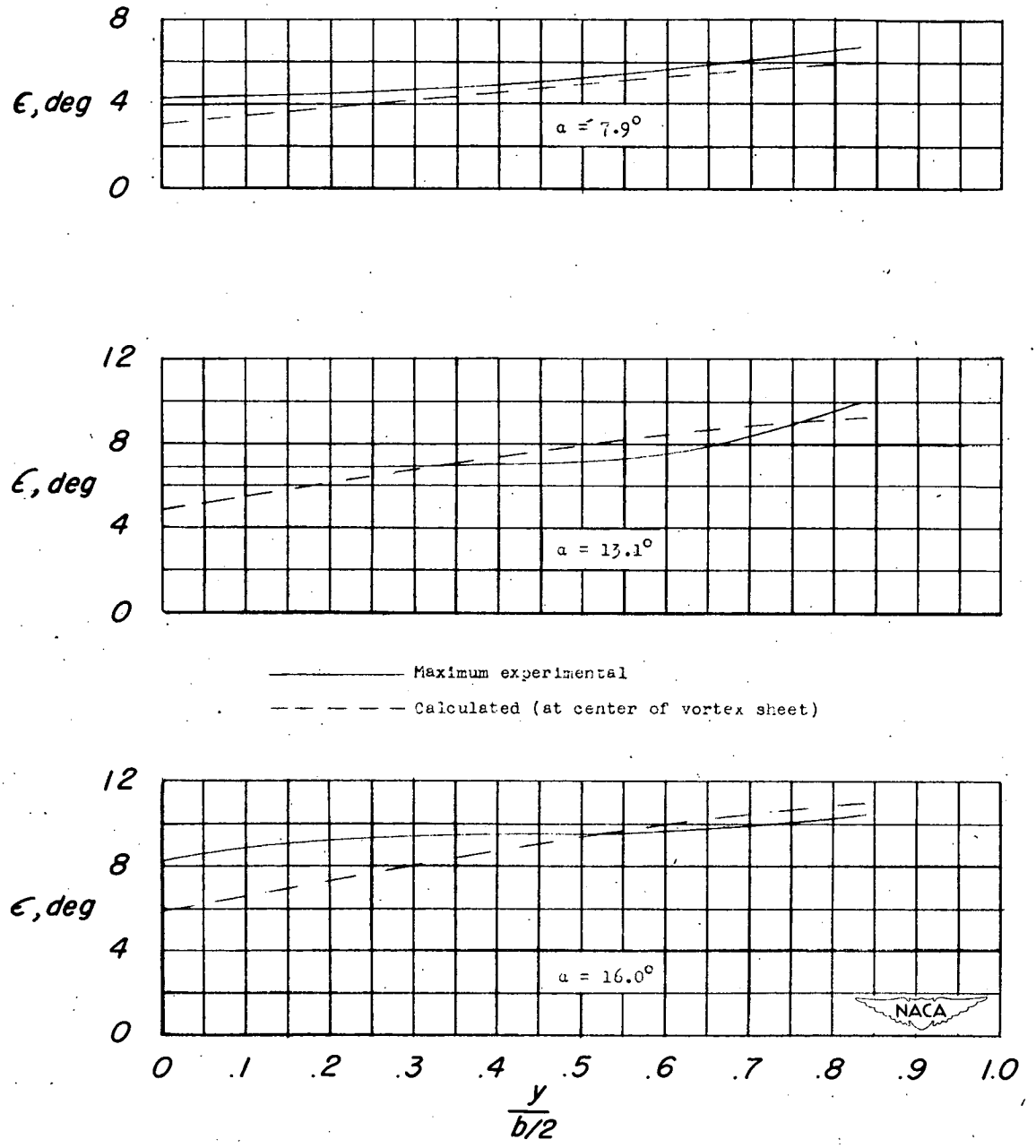

Figure 22.- Spanwise variation of maximum experimental downwash and calculated downwash at the center of the vortex sheet.